NANYANG TECHNOLOGICAL UNIVERSITY

SLOW VISCOUS FLOW OF TWO PARTICLES IN A CYLINDRICAL TUBE

YAO XIN

SCHOOL OF MECHANICAL AND AEROSPACE ENGINEERING

2016

SLOW VISCOUS FLOW OF TWO PARTICLES IN A CYLINDRICAL TUBE

YAO XIN

School of Mechanical & Aerospace Engineering

A thesis submitted to the Nanyang Technological University
in partial fulfilment of the requirement for the degree of
Doctor of Philosophy

2016

Acknowledgments

I would like to express my heartfelt gratitude to my supervisor: Assistant Professor Marcos for his invaluable advice and tutelage of my study throughout the past four years. He continually guides my research and monitors the process of my study. It is a great honor working with him.

My greatest gratitude also goes to Associate Professor Wong Teck Neng for introducing me to the interesting area of microfluidic system and constant guidance in my research.

I would also like to thank my colleagues for their kind help and support: Huang Yi, Feng Huicheng, Xie Jinlong, Ding Zijing, Tran Ngoc Phu, Tran Duc Quang, Kong Tian Fook, Koh Boon Yong James, Shen Xinhui, Tan Pei Yen and Benjamin Tay Zikai.

Abstract

The motion of small particles in a cylindrical tube at low Reynolds number can be found in many fields, ranging from the industrial and environmental applications such as fluidization and filtration, to biomedical applications such as drug delivery in blood vessels. The major challenges in the elucidation of the hydrodynamic behavior of these systems are particle interactions within the tube, which can facilitate analysis of the aggregation and collision of particles. More specifically, the fundamental knowledge of these mechanisms provides significant insight into modelling heat and mass transfer processes of particles. However, most of the current studies on this motion concentrate on a single particle or particles along the axis with same size. The mathematical treatment of multi particles interactions in a tube is still unclear.

A logical beginning towards illustration of these behaviors is addressed in this thesis by considering the flow dynamics of two spherical particles with arbitrary positions traveling within a cylindrical tube at low Reynolds number. Such case is not only of fundamental interest of aforementioned applications, but also can significantly contribute to understand hydrodynamic interactions of multi particles flow field in the tube.

In order to analyze the detailed hydrodynamic interaction between the two particles, we developed a mathematical model adopting the method of reflections. In general, when the two particles travel within a cylindrical tube, each of them has the translational velocity together with the rotational velocity. Due to the no-slip, three boundary conditions are applied for the entire flow

field: the surfaces of the two particles and the wall of the tube. To make the flow field analytically solvable, the method of reflections is utilized to treat the boundary conditions separately. We employ the Lamb's general solution based on spherical harmonics and cylindrical harmonics to solve the flow field around the particles and the flow within the tube, respectively.

By employing this mathematical procedure, we compute the hydrodynamic force coefficients of the particles which are dependent on the distance among the cylinder wall and the two particles. The hydrodynamic forces are also a function of particle velocities and background velocity. Our results are in agreement with the existing theory of a single particle traveling in the tube when the distance between the two particles increases. We found that the particle-particle interaction can be neglected when the separation distance is three times larger than the sum of particles radii. Furthermore, the direction of Poiseuille Flow, particle position relative to the axis and particle size can make the two particles attract and repel. Unlike the single particle case, the two particles can move laterally due to the hydrodynamic interaction. Such analysis can give us insights to understand the mechanisms of collision and aggregation of particles.

Contents

Acknowledgments ..... **I**

Abstract ..... **III**

List of Figures ..... **IX**

List of Notation ..... **XIII**

1 Introduction **1**

1.1 Background 1

1.2 Objective 5

1.3 Scope 6

2 Literature Review **7**

2.1 Slow viscous flow of a single particle 7

2.1.1 Slow viscous flow of a single particle in an unbounded fluid 7

2.1.2 Slow viscous flow of a single particle close to plane surfaces 9

2.1.3 Slow viscous flow of a single particle in an axisymmetric container 11

2.1.4 Slow viscous flow of a single particle close to a free surface 12

2.2 Slow viscous flow of two or more spheres 14

2.2.1 Slow viscous flow of two or more spheres in an unbounded fluid 14

2.2.2 Slow viscous flow of two or more spheres in a cylindrical tube 19

2.3 Current study 21

3 Problem Formulation 23

3.1 Governing equations and Boundary conditions 23

3.2 The Method of Reflections 25

3.3 Spherical harmonics for the flow around the particle 29

3.4 Cylindrical harmonics for the flow field of cylinder 33

3.5 Coordinate transformation 39

3.6 Calculation procedure and velocities of particles 42

4 Result and Discussion 49

4.1 Two spheres along the axis of the cylindrical tube 50

4.1.1 Two particles with same size 50

4.1.2 Two particles with different sizes 58

4.2 Two spheres with one off the axis 69

4.2.1 Two particles with same size 70

4.2.2 Two particles with different sizes 77

4.3 Two particles in the same cross sectional area 84

5 Conclusions and Future Work 89

5.1 Conclusions 89

5.2 Future work 92

Reference 93

Appendix.....99

List of Figures

Figure 3.1: Sketch of two particles moving in a cylindrical tube.....23

Figure 3.2: The method of reflections procedure 27

Figure 3.3: (a) axonometric drawing of the coordinate system of two particles in a cylindrical tube; (b) projection of the coordinate system of two particles in a cylindrical tube along the axis. 40

Figure 3.4: Calculation procedure 42

Figure 4.1: Schematics of two rigid particles moving in a cylindrical tube. 49

Figure 4.2: Schematic of two particles along the axis of the tube. 50

Figure 4.3: Streamlines of two particles with the same size along the axis in the tube (Region marked in Figure 4.2 with dashed rectangle). 51

Figure 4.4: Velocity profile along the radial direction of the two particles with the same size 52

Figure 4.5: Normalized drag force coefficient D ($D = D_a = D_b$) with two different particle sizes. 53

Figure 4.6: Normalized drag force coefficient K^* ($K^* = K_{ab} = K_{ba}$) with different particle sizes.....54

Figure 4.7: Normalized drag force coefficient K ($K = K_a = K_b$) with different particle sizes.....55

Figure 4.8: Normalized velocity of the two particles U_z ($U_z = U_{az} = U_{bz}$) with different particle sizes. 57

Figure 4.9: Normalized drag force coefficient D_a for two particles with different sizes. The horizontal line refers to the coefficient of a single particle case with a/R_0=0.1. 58

Figure 4.10: Normalized drag force coefficient D_b. It is plotted as L/R_0. We choose a/R_0=0.1 and (a) b/a=2, (b) b/a=3, (c) b/a=4, (d) b/a=5, respectively. The horizontal line refers to the coefficient of single particle case accordingly.59

Figure 4.11: Streamlines with a/R_0=0.1 and b/a=3. We choose (a) L/R_0=0.405, (b) L/R_0=0.5, (c) L/R_0= 0.9, respectively. Since the geometry is under axisymmetric condition, we plot half of the streamlines with U_a=U_b=0 to represent the flow field. 61

Figure 4.12: Velocity profile along the radial direction of the two particles with a/R_0=0.1 and b/a=3. We choose (a) L/R_0=0.405, (b) L/R_0=0.5, (c) L/R_0= 0.9, respectively. 62

Figure 4.13: Normalized drag force coefficients K_a with different radii ratios..63

Figure 4.14: Normalized drag force coefficient D_b with different radii ratios. ..64

Figure 4.15: Normalized drag force coefficients K^* ($K^* = K_{ab} = K_{ba}$) with different radii ratios. 65

Figure 4.16: (a) Normalized velocity of particle *A*; (b) Normalized velocity of particle *B*. 66

Figure 4.17: Schematics of two rigid particles with the symmetric positions in a cylindrical tube. Particle *A* is located on the axis and Particle *B* has a lateral distance perpendicular to the axis named as L_b. 69

Figure 4.18: Normalized velocities the two particles in *X*-direction with $a/R_0=b/R_0=0.02$ and $L/R_0=0.05$.....70

Figure 4.19: Normalized velocities the two particles in *X*-direction with $a/R_0=b/R_0=0.02$ and $L/R_0=0.02$.....72

Figure 4.20: Normalized velocities the two particles in *Z*-direction with $a/R_0=b/R_0=0.02$ and $L/R_0=0.05$.....73

Figure 4.21: Normalized velocities the two particles in *Z*-direction with $a/R_0=b/R_0=0.02$ and $L/R_0=0.02$.....74

Figure 4.22: Normalized rotational velocities the two particles in *Y*-direction with $a/R_0=b/R_0=0.02$ and $L/R_0=0.05$. 75

Figure 4.23: Normalized rotational velocities the two particles in *Y*-direction with $a/R_0=b/R_0=0.02$ and $L/R_0=0.02$. 76

Figure 4.24: Normalized translational velocities of the two particles in *X*-direction with $a/R_0=0.05$, $b/R_0=0.1$ and $L/R_0=0.2$. 77

Figure 4. 25: Normalized translational velocities of the two particles in *X*-direction with $a/R_0=0.05$, $b/R_0=0.1$ and $L/R_0=0.1$. 79

Figure 4.26: Normalized translational velocities of the two particles in *Z*-direction with $a/R_0=0.05$, $b/R_0=0.1$ and $L/R_0=0.2$. 80

Figure 4.27: Normalized translational velocities the two particles in *Z*-direction with $a/R_0=0.05$, $b/R_0=0.1$ and $L/R_0=0.1$. 80

Figure 4.28: Normalized rotational velocities of the two particles in *Y*-direction with $a/R_0=0.05$, $b/R_0=0.1$ and $L/R_0=0.2$. 81

Figure 4.29: Normalized rotational velocities of the two particles in *Y*-direction with a/R_0=0.05, b/R_0=0.1 and L/R_0=0.1. 82

Figure 4.30: Schematics of two rigid particles in the same cross sectional area in a cylindrical tube. 84

Figure 4.31: Normalized translational velocities of the two particles in the same cross sectional area. 85

Figure 4.32: Normalized rotational velocities of the two particles in the same cross sectional area: ω_{aX}/U_0 and ω_{bx}/U_0. 86

Figure 4.33: Normalized rotational velocities of the two particles in the same cross sectional area: ω_{aY}/U_0 and ω_{by}/U_0. 87

List of Notation

U_i	Translational velocity of particle *i*
ω_i	Rotational velocity of particle *i*
$\vec{F}_i^{(j)}$	j^{th} reflection drag force of boundary *i*
$\vec{T}_i^{(j)}$	j^{th} reflection torque of boundary *i*
R_0	Radius of cylinder
L_i	Distance of between center of the particle *i* and the axis of tube
L	Distance between two particles along the tube
X_i, Y_i, Z_i	Cartesian coordinates variables of boundary *i*
r_i, θ_i, φ_i	Spherical coordinates variables of particle *i*
R, Φ, Z	Cylindrical coordinates variables
a	radius of particle *A*
b	radius of particle *B*
v	Velocity of flow
p	Dynamic pressure
$\vec{v}_i^{(j)}$	j^{th} reflection velocity of boundary *i*
$p_i^{(j)}$	j^{th} reflection pressure of boundary *i*
$\vec{V}_i$	Velocity on the particle *i* surface
p_n, χ_n, Φ_n	n^{th} solid spherical harmonics
P_n	Legendre polynomials

P_n^m	Associated Legendre Polynomials
T_n^m	Legendre polynomials of the first kind

Chapter 1

Introduction

1.1 Background

The motion of particles at low Reynolds number is ubiquitous. This problem is of interest in connection with a great variety of natural and industrial phenomena. In atmospheric circulation, the movements of particles contribute to the formation of aerosols, such as fog and clouds, which play crucial roles in influencing human health, relative air moisture and earth climate system [1, 2]. Meanwhile, the mass transfer process in the ocean is greatly affected by the hydrodynamic behaviors of moving particles. Typical examples include particle aggregation and sedimentation, which are important to the formation of organic and inorganic source [3, 4]. Additionally, the motion of particles appears in a wide range of industrial applications, such as fluidization, elutriation and filtration [5].

The systematic investigation of particles traveling in an unbounded fluid at low Reynolds number involves both analytical and numerical studies tracing back to the work of Brenner [6, 7]. He found that the hydrodynamic resistance of a single particle can be represented as a symmetric tensor based on the external geometry of the particle. Later, the steady motion of two rigid spheres in an unbounded fluid has been studied by Stimson & Jeffery [8], Goldman et al. [9], Jeffrey & Onishi [10], Kim & Mifflin [11] and the unsteady flow field by Ardekani & Rangel [12]. Furthermore, Stokes flow past three spheres was

analyzed by Kim [13] theoretically and Wilson [14] numerically. The physical parameters such as drag force, torque, stresslet and pressure drop have mainly been considered from numerical and analytical point of view.

Unlike in an unbounded fluid, the presence of a boundary will significantly affect the flow behavior. One typical example of a commonly used boundary is a cylindrical tube. This problem is of interest in connection with a great variety of phenomena, ranging from the industrial and environmental applications such as fluidization, elutriation and filtration [15, 16]. The cylindrical tube serves as transfer device: to generate flow carrying particles in a certain direction; to separate particles due to the surface properties; to transfer energy through the solid surface. Additionally, this motion has been used as a model for the flow of chemical drugs [17]. It is known, in the medical therapy, the dissolved drug will be dispersed in blood circulation and lymph circulation through capillaries. It also concerns the detailed flow field of particles in microchannel for microfluidic system, with the prospect of exploring the adaptability of such an instrument to industrial applications. Meanwhile, it is widely accepted that particulate interaction plays a critical role in these flow fields. Such hydrodynamic mechanism is responsible for the aggregation and collision of particles in the tube. Similarly, these processes can be exploited in microfluidic systems for particle separation. Problems of spherical particles travelling in a tube involve hydrodynamic interactions due to multiple objects. The characteristics of the flow field such as drag force will be more complex depending on the configuration of the geometry. Therefore, there is a

compelling need to understand the flow characteristics involving multiple particles within the tube.

Generally, slow viscous flow containing particles moving along the tube, is driven by an externally applied force, such as pressure gradient, electric field and magnetic force [15, 18, 19]. The Reynolds number based on the particle scales is much smaller than 1. Such flow is governed by the Stokes equation in which the drag force is linearly proportional to translational velocity. In a low Reynolds number world, viscous forces dominate inertial effects. Physically, inertia is the character of the particle to remain in motion. On the other hand, viscous forces are the original source of the drag acting on the particle traveling through the fluid. These mechanisms make the particle move or stop instantaneously under application or removal of external forces. When the concentration of particles is small, each particle can be regarded as a single particle moving in the fluid. However, at large concentration, particle interactions will dominate the hydrodynamic behaviors. Such effects can lead to significant changes of the flow field, which is responsible for the aggregation and collision of particles in the tube.

Brenner & Happel considered the flow dynamics of a single particle traveling within a cylindrical tube and found the drag force is larger than that in an unbounded fluid [20]. Later, another model was proposed by Greenstein & Happel [21]. Meanwhile, the hydrodynamic mechanism of a particle with an arbitrary viscosity property and slip surface translating through another immiscible fluid is numerically and theoretically investigated by Keh & Chang

[22]. Recently, a different approach was pursued by Bhattacharya et al. [17], which is capable of solving general problems containing particles within cylindrical tubes. The first step towards elucidation of the entire flow field is to consider the flow dynamics of two particles traveling within a cylindrical tube at low Reynolds number. Theoretical approaches have been conducted to investigate this case [23-25]. Their main focus has been on the parameterizations of the drag force and torque acting on the spherical particles. However, these studies are limited to symmetrical positions or constant velocities and the details of the flow field in such system have not been well studied.

The slow viscous flow around two particles in a cylindrical tube is obtained theoretically in this study. We employ the Lamb's general solution based on spherical harmonics and cylindrical harmonics to solve the flow field around the particles and the flow within the tube, respectively. The method of reflections is adopted to satisfy the boundary conditions. We compute the drag force and torque coefficients of the particles which are dependent on the distance among the cylinder wall and the two particles. These coefficients are also a function of particles velocities and background velocity. Our results are in agreement with the existing theory of single particle traveling in the tube when distance between two particles increases. Finally, we determine the characteristic distance where particle- particle interaction can be neglected. We can then extend the two-particle approach to multiple particles problem by extending the boundary conditions based on the method of reflections. Such

analysis could give us insights to understand the mechanisms of collision and aggregation of particles.

1.2 Objective

The main objective of this project is to analyze the flow dynamics of two particles traveling within a cylindrical tube at low Reynolds number. A systematic procedure is proposed. There are several crucial parameters to describe the hydrodynamic behaviors due to various geometries; they are the drag forces, torques and velocities of particles including both translational and rotational velocities. The previous approaches are still not adequate to solve the general motion of two particles within the tube with arbitrary velocities. Therefore, the current work aims to construct a new mathematical procedure which can solve the flow field analytically. We can then extend the two-particle approach to multiple particles problem by extending the boundary conditions based on the method of reflections. Constructing such models would contribute to the understanding of the particle interactions. Such mechanism can be utilized to predict particle aggregation and collision.

1.3 Scope

The scope of this work consists of the following parts:

a) To construct a mathematical procedure capable of solving the flow field of two particles traveling in an infinite tube at low Reynolds number.

b) To determine the effect of geometries on the hydrodynamic force and torque acting on the particles at low Reynolds number within the tube.

c) To calculate of translational and rotational velocities of particles.

d) To determine the characteristic distance of particle interactions with various flow conditions before the particle-particle interaction can be neglected.

Chapter 2

Literature Review

The motion of particles and liquid droplets translating in a viscous fluid is one of the most classical problems, which can be traced back to Stokes's investigation of a rigid particle in an unbounded fluid. Slow viscous flow involving micrometer-sized objects exhibits unique physics particular performances which are quite different from large scales. Since such typical scales supply a high surface to volume ratio, unusual transfer phenomena appear. As the dimensions contract, the surface forces with the first power or the second power of the typical scale length will be more significant than the body forces with the third power.

2.1 Slow viscous flow of a single particle

2.1.1 Slow viscous flow of a single particle in an unbounded fluid

It is known that the flow behavior of a sphere at low Reynolds number is a typical model of heat and mass transfer applications such as filtration and sedimentation. One of the most comprehensive researches on the creeping motion of a sphere was reported by Brenner [6, 7]. He found that the hydrodynamic resistance of a particle translating in an unbound fluid can be represented as a symmetric tensor based on the external geometry of the particle. Meanwhile, the result was similar for rotational velocity except that the rotational tensor was a function of the position vector. Furthermore, Brenner

formulated the scheme of the hydrodynamic force and torque acting on a particle in a shear flow [26]. The tensor between the hydrodynamic resistances and the properties of the fluid were presented. Without loss in generality, the tensor was a function of the geometry of the particle. Meanwhile, he also made the extension of this problem which the flow field was an arbitrary Stokes flow [27].

In oceans and lakes which can be treated as unbounded fluid, the density varies due to the temperature or salinity. This ubiquitous phenomenon is known as stratified fluid. The presence of stratification significantly influences the motion of particles in the flow. On account of this widespread problem, the effect of stratification has received attention. The investigation of a spherical particle settling in a stratified fluid at low Reynolds number combining the experimental and numerical simulation data was presented [28]. The result showed the first experimental evidence of stratification enhancing drag force which depended on the viscous Richardson number in a stratified fluid at low Reynolds number. Ardekani & Stocker focused on the fundamental solutions of slow viscous flow in a stratified fluid known as ‘‘Stratlets’’ [29]. As compared with the Stokes flow in homogeneous fluid, the analysis presented the fundamental length scale of the flow in a stratified fluid. This approach utilized the Fourier transform to derive the solution which was computed numerically through the Fast Fourier Transform. The structure of the stratification was one such factor that influence on the flow field of small organisms by generating toroidal eddies.

The material of the particle can be different according to the scope of application. In a low Reynolds number environment, the flow through porous particles occurs commonly such as lubrication and oil recovery. Therefore, understanding the mechanism of porous particles in a viscous flow can contribute to improve the efficiency of mass transfer. Prakash & Sekhar reported the hydrodynamics of the porous sphere in an unsteady stokes flow. The unsteady Stokes equation was applied for the exterior region of the porous sphere [30]. The drag force and torque can be acquired with Faxén's law. At the same time, Brinkman equation was used to calculate the flow field of the interior area which is an extension of Stokes equation. They showed the inverse relation of the drag force and Darcy number in the uniform flow and the positive relation of the interface velocity and Darcy number with different frequency of the oscillation of the unsteady Stokes flow. The creeping motion of a porous cylindrical shell was also studied [31]. The mathematical treatment adopted the stream functions by means of the cell method technique based on different conditions. Saad investigated the same problem with the effect of stress jump condition and compared the result with the previous work [32]. The properties of the material and boundary condition can effect on the flow field significantly.

2.1.2 Slow viscous flow of a single particle close to plane surfaces

In general, slow viscous flow of particles involves the presence of boundaries. Unlike the creeping motion in an unbounded fluid, the additional boundary can

result in hydrodynamic effect on the flow field. Boundary effect on the viscous flow contains various cases. When a spherical particle translated towards to a steady plane, the resistance was larger than it in an unbounded viscous fluid or close to a free surface [33]. Goldman, Cox and Brenner analyzed the translation and rotation of a sphere parallel to a plane surface [34]. They succeeded in solving this motion with small gap between the sphere and the plane. Further improvement was also reported. Based on the bipolar coordinate system, an analytical solution was obtained for the motion of a sphere towards to a plane in a simple viscous shear flow [35]. This solution can be adopted for a wide range of the ratio of the particle radius and distance of the center to the wall. Dagan, Pfeffer and Weinbaum showed the theoretical result of the general creeping motion of a sphere close to a finite plain surface [36]. The physical model was axisymmetric and mathematical procedure was based on the stream function and cylindrical harmonics. The drag force of various background flows acting on the sphere was presented.

In a later treatment, the exact solution of the flow field in a viscous fluid resulting from a steady particle in touch with a fixed plane wall was derived [37]. The surrounding fluid was supposed to be a simple uniform shear flow. Goren calculated the normal force acting on a sphere in contact with a steady wall in axisymmetric stagnation flow and plain stagnation flow [38].

For the presence of two plane walls, the analytical investigation based on the method of reflections was given [39]. There are varieties of numerical techniques which are suitable to Stokes flow. Ganatos, Weinbaum and Preffer

showed the solution of the perpendicular and parallel motion of a sphere between two plane walls [40, 41]. They provided an analytical procedure according to the stream function. Dvinsky & Popel presented a general numerical procedure for the two dimensional Stokes flow of a cylinder between two planar walls [42, 43]. The background flow can be quiescent fluid, Poiseuille and Couette flow. The motion of a particle translating and rotating between two parallel wall surfaces was investigated with a new boundary-integral algorithm. The mathematic model had a wide range of particles and depths of channels [44, 45]. For the spherical particle which is of slip surface, Chang & Keh showed the semianalytical study of the hydrodynamic mechanism of a fluid sphere and a particle with an arbitrary viscosity property, translating through another immiscible fluid perpendicular to two parallel surface walls at a random position at low Reynolds number [46].

2.1.3 Slow viscous flow of a single particle in an axisymmetric container

The most common boundary-value problem encountered in slow viscous flow is that of a sphere moving in an axisymmetric container. This kind of motion is a crucial phenomenon in nature and industrial process such as filtration and suspension in microfluidic systems.

The problem of viscous fluid through a cylindrical tube involving particles is of interest in matter of various cases, such as fluidization and translating beds of solids. A rational beginning towards illustration of the mechanism of these

applications was undertaken by considering a single sphere translating along the axis within a cylindrical duct at low Reynolds number [20, 21]. The spherical particle was set up in an arbitrary position moving with a constant velocity along the axis of the cylinder. The crucial parameters of this problem were the ratio of spherical particle to cylindrical tube radius and the relative distance of the sphere from the axis of the cylinder. The general solution directed by Lamb was used for the spherical coordinate and cylindrical harmonics for the tube. The method of reflections was applied for constructing the entire procedure. The final results of the drag force and torque were obtained. However, this solution was limited to the case that the ratio of the sphere to cylinder radius was small. For the dramatical interactions between the particle and wall, a new mathematical procedure should be derived.

Keh and Chang studied this motion with slip boundary condition of the sphere [22]. The drag force acting on the surface of the particle was presented. Based on the Dirichlet boundary condition, a semi-analytical approach can be adopted to solve the general motion of particle within cylinder at low Reynolds number [17].

2.1.4 Slow viscous flow of a single particle close to a free surface

In relation to the filtration and separation processes, the flow field of viscous fluid resulting from a particle or droplet can be significantly affected by the disturbance of the interface between immiscible fluids. The presence of the interfaces would have an effect on the drag force.

Lee, Chadwick and Leal investigated the motion of a sphere close to planar interface [47]. They derived the point force in the presence of the free surface and made an extension to define the flow field around the sphere. The general solution of creeping flow in bipolar-coordinates was subsequently concluded by Lee and Leal [48]. They calculated the drag force and torque of the sphere translating and rotating near the free surface and compared the numerical exact solution with the previous one. Much later, Berdan and Leal studied the motion of a sphere close to a free surface with small deformation theoretically [49]. Lee and Leal presented the numerical result of a sphere translating normal to the interface [50]. Yang and Leal used general solution for singularities to investigate the flow field of a slender close to a plain free surface [51]. The fluid was assumed to be steady at infinity and the particle was of arbitrary position relative to the surface. They also extended the theoretical work which the background flow was adopted to be linear undisturbed flow [52]. For a droplet near to a deformable surface, Yang and Leal derived the analytical solution based on the fundamental singularity solutions [53]. Their approximate drag force results were in agreement with the exact solution in some particular situations. Chi and Leal presented a theoretical study of a droplet towards a fluid interface by means of the boundary integral method [54]. Their solution contained large deformations of the droplet and interface with different capillary numbers and viscosity ratios. Danov, Gurkov, Raszillier and Durst presented the relationships of the intrinsic properties of the fluid and the drag force of the droplet. At small distances between the sphere and the viscous

interface, a crucial effect based on the surface viscosity gave rise to the augments of drag force and torque [55].

Owing to the retardation of the interface, the velocity field of translation is more sensitive to the distance than the rotation. In a simple shear flow parallel to a viscous interface, the translational and rotational velocities of a spherical particle were functions of particle distance from the interface and the viscosity ratio [56]. Furthermore, in some special situations, the sphere could move across the surface into the other fluid. Referring to such cases, before the particle can pass through the interface, the thin film of liquid occupying the region between them must be compressed out. This model is the film drainage problem including substantial parameters such as viscosity ration, density difference, surface tension and relative position of the particle and interface [57].

2.2 Slow viscous flow of two or more spheres

2.2.1 Slow viscous flow of two or more spheres in an unbounded fluid

The inter-particle interactions need to be involved in actual particles or droplets motions which are so frequently encountered in mass transfer and fabrication processes.

A large body of literature has considered the motion of particles traveling in an unbounded fluid at low Reynolds number. Due to the complexity of particle

motion, a logic start to illustrate the hydrodynamic mechanism is to analyze the motion of two particles in an unbounded fluid. Stimson and Jeffery derived the exact solution of two particle traveling with identical velocities parallel to the line of centers [8]. The stream function was adopted to study the flow field. Later, Goldman et al calculated the exact numerical values for the velocities of two identical particles setting in an unbounded fluid by employing the Bipolar coordinates [9]. Oneill and Majumdar extended previous work and investigated the asymmetrical creeping flow caused by the movements of two particles [58, 59]. They presented a comprehensive study of the dimensionless force coefficients with various geometries and investigated the hydrodynamic behaviors when the two particles were very close. In another direction, slow viscous flow of particles with slip boundary condition has also been considered by Keh & Chen [60] and Saad [61].

In a low Reynolds number world, the inertia effect can be neglected requiring the mobility functions can be derived from the resistance functions. Jeffrey and Onishi showed the calculation of the drag force and mobility functions of two sphere at low Reynolds number [10]. They described the hydrodynamic interactions between spheres as a series by means of the linearity of the governing equation. Kim and Mifflin calculated the resistance and mobility function [11] using a boundary collocation technique. These functions can characterize the relationship between the movement and force coefficients of particles. Furthermore, Yoon and Kim showed a simple and direct method to calculate the mobility functions for the velocities and stresslets of two identical

particles [62]. Their results are also applicable for touching particles. Later, these functions have also been investigated by Ying & Peters with singular perturbation scheme [63] and summarized by Jeffrey [64].

When the two particles contact with each other, the standard theory for the particle motion needs to be modified due to the specific surface shape. Cooley and Oneill provided the exact solution of two particles moving with identical velocity along their line of centers uniformly using stream function [65]. Meanwhile, Oneill presented an asymptotic theory for studying the motion of two particles almost in contact rotating with identical and opposite velocities [66]. Later, more accurate theoretical solutions have been given by Nir & Acrivos using tangent-sphere coordinates [67] and Sun & Chwang using an extended successive reflection method [68]. Their investigation validated two dynamic states in contact: pure rolling and rolling with slip. These phenomena have also been confirmed experimentally by Ekiel-Jezewska et al. [69, 70] and Zhao & Davis [71].

In order to investigate the unsteady motion of two solid spherical particles in an unbounded fluid, Ardekani and Rangel introduced two approaches combining with the method of reflections to calculate the force acting on the surface of the particles [12]. The result of these two cases showed that the Basset force according with the motion of the particles was larger than the force for an individual sphere.

For more particles cases, Brenner and Oneill presented a general theory to analyze resistance of an aggregate of particles of arbitrary shape traveling in a

linear shear flow [72]. They found that the hydrodynamic force of particles can be expressed by two intrinsic matrixes. Kim derived the analytical solution for Stokes flow past three particles based on the Legendre expansion [13]. Later, Clercx and Schram developed a method to construct the mobility function of three hydrodynamically interacting spheres with arbitrary positions [73]. Cichocki et al. numerically investigated the resistance and mobility function of many particles which can be extended for practical calculation [74]. Furthermore, Haber and Brenner studied the hydrodynamic drag force and torque acted on non-identical spheres in a quadratic flow at infinity. Explicit function has been expressed for the case of two particles [75]. Filippov proposed a scheme to calculate the drag force and torque acting on clusters of arbitrary spherical particles with slip boundary condition [76]. Ekiel-Jezewska and Wajnryb analyzed the dynamics of three identical particles falling due to gravity. The stability of different configurations and phase portraits for two symmetrical motions have been discussed [77]. Wilson presented a numerical method to track the mechanism of three spheres at low Reynolds number which is based on the Lamb's general solution and the method of reflections [14]. The data gave an existence that the largest error appeared at a distance between particles around 0.1 radius. Recently, Ekiel-Jezewska and Felderhof derived the exact solutions for the two and three spheres hydrodynamic interactions [78]. The expressions are a combination of a solution for particle with no-slip and Green tensor.

The hydrodynamic interactions which depend on the spatial distance between droplets were experimentally and theoretically reported. The agreement of experimental data with droplet motion containing the drag correction in chain was testified [79]. Faltas, Sherief and Ashmawy studied the hydrodynamic interactions of two unequal spherical particles with different rotational movement along the same direction connecting their geometry center in the micro polar fluid [80]. Fuentes, Kim and Jeffrey gave the investigation of two unequal droplets at low Reynolds number which provided a closed analytical expression for the interactions [81, 82]. The surface tension was assumed to be high enough which made the droplets keep spherical shape. Exact solutions of the velocity field for Stokeslets and singularities close to a viscous droplet were obtained. Stoos, Yang and Leal analyzed the interactions between a small droplet and a much larger viscous droplet moving in a quiescent fluid [83]. The mathematical solution was a balanced expansion of the local boundary conditions and the disturbed flow. Keh and Tseng presented an analytical-numerical study for interactions of a group of droplets in a viscous fluid through the boundary collocation technique [84]. A general solution of the resistance and mobility function was given with a good agreement with previous work in some special cases. Baldessari and Leal solved the motion of two contacted spherical droplets in uniaxial background flow at low Reynolds number [85]. The stream function was employed for the axisymmetric creeping motion. Pozrikidis studied the motion of two spherical fluid droplets suspending in an unbounded fluid at low Reynolds number [86]. The

investigation of this problem would contribute to the understanding of the breakup and deformation of droplets and bubbles.

2.2.2 Slow viscous flow of two or more spheres in a cylindrical tube

Unlike in an unbounded fluid, the extra surface will make an inevitable influence on the flow behavior of particles. One typical example of a commonly used boundary is a cylindrical tube. As is well known, the flow field has a parabolic profile within the tube with maximum value at the center. Due to the interactions among the spheres and the cylindrical wall, the sphere can move towards or away from the other one. To better highlight the collision and aggregation of particles in the tube, it is necessary to analyze the hydrodynamic force coefficients and particle velocities.

Greenste and J. Happel presented numerical values of the force and torque of two particles within a cylindrical tube in a viscous fluid using the method of reflections [24]. However, the physical model is based on a specific configuration and boundary condition. The two particles were placed symmetrically about the axis of the cylinder traveling in a direction normal to the line connecting their centers with constant translational and rotational velocities. Sonshine and Brenner investigated the motion of two or more particles translating along the axis of an infinite cylindrical tube [23]. The spheres had the identical size and were equally settled. They calculated the drag force encountered by the sphere and found that the hydrodynamic interaction

caused by adjacent sphere could decrease the drag force. Wang and Skalak derived the general solution of the same physical model employing stream function [87]. They presented numerical results for the pressure difference and drag force for a range of configurations, together with stream lines and velocity profile. Later, Chen and Skalak extended previous mathematical model [88]. They analyzed the slow viscous flow of a line of spheroidal particles within a cylindrical tube and showed the drag force was primarily related to the spheroidal diameter perpendicular to the axis of the tube. Both prolate spheroids and oblate spheroids were also equally placed along the axis. Leichtberg, Pfeffer and Weinbaum investigated the Stokes flow past finite coaxial clusters of spheres equally spaced along the axis of a cylindrical tube using a Fourier transform of the general disturbance [89]. They presented the drag force solution and for a wide range of particle spacing and particle to cylinder radii ratios. Meanwhile, the velocities of each particle has been calculated which demonstrate the hydrodynamic interactions among particles. Recently, Navardi and Bhattacharya proposed a general methodology to calculate the hydrodynamic force of two particles traveling in a cylindrical tube [25]. The drag force and torque can be obtained due to specific motion with arbitrary radial positions. Nevertheless, the velocities including translation and rotation of the two particles have not been investigated.

2.3 Current study

The motion of small particles in a cylindrical tube can be found in many fields, ranging from the industrial and environmental applications such as fluidization and filtration, to biomedical applications such as drug delivery in blood vessels. When fluid passes particles, the flow field could make them collide or aggregate due to particle interactions. The characteristics of the flow field, such as drag force, will be more complex depending on the geometric configuration of the particles. The analytical solution of one single particle moving inside the cylindrical tube has been previously studied. Neither of the aforementioned investigation is, however, applicable to solve the general motion of two particles traveling within a cylindrical tube. This is why the previous theories are inadequate in analyzing various physically significant phenomena such as collision and aggregation of particles. Also, the existing theories were primarily concentrated on the motion of particles equally placed along the axis with identical size or only the hydrodynamic forces of two particles with arbitrary position. However, in the presence of general configuration, the particle can move perpendicular to the axis, together with rotation due to the hydrodynamic interaction between particles. To our knowledge, such systematic analysis on the flow behavior of the multi particles traveling in a cylindrical tube is still not available. Therefore, there is a compelling need for constructing a theoretical model to quantify particle interactions for the flow characteristics involving multiple particles. A logical beginning towards illustration of these behaviors can be addressed by considering the flow dynamics of two spherical particles

traveling within a cylindrical tube at low Reynolds number. This motivates us to analyze the mechanism of this case. The following chapters will propose a comprehensive procedure to solve the problem. We can then extend the two-particle approach to multiple particles problem by extending the boundary conditions based on the method of reflections. Such analysis can give us insights to understand the mechanisms of collision and aggregation of particles.

Chapter 3

Problem Formulation

The mathematical formulation is set up. Lamb's general solution is used to calculate the flow field around the particle in spherical coordinates. We extend the previous method presented by Brenner and Happel [20] and construct a general solution in cylindrical coordinates. The solutions adopted in different coordinate systems are combined with the method of reflections [90, 91].

3.1 Governing equations and Boundary conditions

In order to investigate the hydrodynamic interaction of particles in a low Reynolds number flow, we develop a mathematical model to analyze the flow dynamics of two particles moving in a cylindrical tube at low Reynolds number.

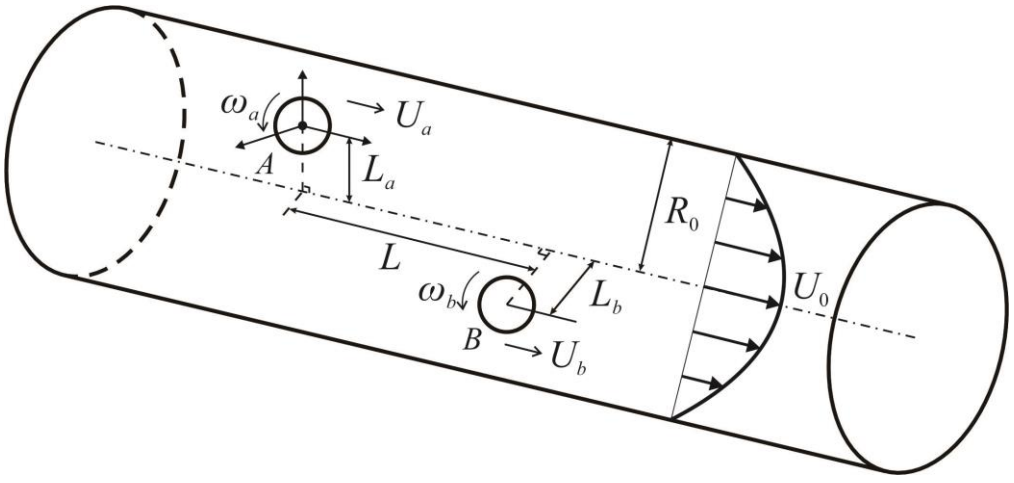

Figure 3.1: Sketch of two particles moving in a cylindrical tube

Two particles, named as particle *A* and particle *B* with radius *a* and *b* respectively, are placed in arbitrary positions in a tube radius R_0. The background flow field of the cylinder is of parabolic profile with the maximum value U_0 at the axis known as the Poiseuille Flow. Each particle has a translational velocity *U* and a rotational velocity ω with subscript *a* and *b* with respect to particle *A* and particle *B*. L_a represents the distance between the center of particle *A* and the axis of the tube, the same for L_b in relation to particle *B*. *L* is the particle spacing.

At low Reynolds number, the governing equation for the steady motion of Newtonian fluid are the Stokes equation:

$$\nabla^2 \vec{v} = \frac{1}{\mu} \nabla p \tag{3.1}$$

Together with the continuity equation

$$\nabla \cdot \vec{v} = 0 \tag{3.2}$$

Using a reference frame attached to the center of particle *A* (variable $\vec{Z}$ described the axial direction of the coordinates), the boundary conditions are:

$$\begin{cases} \vec{v} = \vec{\omega}_a \times \vec{r}_a & at \quad r_a = a \\ \vec{v} = \vec{Z}(U_b - U_a) + \vec{\omega}_b \times \vec{r}_b & at \quad r_b = b \\ \vec{v} = -U_a \vec{Z} & at \quad R = R_0 \end{cases} \tag{3.3}$$

With no slip, particle *A* only has a rotational velocity while particle *B* has the relative translational velocity and rotational velocity.

3.2 The Method of Reflections

As described earlier, there are three boundary conditions in the model and the governing equation cannot be solved directly. In this study, we conduct the calculations by utilizing the method of reflections due to the complex interactions among the particles and the cylindrical tube. This method can be adopted for multiple objects and is proposed by previous researchers [90, 91]. By using the method of reflections, the velocity and pressure fields can be expressed as an infinite series since the governing equations and boundary conditions are linear.

$$\vec{v} = \vec{v}_c^{(0)} + \vec{v}_a^{(1)} + \vec{v}_b^{(2)} + \vec{v}_c^{(3)} + \vec{v}_a^{(4)} + \vec{v}_b^{(5)} + \cdots \tag{3.4}$$

$$p = p_c^{(0)} + p_a^{(1)} + p_b^{(2)} + p_c^{(3)} + p_a^{(4)} + p_b^{(5)} + \cdots \tag{3.5}$$

where the superscript *i* refers to the *i*th reflection and subscript (*a*, *b*, *c*) refers to the boundary conditions satisfied for particle *A*, particle *B* and cylinder, respectively. The whole flow field is the summation of the series and the added term in the calculation can be considered as a modification of the previous result (summation of previous terms). Each term of *v* and *p*, separately satisfy Eq (3.1) (3.2) and the boundary condition resulting from previous term. For example, if the subscript of the last term is *b*, the summation of the terms will satisfy the boundary condition of particle *B*. Therefore, the following relations can be derived.

We start the calculation with the initial flow field $\vec{v}_c^{(0)}$ corresponds to the pressure-driven parabolic flow in a cylinder:

$$\vec{v}_c^{(0)} = \vec{Z}\left[U_0(1-R^2/R_0^2)\right] - \vec{U}_a \tag{3.6}$$

Then we add a reflection due to the presence of particle *A*. The subsequent reflection $\vec{v}_a^{(1)}$ can be obtained from the boundary condition of particle *A*. The entire flow field, which is the summation of the first two terms, satisfies the boundary condition of particle *A*:

$$\vec{v}_c^{(0)} + \vec{v}_a^{(1)} = \vec{\omega}_a \times \vec{r}_a \quad at \quad r_a = a \tag{3.7}$$

This makes:

$$\vec{v}_a^{(1)} = \begin{cases} -\vec{v}_c^{(0)} + \vec{\omega}_a \times \vec{r}_a & at \quad r_a = a \\ 0 & at \quad z = \pm\infty \end{cases} \tag{3.8}$$

Similarly, the next reflection due to particle *B*, the added term need to make the summation satisfy the boundary condition of particle *B*.

$$\vec{v}_c^{(0)} + \vec{v}_a^{(1)} + \vec{v}_b^{(2)} = \vec{Z}(U_b - U_a) + \vec{\omega}_b \times \vec{r} \quad at \quad r_b = b \tag{3.9}$$

So we have:

$$\vec{v}_b^{(2)} = \begin{cases} -\vec{v}_a^{(1)} - \vec{v}_c^{(0)} + \vec{Z}(U_b - U_a) + \vec{\omega}_b \times \vec{r}_b & at \quad r_b = b \\ 0 & at \quad z = \pm\infty \end{cases} \tag{3.10}$$

In order to make the result closer to the exact flow field, more terms should be added by repeating the process. Therefore, the following reflection ($\vec{v}_c^{(3)}$) is conducted based on the boundary condition of the tube. The summation is required to satisfy the boundary condition:

$$\vec{v}_c^{(0)} + \vec{v}_a^{(1)} + \vec{v}_b^{(2)} + \vec{v}_c^{(3)} = -U_a\vec{Z} \qquad at \quad R = R_0 \tag{3.11}$$

This makes:

$$\vec{v}_c^{(3)} = \begin{cases} -\vec{v}_a^{(1)} - \vec{v}_b^{(2)} & at \quad R = R_0 \\ 0 & at \quad z = \pm\infty \end{cases} \tag{3.12}$$

Then the following reflections ($\vec{v}_a^{(4)}$ and $\vec{v}_b^{(5)}$) can be calculated by satisfying the boundary condition of particle *A* and *B*, respectively .The procedure continues repetitively by adding more terms and as the number of terms goes to infinity, the solution will be closer to the exact flow field.

Based on this relationship and the method of reflections, the process of the generation of the total velocity fields can be summarized in a flow chart (Figure 3.2).

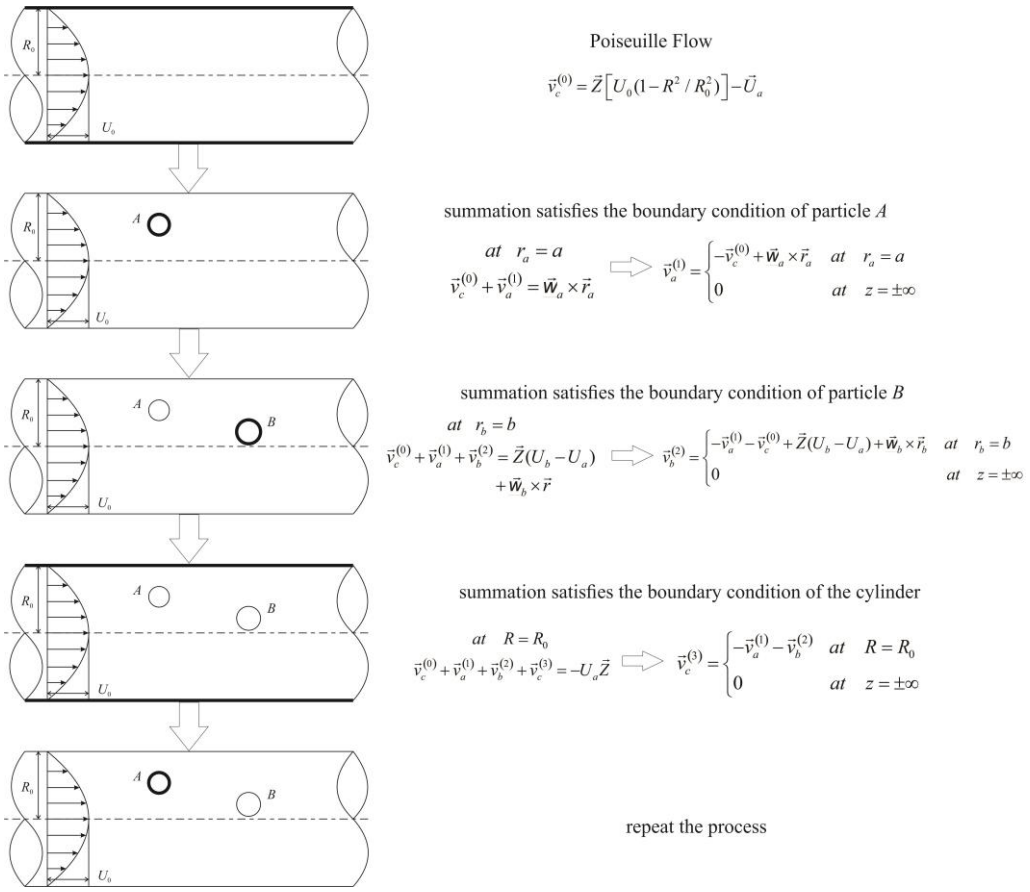

Figure 3.2: The method of reflections procedure

The pressure can then be acquired from the governing equations related to velocity.

Note that the sequential steps are similar to the perturbation method. Thus, it is necessary to consider the convergence of the method of reflections.

In general, the first reflection $v_a^{(1)}$ arising from $v_c^{(0)}$ brings in the representative geometry dimension a (the radius of particle A) in the form a/r with positive power, where r is the radial variable of the spherical coordinate with reference to particle A. The next reflection $v_b^{(2)}$ (only consider particle A and B, the principle is similar for wall of the cylinder) introduces the term a/L. L is the characteristic dimension between the two particles. Further improvement which is the term $v_a^{(4)}$ will possess a magnitude in the order of $O(a^2/L^2)$. Therefore, the subsequent reflection can correct the error of the flow field to higher order, depending on the number of terms.

Once the flow field is acquired to a desired accuracy, the drag force $\vec{F}$, which is operated on the surface of the particle by the surrounding fluid, is a summation of the contributions resulting from each reflected velocity.

$$\vec{F} = \vec{F}^{(1)} + \vec{F}^{(2)} + \vec{F}^{(3)} + \vec{F}^{(4)} + \cdots \tag{3.13}$$

Similarly, the torque is:

$$\vec{T} = \vec{T}^{(1)} + \vec{T}^{(2)} + \vec{T}^{(3)} + \vec{T}^{(4)} + \cdots \tag{3.14}$$

Since the method of reflections can treat the boundary conditions individually, it is necessary to obtain the general solution for the flow field around the

particle and within the cylindrical tube and the detailed calculation procedure is shown in section 3.6.

3.3 Spherical harmonics for the flow around the particle

Lamb provided a general solution for the flow field outside the particle at low Reynolds number in spherical coordinate system [92]. After taking the divergence of the Stokes equation (Eq.(3.1)), it is straightforward that the pressure satisfies the Laplace equation.

$$\nabla^2 p = 0 \tag{3.15}$$

So the pressure field can be expanded with the solid spherical harmonics [90]:

$$p = \sum_{n=-\infty}^{\infty} \gamma_n \tag{3.16}$$

Upon adopting the homogeneous and special solutions of the equations, the expansion constructs the general solution [90]:

$$\vec{v} = \sum_{n=-\infty}^{\infty} \left[\nabla \times (\vec{r}\chi_n) + \nabla \Phi_n + \frac{(n+3)}{2\mu(n+1)(2n+3)} r^2 \nabla \gamma_n - \frac{n}{\mu(n+1)(2n+3)} \vec{r}\gamma_n \right] \tag{3.17}$$

where γ_n, Φ_n and χ_n are solid spherical harmonics which are of the normal form [91]:

$$\gamma_n = r^n \sum_{m=0}^{n} P_n^m (\cos\theta)\left(a_{mn} \cos m\varphi + \tilde{a}_{mn} \sin m\varphi\right) \tag{3.18}$$

$$\Phi_n = r^n \sum_{m=0}^{n} P_n^m (\cos\theta)\left(b_{mn} \cos m\varphi + \tilde{b}_{mn} \sin m\varphi\right) \tag{3.19}$$

$$\chi_n = r^n \sum_{m=0}^{n} P_n^m(\cos\theta)\left(c_{mn}\cos m\varphi + \tilde{c}_{mn}\sin m\varphi\right) \tag{3.20}$$

P_n^m is the Associated Legendre Polynomial. Due to the properties of the Legendre Polynomial, the connections of the boundary condition and the solid spherical harmonics are as follows [90]:

$$\sum_{n=-\infty}^{\infty}\left[\frac{na}{2\mu(2n+3)}\left(\frac{a}{r}\right)^n \gamma_n + \frac{n}{a}\left(\frac{a}{r}\right)^n \Phi_n\right] = \frac{\vec{r}}{r}\cdot\vec{V} \tag{3.21}$$

$$\sum_{n=-\infty}^{\infty}\left[\frac{n(n+1)a}{2\mu(2n+3)}\left(\frac{a}{r}\right)^n \gamma_n + \frac{n(n-1)}{a}\left(\frac{a}{r}\right)^n \Phi_n\right] = -r\nabla\cdot\vec{V} \tag{3.22}$$

$$\sum_{n=-\infty}^{\infty}\left[n(n+1)\left(\frac{a}{r}\right)^n \chi_n\right] = \vec{r}\cdot\nabla\times\vec{V} \tag{3.23}$$

$\vec{V}$ represents the boundary condition which is the velocity on the sphere surface. These relationships cover both the regions inside and outside the sphere.

In order to eliminate the summation and solve the solid spherical harmonics, the right hand side of these equations must be transformed into similar form. It is concluded that a function $f(\theta, \varphi)$ can be expanded in a series of surface spherical harmonics [93, 94].

$$f(\theta,\varphi) = \sum_{n=0}^{\infty}\left\{A_n P_n(\mu) + \sum_{m=1}^{n}\left(A_n^m \cos m\varphi + B_n^m \sin m\varphi\right)T_n^m(\mu)\right\} \tag{3.24}$$
$$\left(\text{for } 0 \le \theta \le \pi, 0 \le \varphi \le 2\pi\right)$$

where P_n and T_n^m are Legendre polynomials and associated Legendre polynomials, respectively. A_n, A_n^m and B_n^m are coefficients of transformation with following formulas [94]:

$$A_n = \frac{2n+1}{4\pi}\int_0^{2\pi}\int_{-1}^{1} f\left(\theta',\varphi'\right)P_n\left(\mu'\right)d\mu' d\varphi' \tag{3.25}$$

$$A_n^m = \frac{2n+1}{2\pi}\frac{(n-m)!}{(n+m)!}\int_0^{2\pi}\int_{-1}^{1} f\left(\theta',\varphi'\right)T_n^m\left(\mu'\right)\cos m\varphi' d\mu' d\varphi' \tag{3.26}$$

$$B_n^m = \frac{2n+1}{2\pi}\frac{(n-m)!}{(n+m)!}\int_0^{2\pi}\int_{-1}^{1} f\left(\theta',\varphi'\right)T_n^m\left(\mu'\right)\sin m\varphi' d\mu' d\varphi' \tag{3.27}$$

Thus, based on the transformation of surface spherical harmonics, a set of algebra equations can be generated. Since the general solution is applicable for the flow inside and outside the sphere, it is necessary to consider them separately.

Region inside the sphere

According to the flow field occupies the region inside the sphere, with the face that the velocity should be finite, it provides the simplification to positive spherical harmonics:

$$\gamma_n = \Phi_n = \chi_n = 0, \quad n \le 0 \tag{3.28}$$

This makes the general solution [90]:

$$\vec{v} = \sum_{n=1}^{\infty}\left[\nabla\times(\vec{r}\chi_n) + \nabla\Phi_n + \frac{(n+3)}{2\mu(n+1)(2n+3)}r^2\nabla\gamma_n - \frac{n}{\mu(n+1)(2n+3)}\vec{r}\gamma_n\right] \tag{3.29}$$

According to the transformation (Eq(3.24)), the right hand side of Eq(3.21) (3.22)(3.23) can be expanded as [90]:

$$\frac{\vec{r}}{r}\cdot\vec{V} = \sum_{n=1}^{\infty} X_n \tag{3.30}$$

$$-r\nabla\cdot\vec{V}=\sum_{n=1}^{\infty}Y_n \tag{3.31}$$

$$\vec{r}\cdot\nabla\times\vec{V}=\sum_{n=1}^{\infty}Z_n \tag{3.32}$$

So the fundamental relations for the region interior to a sphere are [90]:

$$\sum_{n=1}^{\infty}\left[\frac{na}{2\mu(2n+3)}\left(\frac{a}{r}\right)^n p_n+\frac{n}{a}\left(\frac{a}{r}\right)^n\Phi_n\right]=\sum_{n=1}^{\infty}X_n \tag{3.33}$$

$$\sum_{n=1}^{\infty}\left[\frac{n(n+1)a}{2\mu(2n+3)}\left(\frac{a}{r}\right)^n p_n+\frac{n(n-1)}{a}\left(\frac{a}{r}\right)^n\Phi_n\right]=\sum_{n=1}^{\infty}Y_n \tag{3.34}$$

$$\sum_{n=1}^{\infty}\left[n(n+1)\left(\frac{a}{r}\right)^n\chi_n\right]=\sum_{n=1}^{\infty}Z_n \tag{3.35}$$

Rearranging, we can obtain:

$$p_n=\frac{\mu(2n+3)}{n}\frac{1}{a}(\frac{r}{a})^n[Y_n-(n-1)X_n] \tag{3.36}$$

$$\Phi_n=\frac{1}{2n}a(\frac{r}{a})^n[(n+1)X_n-Y_n] \tag{3.37}$$

$$\chi_n=\frac{1}{n(n+1)}(\frac{r}{a})^n Z_n \tag{3.38}$$

Based on the velocity on the surface of the sphere, the flow field arising from the effect of the boundary conditions can be solved.

Region outside the sphere

Similarly with the previous analysis, since the velocity has to disappear at infinity, the harmonics functions should be restricted with negative order. The general solution outside the sphere is [90]:

$$\vec{v}-\vec{v}_{\infty}=\sum_{n=1}^{\infty}\left[\begin{array}{l}\nabla\times(\vec{r}\,\chi_{-(n+1)})+\nabla\Phi_{-(n+1)}\\ -\dfrac{(n-2)}{\mu 2n(2n-1)}r^{2}\nabla p_{-(n+1)}+\dfrac{(n+1)}{\mu n(2n-1)}\vec{r}p_{-(n+1)}\end{array}\right] \tag{3.39}$$

where $\vec{v}_{\infty}$ is the background flow.

By employing the boundary conditions and surface spherical harmonics, the solution is [90]

$$p_{-(n+1)}=\frac{\mu(2n-1)}{n+1}\frac{1}{a}(\frac{a}{r})^{n+1}[(n+2)X_n+Y_n] \tag{3.40}$$

$$\Phi_{-(n+1)}=\frac{1}{2(n+1)}a(\frac{a}{r})^{n+1}(nX_n+Y_n) \tag{3.41}$$

$$\chi_{-(n+1)}=\frac{1}{n(n+1)}(\frac{a}{r})^{n+1}Z_n \tag{3.42}$$

In this study, the two particles are solid spheres. So we only focus the flow field around the two particles without the region inside. In our study, we find that the first five terms of the spherical harmonics are enough to get the accurate solution. By including the five terms, the solution can satisfy the boundary condition with the difference less than 0.1%.

3.4 Cylindrical harmonics for the flow field of cylinder

In cylindrical coordinates, the velocity components are shown by (R, Φ, Z). The general solution is given by Happel & Brenner [90]:

$$\vec{v}=\sum_{k=-\infty}^{\infty}\left[\nabla\times(\vec{i}_Z\Omega_k)+\nabla\Psi_k+R\frac{\partial}{\partial R}\nabla\Pi_k+\vec{i}_Z\frac{\partial\Pi_k}{\partial Z}\right] \tag{3.43}$$

$$p = -2\mu \sum_{k=-\infty}^{\infty} \frac{\partial^2 \Pi_k}{\partial Z^2} \tag{3.44}$$

where Ω_k, Ψ_k and Π_k are cylindrical harmonics functions. We assume the standard forms:

$$\Pi_k = \frac{1}{\pi}\begin{pmatrix} \cos k\Phi \int_0^\infty \frac{1}{\lambda}\pi_{ak}(\lambda) I_k(\lambda R)\sin \lambda Z d\lambda \\ +\sin k\Phi \int_0^\infty \frac{1}{\lambda}\pi_{bk}(\lambda) I_k(\lambda R)\sin \lambda Z d\lambda \\ +\cos k\Phi \int_0^\infty \frac{1}{\lambda}\pi_{ck}(\lambda) I_k(\lambda R)\cos \lambda Z d\lambda \\ +\sin k\Phi \int_0^\infty \frac{1}{\lambda}\pi_{dk}(\lambda) I_k(\lambda R)\cos \lambda Z d\lambda \end{pmatrix} \tag{3.45}$$

$$\Psi_k = \frac{1}{\pi}\begin{pmatrix} \cos k\Phi \int_0^\infty \frac{1}{\lambda}\psi_{ak}(\lambda) I_k(\lambda R)\sin \lambda Z d\lambda \\ +\sin k\Phi \int_0^\infty \frac{1}{\lambda}\psi_{bk}(\lambda) I_k(\lambda R)\sin \lambda Z d\lambda \\ +\cos k\Phi \int_0^\infty \frac{1}{\lambda}\psi_{ck}(\lambda) I_k(\lambda R)\cos \lambda Z d\lambda \\ +\sin k\Phi \int_0^\infty \frac{1}{\lambda}\psi_{dk}(\lambda) I_k(\lambda R)\cos \lambda Z d\lambda \end{pmatrix} \tag{3.46}$$

$$\Omega_k = \frac{1}{\pi}\begin{pmatrix} \cos k\Phi \int_0^\infty \frac{1}{\lambda}\omega_{ak}(\lambda) I_k(\lambda R)\sin \lambda Z d\lambda \\ +\sin k\Phi \int_0^\infty \frac{1}{\lambda}\omega_{bk}(\lambda) I_k(\lambda R)\sin \lambda Z d\lambda \\ +\cos k\Phi \int_0^\infty \frac{1}{\lambda}\omega_{ck}(\lambda) I_k(\lambda R)\cos \lambda Z d\lambda \\ +\sin k\Phi \int_0^\infty \frac{1}{\lambda}\omega_{dk}(\lambda) I_k(\lambda R)\cos \lambda Z d\lambda \end{pmatrix} \tag{3.47}$$

π_{ik}, ψ_{ik} and ω_{ik}, where $i = a, b, c, d$ are unknown functions of λ with respect to Π_k, Ψ_k and Ω_k. So the velocity components can be described as:

$$\vec{v}=\sum_{k=-\infty}^{\infty}\left[\begin{array}{c}\left(\frac{1}{R}\frac{\partial\Omega_k}{\partial\Phi}+\frac{\partial\Psi_k}{\partial R}+R\frac{\partial^2\Pi_k}{\partial R^2}\right)\vec{i}_R\\+\left(\frac{1}{R}\frac{\partial\Psi_k}{\partial\Phi}-\frac{\partial\Omega_k}{\partial R}+\frac{\partial^2\Pi_k}{\partial R\partial\Phi}-\frac{1}{R}\frac{\partial\Pi_k}{\partial\Phi}\right)\vec{i}_\Phi\\+\left(\frac{\partial\Psi_k}{\partial Z}+R\frac{\partial^2\Pi_k}{\partial R\partial Z}+\frac{\partial\Pi_k}{\partial Z}\right)\vec{i}_Z\end{array}\right] \tag{3.48}$$

In order to construct a relationship between the cylindrical harmonic functions and boundary conditions, we assume the boundary conditions at the wall of tube (R=R_0) has the following form:

$$B\left(R_0,\Phi,Z\right)=B_R\vec{i}_R+B_\Phi\vec{i}_\Phi+B_Z\vec{i}_Z \tag{3.49}$$

So we have:

$$B_R=\sum_{k=-\infty}^{\infty}\left\{\begin{array}{l}\frac{\cos k\Phi}{\pi}\int_0^\infty\left[\begin{array}{r}\psi_{ck}(\lambda)I_k^{'}(\lambda R_0)+\omega_{dk}(\lambda)\frac{kI_k(\lambda R_0)}{\lambda R_0}\\+\pi_{ck}(\lambda)\lambda R_0 I_k^{''}(\lambda R_0)\end{array}\right]\cos\lambda Z d\lambda\\+\frac{\cos k\Phi}{\pi}\int_0^\infty\left[\begin{array}{r}\psi_{ak}(\lambda)I_k^{'}(\lambda R_0)+\omega_{bk}(\lambda)\frac{kI_k(\lambda R_0)}{\lambda R_0}\\+\pi_{ak}(\lambda)\lambda R_0 I_k^{''}(\lambda R_0)\end{array}\right]\sin\lambda Z d\lambda\\+\frac{\sin k\Phi}{\pi}\int_0^\infty\left[\begin{array}{r}\psi_{dk}(\lambda)I_k^{'}(\lambda R_0)-\omega_{ck}(\lambda)\frac{kI_k(\lambda R_0)}{\lambda R_0}\\+\pi_{dk}(\lambda)\lambda R_0 I_k^{''}(\lambda R_0)\end{array}\right]\cos\lambda Z d\lambda\\+\frac{\sin k\Phi}{\pi}\int_0^\infty\left[\begin{array}{r}\psi_{bk}(\lambda)I_k^{'}(\lambda R_0)-\omega_{ak}(\lambda)\frac{kI_k(\lambda R_0)}{\lambda R_0}\\+\pi_{bk}(\lambda)\lambda R_0 I_k^{''}(\lambda R_0)\end{array}\right]\sin\lambda Z d\lambda\end{array}\right\} \tag{3.50}$$

$$B_{\Phi}=\sum_{k=-\infty}^{\infty}\left\{\begin{array}{l}\dfrac{\cos k\Phi}{\pi}\displaystyle\int_0^{\infty}\left[\begin{array}{l}\pi_{dk}(\lambda)kI_k^{'}(\lambda R_0)-\pi_{dk}(\lambda)\dfrac{kI_k(\lambda R_0)}{\lambda R_0}\\ -\omega_{ck}(\lambda)I_k^{'}(\lambda R_0)+\psi_{dk}(\lambda)\dfrac{kI_k(\lambda R_0)}{\lambda R_0}\end{array}\right]\cos\lambda Zd\lambda\\ +\dfrac{\cos k\Phi}{\pi}\displaystyle\int_0^{\infty}\left[\begin{array}{l}\pi_{bk}(\lambda)kI_k^{'}(\lambda R_0)-\pi_{bk}(\lambda)\dfrac{kI_k(\lambda R_0)}{\lambda R_0}\\ -\omega_{ak}(\lambda)I_k^{'}(\lambda R_0)+\psi_{bk}(\lambda)\dfrac{kI_k(\lambda R_0)}{\lambda R_0}\end{array}\right]\sin\lambda Zd\lambda\\ +\dfrac{\sin k\Phi}{\pi}\displaystyle\int_0^{\infty}\left[\begin{array}{l}\pi_{ck}(\lambda)kI_k^{'}(\lambda R_0)-\pi_{ck}(\lambda)\dfrac{kI_k(\lambda R_0)}{\lambda R_0}\\ -\omega_{dk}(\lambda)I_k^{'}(\lambda R_0)+\psi_{ck}(\lambda)\dfrac{kI_k(\lambda R_0)}{\lambda R_0}\end{array}\right]\cos\lambda Zd\lambda\\ +\dfrac{\sin k\Phi}{\pi}\displaystyle\int_0^{\infty}\left[\begin{array}{l}\pi_{ak}(\lambda)kI_k^{'}(\lambda R_0)-\pi_{ak}(\lambda)\dfrac{kI_k(\lambda R_0)}{\lambda R_0}\\ -\omega_{bk}(\lambda)I_k^{'}(\lambda R_0)+\psi_{ak}(\lambda)\dfrac{kI_k(\lambda R_0)}{\lambda R_0}\end{array}\right]\sin\lambda Zd\lambda\end{array}\right\} \tag{3.51}$$

$$B_Z=\sum_{k=-\infty}^{\infty}\left\{\begin{array}{l}\dfrac{\cos k\Phi}{\pi}\displaystyle\int_0^{\infty}\left[\begin{array}{r}\psi_{ak}(\lambda)I_k(\lambda R_0)+\pi_{ak}(\lambda)\lambda R_0I_k^{'}(\lambda R_0)\\ +\pi_{ak}(\lambda)I_k(\lambda R_0)\end{array}\right]\cos\lambda Zd\lambda\\ +\dfrac{\cos k\Phi}{\pi}\displaystyle\int_0^{\infty}\left[\begin{array}{r}-\psi_{ck}(\lambda)I_k(\lambda R_0)-\pi_{ck}(\lambda)\lambda R_0I_k^{'}(\lambda R_0)\\ -\pi_{ck}(\lambda)I_k(\lambda R_0)\end{array}\right]\sin\lambda Zd\lambda\\ +\dfrac{\sin k\Phi}{\pi}\displaystyle\int_0^{\infty}\left[\begin{array}{r}\psi_{bk}(\lambda)I_k(\lambda R_0)+\pi_{bk}(\lambda)\lambda R_0I_k^{'}(\lambda R_0)\\ +\pi_{bk}(\lambda)I_k(\lambda R_0)\end{array}\right]\cos\lambda Zd\lambda\\ +\dfrac{\sin k\Phi}{\pi}\displaystyle\int_0^{\infty}\left[\begin{array}{r}-\psi_{dk}(\lambda)I_k(\lambda R_0)-\pi_{dk}(\lambda)\lambda R_0I_k^{'}(\lambda R_0)\\ -\pi_{dk}(\lambda)I_k(\lambda R_0)\end{array}\right]\sin\lambda Zd\lambda\end{array}\right\} \tag{3.52}$$

We now proceed to construct algebra equations between the coefficients and boundary conditions. A considerate mathematical treatment must be applied in

order to eliminate the variable Φ of the right hand side of the equation. Owing to the Orthogonality Relations:

$$\int_0^{2l} \cos\frac{m\pi x}{l}\cos\frac{n\pi x}{l}\,dx = \begin{cases} 0 & m \neq n \\ l & m = n \neq 0 \\ 2l & m = n = 0 \end{cases} \tag{3.53}$$

$$\int_0^{2l} \sin\frac{m\pi x}{l}\sin\frac{n\pi x}{l}\,dx = \begin{cases} 0 & m \neq n \\ l & m = n \neq 0 \\ 2l & m = n = 0 \end{cases} \tag{3.54}$$

the cancellation of Φ is achievable. For $k \neq 0$, Eq. (3.50) can be transformed as:

$$\begin{aligned} \int_0^{2\pi} \cos k\Phi B_R\, d\Phi = \int_0^{\infty} & \left[\psi_{ck}(\lambda) I_k'(\lambda R_0) + \pi_{ck}(\lambda)\lambda R_0 I_k''(\lambda R_0) \right. \\ & \left. + \frac{\omega_{dk}(\lambda)}{\lambda R_0} k I_k(\lambda R_0) \right] \cos\lambda Z d\lambda \\ + \int_0^{\infty} & \left[\psi_{ak}(\lambda) I_k'(\lambda R_0) + \pi_{ak}(\lambda)\lambda R_0 I_k''(\lambda R_0) \right. \\ & \left. + \frac{\omega_{bk}(\lambda)}{\lambda R_0} k I_k(\lambda R_0) \right] \sin\lambda Z d\lambda \end{aligned} \tag{3.55}$$

$$\begin{aligned} \int_0^{2\pi} \sin k\Phi B_R\, d\Phi = \int_0^{\infty} & \left[\psi_{dk}(\lambda) I_k'(\lambda R_0) + \pi_{dk}(\lambda)\lambda R_0 I_k''(\lambda R_0) \right. \\ & \left. - \frac{\omega_{ck}(\lambda)}{\lambda R_0} k I_k(\lambda R_0) \right] \cos\lambda Z d\lambda \\ + \int_0^{\infty} & \left[\psi_{bk}(\lambda) I_k'(\lambda R_0) + \pi_{bk}(\lambda)\lambda R_0 I_k''(\lambda R_0) \right. \\ & \left. - \frac{\omega_{ak}(\lambda)}{\lambda R_0} k I_k(\lambda R_0) \right] \sin\lambda Z d\lambda \end{aligned} \tag{3.56}$$

The Fourier integral [95] can be used to eliminate variable *Z*:

$$f(x) = \int_0^{\infty} \left[A(w)\cos wx + B(w)\sin wx \right] dw \tag{3.57}$$

where

$$A(w)=\frac{1}{\pi}\int_{-\infty}^{\infty} f(\upsilon)\cos w\upsilon d\upsilon \tag{3.58}$$

$$B(w)=\frac{1}{\pi}\int_{-\infty}^{\infty} f(\upsilon)\sin w\upsilon d\upsilon \tag{3.59}$$

So Eq. (3.55) can be written as:

$$\frac{1}{\pi}\int_{-\infty}^{\infty}\int_{0}^{2\pi}\cos k\Phi B_R d\Phi\cos\lambda Z dZ=\psi_{ck}(\lambda)I_k^{'}(\lambda R_0)+\pi_{ck}(\lambda)\lambda R_0 I_k^{''}(\lambda R_0)+\frac{\omega_{dk}(\lambda)}{\lambda R_0}kI_k(\lambda R_0) \tag{3.60}$$

$$\frac{1}{\pi}\int_{-\infty}^{\infty}\int_{0}^{2\pi}\cos k\Phi B_R d\Phi\sin\lambda Z dZ=\psi_{ak}(\lambda)I_k^{'}(\lambda R_0)+\pi_{ak}(\lambda)\lambda R_0 I_k^{''}(\lambda R_0)+\frac{\omega_{bk}(\lambda)}{\lambda R_0}kI_k(\lambda R_0) \tag{3.61}$$

Similarly, Eq. (3.56) becomes:

$$\frac{1}{\pi}\int_{-\infty}^{\infty}\int_{0}^{2\pi}\sin k\Phi B_R d\Phi\cos\lambda Z dZ=\psi_{dk}(\lambda)I_k^{'}(\lambda R_0)+\pi_{dk}(\lambda)\lambda R_0 I_k^{''}(\lambda R_0)-\frac{\omega_{ck}(\lambda)}{\lambda R_0}kI_k(\lambda R_0) \tag{3.62}$$

$$\frac{1}{\pi}\int_{-\infty}^{\infty}\int_{0}^{2\pi}\sin k\Phi B_R d\Phi\sin\lambda Z dZ=\psi_{bk}(\lambda)I_k^{'}(\lambda R_0)+\pi_{bk}(\lambda)\lambda R_0 I_k^{''}(\lambda R_0)-\frac{\omega_{ak}(\lambda)}{\lambda R_0}kI_k(\lambda R_0) \tag{3.63}$$

Applying the same method, similar equations can be obtained from boundary condition in Φ and Z direction (Eq. (3.51) and Eq. (3.52)), which are applied to

solve the unknown coefficients simultaneously. For k=0, the procedure is similar. Similar with the spherical harmonics, the first five terms of the cylindrical harmonics are enough to get the accurate solution.

3.5 Coordinate transformation

Based on the general solution with respect to sphere and cylinder, the velocity transformation between different coordinates must be considered. In the settlement to follow, it is inevitable to utilize a series of different coordinate systems.

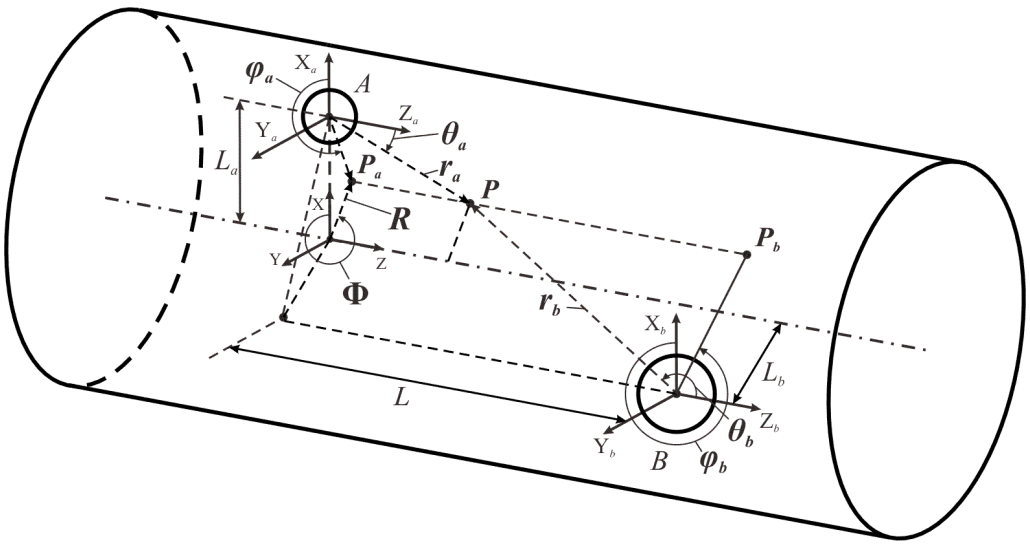

(a)

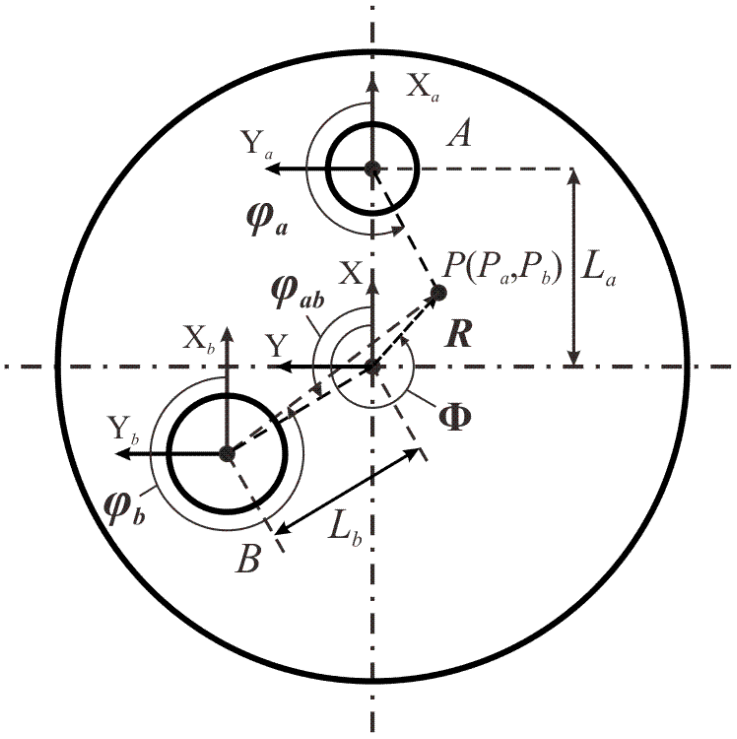

(b)

Figure 3.3: (a) axonometric drawing of the coordinate system of two particles in a cylindrical tube; (b) projection of the coordinate system of two particles in a cylindrical tube along the axis.

Consider an arbitrary point P in space (Figure 3.3); the position can be described with various coordinates. P_a (P_b) is the projection of P on the surface perpendicular to the axis of the tube and passes the center of particle A (B).

The two particles have arbitrary positions. For each particle, there are Cartesian coordinates ($X_{a(b)}$, $Y_{a(b)}$, $Z_{a(b)}$); spherical coordinates ($r_{a(b)}$, $\theta_{a(b)}$, $\varphi_{a(b)}$), which are distinguished by appending the subscripts a and b in relation to particle A and B with the common origin at the sphere center, respectively. We employ two coordinates systems: Cartesian coordinates (X, Y, Z) and cylindrical coordinates (R, Φ, Z), to describe the flow field in the cylindrical tube.

The coordinates' transformation between two particles, it can be acquired through geometry. Relative distances such as L_a, L_b and L are involved in the following relations.

$$r_a \cos\theta_a - r_b \cos\theta_b = L \tag{3.64}$$

$$-r_a \sin\theta_a \cos\varphi_a + r_b \sin\theta_b \cos\varphi_b = L_a - L_b \cos\varphi_{ab} \tag{3.65}$$

$$r_a \sin\theta_a \sin\varphi_a - r_b \sin\theta_b \sin\varphi_b = L_b \sin\varphi_{ab} \tag{3.66}$$

$$\cos^2\theta_a + \sin^2\theta_a = 1 \tag{3.67}$$

$$\cos^2\varphi_a + \sin^2\varphi_a = 1 \tag{3.68}$$

Solving the equations simultaneously, the transformation can be obtained.

Similarly, the coordinates' transformation between particle and tube can be obtained:

$$r_a \cos\theta_a = Z \tag{3.69}$$

$$-r_a \sin\theta_a \cos\varphi_a + R\cos\Phi = L_a \tag{3.70}$$

$$r_a \sin\theta_a \sin\varphi_a = R\sin\Phi \tag{3.71}$$

$$\cos^2\theta_a + \sin^2\theta_a = 1 \tag{3.72}$$

$$\cos^2\Phi + \sin^2\Phi = 1 \tag{3.73}$$

$$r_b \cos\theta_b + L = Z \tag{3.74}$$

$$r_b \sin\theta_b \cos\varphi_b - R\cos\Phi = -L_b \cos\varphi_{ab} \tag{3.75}$$

$$r_b \sin\theta_b \sin\varphi_b - R\sin\Phi = -L_b \sin\varphi_{ab} \tag{3.76}$$

$$\cos^2\theta_b + \sin^2\theta_b = 1 \tag{3.77}$$

3.6 Calculation procedure and velocities of particles

By means of the method of reflections, each velocity can be acquired according to general solution with respect to individual coordinate systems. The superscript of series represents the computation sequence.

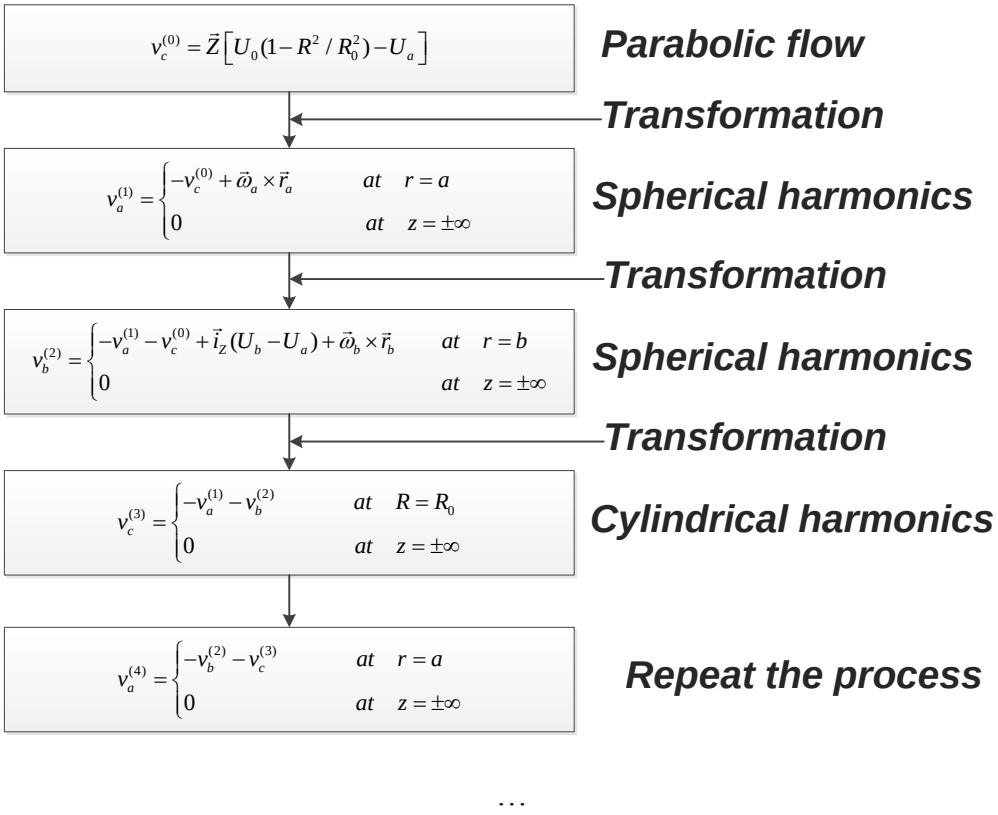

Figure 3.4: Calculation procedure

We start the calculation from the background flow named as $\vec{v}_c{}^{(0)}$ with parabolic profile which is a typical model in a tube at low Reynolds number. As described earlier, the boundary condition of the following reflection $v_a^{(1)}$ due to the presence of particle *A* comes from the previous reflection $\vec{v}_c{}^{(0)}$. Therefore,

the expression of $\vec{v}_c^{(0)}$ derived in cylindrical coordinates should be transformed into spherical coordinates (section 3.5). Then the boundary condition of $v_a^{(1)}$ can be acquired by using the method of reflections (Figure 3.2) and the expression can be calculated with the spherical harmonics (section 3.3). The next reflection $v_b^{(2)}$ can be obtained with the same procedure in the spherical coordinate of particle *B*.

The first three reflections are derived based on the three boundary conditions: two particles and the tube. In order to make the result closer to the exact flow field, more terms should be added by repeating the process. Thus, the following reflection $\vec{v}_c^{(3)}$ is conducted based on the boundary condition of the tube. Due to the procedure described in Figure 3.2, the added reflection is related to the previous result: $v_a^{(1)}$ and $v_b^{(2)}$. So the expressions derived in spherical coordinates of particle *A* and particle *B* should be transformed into cylindrical coordinates (section 3.5). Then the boundary condition of $\vec{v}_c^{(3)}$ can be obtained by utilizing the method of reflections (Figure 3.2) and the velocity expression can be calculated by taking advantage of the cylindrical harmonics (section 3.4). Similar calculations can be adopted with reference to particle *A* and particle *B*. In our study, we find that the first five terms of the spherical harmonics and cylindrical harmonics are enough to get the accurate solution. By including the five terms, the solution can satisfy the boundary condition with the difference less than 0.1%. We can continue the procedure by adding more terms to make the solution closer to the exact flow field. It is noted that the expression of the

velocity of each reflection is a function of the particle velocities including the translational and rotational velocities.

To solve the particle velocities, it is necessary to obtain the hydrodynamic force acting on the particle surfaces. Once the velocity of each reflection step has been solved, it is essential to calculate the drag force and torque of particles. The stress tensor acting on the surface of the particles is given by Lamb [96]:

$$\Pi_r = \frac{\vec{r}}{r} \cdot \Pi = -\frac{\vec{r}}{r} p + \mu\left(\frac{\partial \vec{v}}{\partial r} - \frac{\vec{v}}{r}\right) + \frac{\mu}{r} \nabla(\vec{r} \cdot \vec{v}) \tag{3.78}$$

Application of the general solution in spherical coordinates (Eq (3.17)) ultimately yields [90]:

$$\Pi_r = \frac{\mu}{r} \sum_{n=-\infty}^{\infty} \begin{bmatrix} (n-1)\nabla \times (\vec{r}\chi_n) + 2(n-1)\nabla\Phi_n \\ -\dfrac{(2n^2+4n+3)}{\mu(n+1)(2n+3)} \vec{r} p_n + \dfrac{n(n+2)}{\mu(n+1)(2n+3)} r^2 \nabla p_n \end{bmatrix} \tag{3.79}$$

Therefore, the drag force and torque conducted by the surround fluid on the particles can be acquired by integration of the stress tensor acting throughout the particle surface. Since the general solution is a function of spherical harmonics (represented with H_n in the following equations), there are general surface theories to adopt the integration [90]:

$$\int_s H_n dS = \begin{cases} 4\pi r^2 H_0 & n = 0 \\ 4\pi^2 H_{-1} & n = -1 \\ 0 & \textit{all other } n \end{cases} \tag{3.80}$$

$$\int_s \vec{r} H_n dS = \begin{cases} \dfrac{4\pi r^4}{3} \nabla H_1 & n = 1 \\ \dfrac{4\pi r}{3} \nabla (r^3 H_{-2}) & n = -2 \\ 0 & all\ other\ n \end{cases} \tag{3.81}$$

$$\int_s \nabla H_n dS = \begin{cases} 4\pi r^2 \nabla H_1 & n = 1 \\ 0 & all\ other\ n \end{cases} \tag{3.82}$$

$$\int_s \nabla \times \left(\vec{r} H_n \right) dS = 0 \qquad all \quad n \tag{3.83}$$

Again, the drag force and torque are the integrals of the stress tensor around the surface of the spheres [90]

$$\vec{F} = \int_s \Pi_r dS \tag{3.84}$$

$$\vec{T} = \int_s \vec{r} \times \Pi_r dS \tag{3.85}$$

Thus, the expressions of drag force and torque yield [90]

$$\vec{F} = -4\pi \nabla (r^3 p_{-2}) \tag{3.86}$$

$$\vec{T} = -8\pi\mu \nabla (r^3 \chi_{-2}) \tag{3.87}$$

Therefore, the total drag force and torque can be obtained by summing all the results with Eq. (3.13) and (3.14).

It is noted that the calculation procedure is an iterative process and it should be terminated under specific conditions. Due to the principle of the method of reflections, the magnitude of the drag force and torque will be smaller and smaller during the iteration. In this study, when the magnitude of the drag force and torque are three orders smaller than the sum of the previous results, we can

terminate the calculation because the following results are negligible for the whole results.

Similar with the expression of the velocity, the drag force and torque are also functions of the particle velocities. The Reynolds number represents the ratio of the effect of inertial force to viscous force in the flow. In slow viscous flow, the Reynolds number is smaller than 1. Therefore, it is reasonable that the inertial force need not be considered and the total drag force and torque are zero. So we have:

$$\begin{cases} \vec{F} = \vec{F}^{(1)} + \vec{F}^{(2)} + \vec{F}^{(3)} + \vec{F}^{(4)} + \cdots = 0 \\ \vec{T} = \vec{T}^{(1)} + \vec{T}^{(2)} + \vec{T}^{(3)} + \vec{T}^{(4)} + \cdots = 0 \end{cases} \tag{3.88}$$

By solving these two equations simultaneously, the relationship of translational and rotational velocity of particle and the background flow can be obtained. By substituting the particle velocities back into the expression of the velocity, the flow field can be obtained. Meanwhile, the number of the iteration is related to the specific configuration of the model. If the two particles are small (a/R_0 and b/R_0 <0.25), the calculation can converge within 20 items. However, when the two particles are bigger (a/R_0 and b/R_0 >0.3), the calculation needs more terms to converge.

The calculation procedure presented in this chapter can also be developed for multi particles problem due to the method of reflections. For example, if there are three particles (named as particle *A*, particle *B* and particle *E*) travelling in a cylindrical tube, the velocity field and the pressure field can be expressed as:

$$\vec{v} = \vec{v}_c^{(0)} + \vec{v}_a^{(1)} + \vec{v}_b^{(2)} + \vec{v}_e^{(3)} + \vec{v}_c^{(4)} + \vec{v}_a^{(5)} + \vec{v}_b^{(6)} + \vec{v}_e^{(7)} + \cdots \tag{3.89}$$

$$p = p_c^{(0)} + p_a^{(1)} + p_b^{(2)} + p_e^{(3)} + p_c^{(4)} + p_a^{(5)} + p_b^{(6)} + p_e^{(7)} + \cdots \tag{3.90}$$

The superscript *i* refers to the *i*th reflection and subscript (*a*, *b*, *e*, *c*) refers to the boundary conditions satisfied for particle *A*, particle *B*, particle *E* and cylinder, respectively. Similar with the current calculation, we can derive the boundary conditions due to the method of reflections which is similar to the two particles case. The origin of the coordinate system is also set at the center of particle *A*.

$$\vec{v}_c^{(0)} = \vec{Z}\left[U_0(1 - R^2 / R_0^2)\right] - \vec{U}_a \tag{3.91}$$

$$\vec{v}_a^{(1)} = \begin{cases} -\vec{v}_c^{(0)} + \vec{\omega}_a \times \vec{r}_a & at \quad r_a = a \\ 0 & at \quad z = \pm\infty \end{cases} \tag{3.92}$$

$$\vec{v}_b^{(2)} = \begin{cases} -\vec{v}_a^{(1)} - \vec{v}_c^{(0)} + \vec{Z}(U_b - U_a) + \vec{\omega}_b \times \vec{r}_b & at \quad r_b = b \\ 0 & at \quad z = \pm\infty \end{cases} \tag{3.93}$$

$$\vec{v}_e^{(3)} = \begin{cases} -\vec{v}_b^{(2)} - \vec{v}_a^{(1)} - \vec{v}_c^{(0)} + \vec{Z}(U_e - U_a) + \vec{\omega}_e \times \vec{r}_e & at \quad r_e = e \\ 0 & at \quad z = \pm\infty \end{cases} \tag{3.94}$$

$$\vec{v}_c^{(4)} = \begin{cases} -\vec{v}_a^{(1)} - \vec{v}_b^{(2)} - \vec{v}_e^{(3)} & at \quad R = R_0 \\ 0 & at \quad z = \pm\infty \end{cases} \tag{3.95}$$

The boundary conditions can be derived continually during the calculation with a loop. During each reflection, there will be one more coordinate transformation due to the presence of particle *E*. Then the entire flow field can be solved with the similar procedure of the two particles case.

Chapter 4

Result and Discussion

We consider a physical model of two rigid spherical particles translating and rotating within a long cylindrical tube with radius R_0 at low Reynolds number (Figure 4.1). Each particle has a translational velocity U and a rotational velocity ω with subscript a and b with respect to particle A and particle B, respectively.

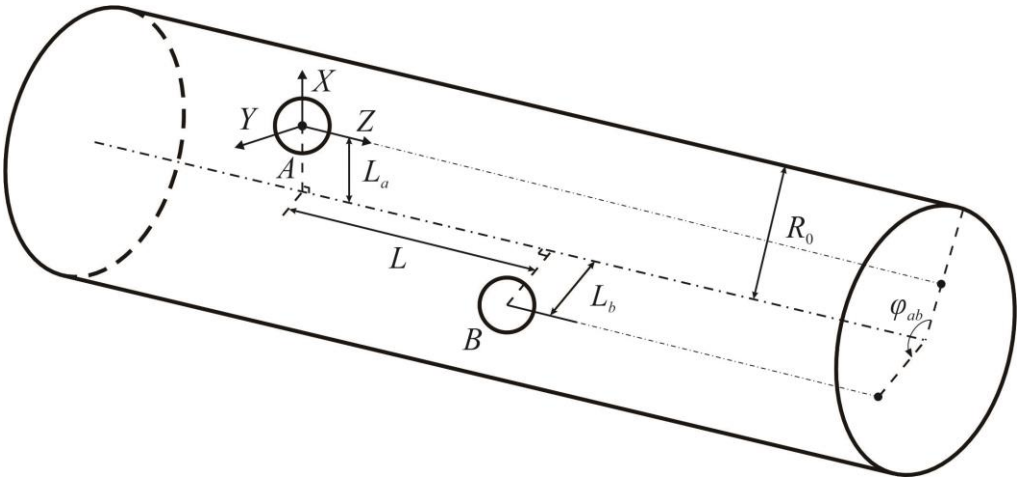

Figure 4.1: Schematics of two rigid particles moving in a cylindrical tube.

Due to the interactions among the two particles and the cylindrical wall, the sphere can move towards or away from the other sphere. To better highlight the interactive process it is necessary to analyze the drag force coefficients and particle velocities.

4.1 Two spheres along the axis of the cylindrical tube

4.1.1 Two particles with same size

We first consider two particles moving along the axis of the tube ($L_a = L_b = \varphi_{ab} = 0$), with axisymmetric condition that each particle only involves translational velocity and drag force in *Z*-direction (Figure 4.2).

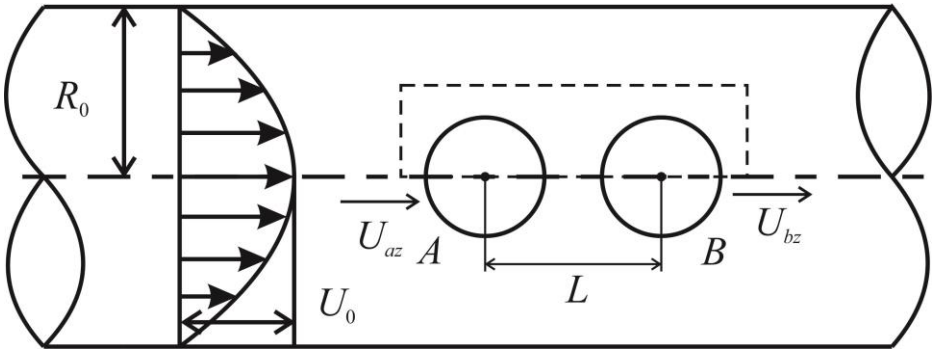

Figure 4.2: Schematic of two particles along the axis of the tube.

When a single particle travels in the tube, the flow pattern is symmetrical front to back. The flow field can be distorted in the presence of the particle due to the hydrodynamic interaction. To better highlight this mechanism, it is necessary to plot the flow pattern. Figure 4.3 shows the streamlines between the two particles (Region marked in Figure 4.2 with dashed rectangle). For convenience, we plot half of the whole flow field due to the axisymmetric geometry. The flow field is symmetric since the two particles are identical, which agrees well with the kinematic reversibility. Due to the hydrodynamic interaction between the particles, the flow around each particle cannot recover back to the upstream streamline as it passes around the particle, as compared to the case of single

particle. Figure 4.4 shows the velocity profile along the radial direction. It can be concluded that due to the presence of the particle, the previous parabolic flow has been pressed into an annular flow between the particle and the wall.

When a particle travels through a fluid, there are drag force and torque acting on it which stem from the frictional action of the fluid. Mathematically, the drag force and torque are the integrals of the stress tensor around the surface of the particle (Eq. (3.84)(3.85)). The stress tensor is attributed to the strain rate which indicates the velocity gradient is responsible for the drag force and torque.

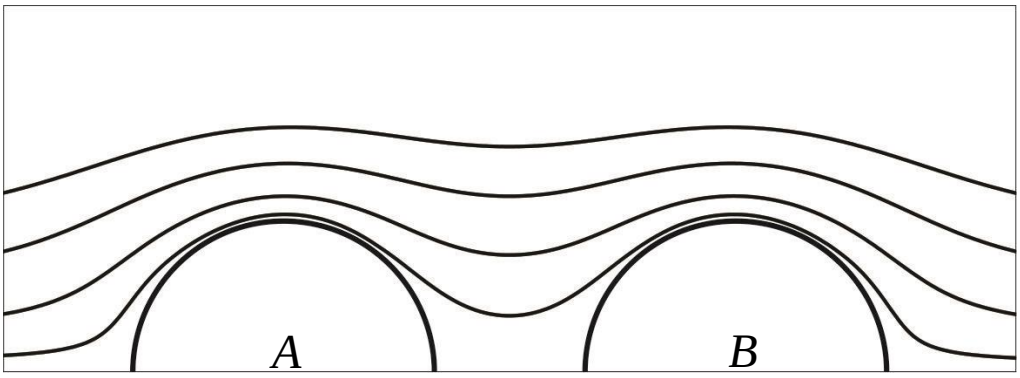

Figure 4.3: Streamlines of two particles with the same size along the axis in the tube (Region marked in Figure 4.2 with dashed rectangle).

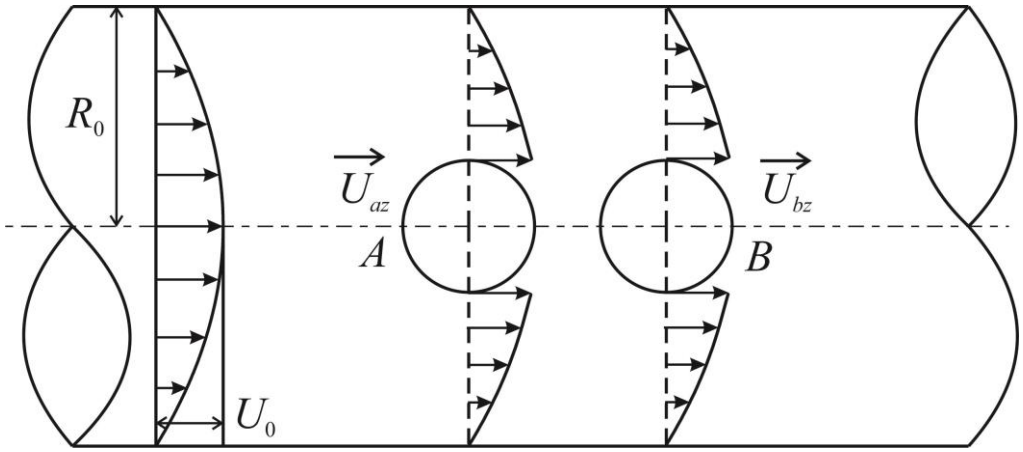

Figure 4.4: Velocity profile along the radial direction of the two particles with the same size

The final expression of the drag force of the spheres can be calculated by summing the individual reflections. Referring to the particle in axial position, the drag force can be described as:

$$\vec{F}_a = 6\pi\mu a \;\; D_a U_0 + K_a U_a + K_{ab} U_b \;\; \vec{Z} \tag{4.1}$$

$$\vec{F}_b = 6\pi\mu a \;\; D_b U_0 + K_{ba} U_a + K_b U_b \;\; \vec{Z} \tag{4.2}$$

where $\vec{F}$ are the drag forces of particles exerted by the fluid with subscript a and b corresponding to particle A and particle B. D_a, D_b and K_a, K_b are the coefficients related to the background flow and the particle velocities, respectively. K_{ab} and K_{ba} are the coefficients referring to the hydrodynamic interaction between the particles. First we consider the two particles with the same size and plot the result as a function of L/R_0. For comparison, we choose $a/R_0 = b/R_0 = 0.1$ and 0.3.

In a low Reynolds number world, the coefficients of the two particles must be identical when they have the same size due to the kinematic reversibility. Our

analytical results have validated that they agree well. In such case, for convenience, the new variable D ($D=D_a=D_b$), K ($K=K_a=K_b$) and K^* ($K^*=K_{ab}=K_{ba}$) are utilized to represent the coefficients.

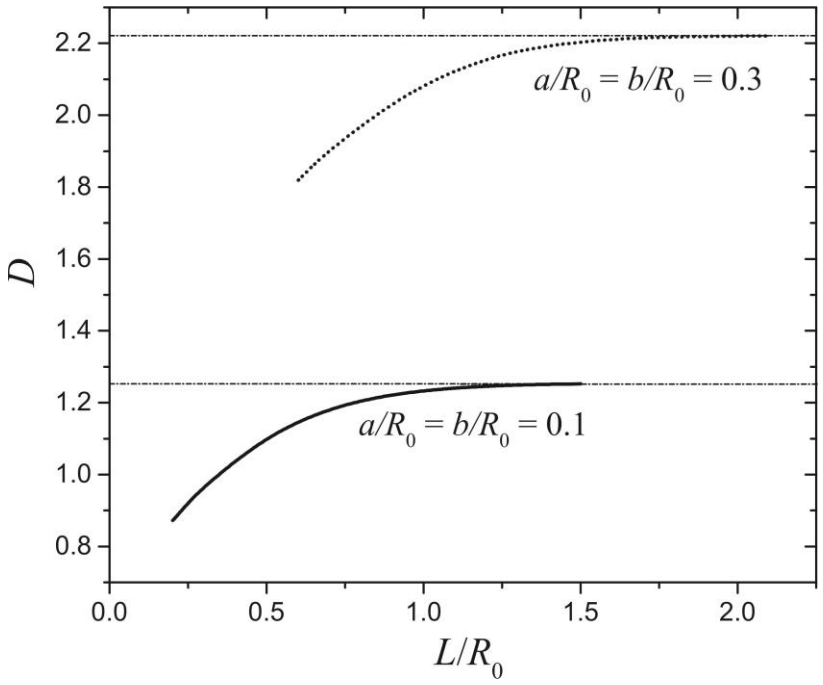

Figure 4.5: Normalized drag force coefficient D ($D = D_a = D_b$) with two different particle sizes.

Figure 4.5 shows the variation of coefficient D ($D = D_a = D_b$) with two different particle sizes. It is not unexpected that the coefficient D is positive, since the drag force is in the same direction as the flow. The coefficient increases monotonically from a minimum value to a constant elucidated by a horizontal line which indicates that the interaction between particles is negligible. When the two particles are closer, the streamlines are deformed by the neighboring particle and the fluid between them has negligible velocity gradient (Figure 4.3).

As expected, this behavior causes the smaller drag force acting on the surface particle. Hence the closer the two particles are from each other, the smaller is the necessary values for coefficient *D*. In addition, the bigger particle has a larger drag force coefficient due to the stronger wall effect. This result also agrees well with the previous work [90]. Also, the characteristic distance related to the particle interaction can be obtained. When $a/R_0 = b/R_0$=0.1 and L/R_0>1.0, the difference between the coefficient *D* and the single particle case is less than 1 percent, which manifests the hydrodynamic interaction is negligible. The same conclusion can be obtained for $a/R_0 = b/R_0 = 0.3$ with L/R_0>1.5.

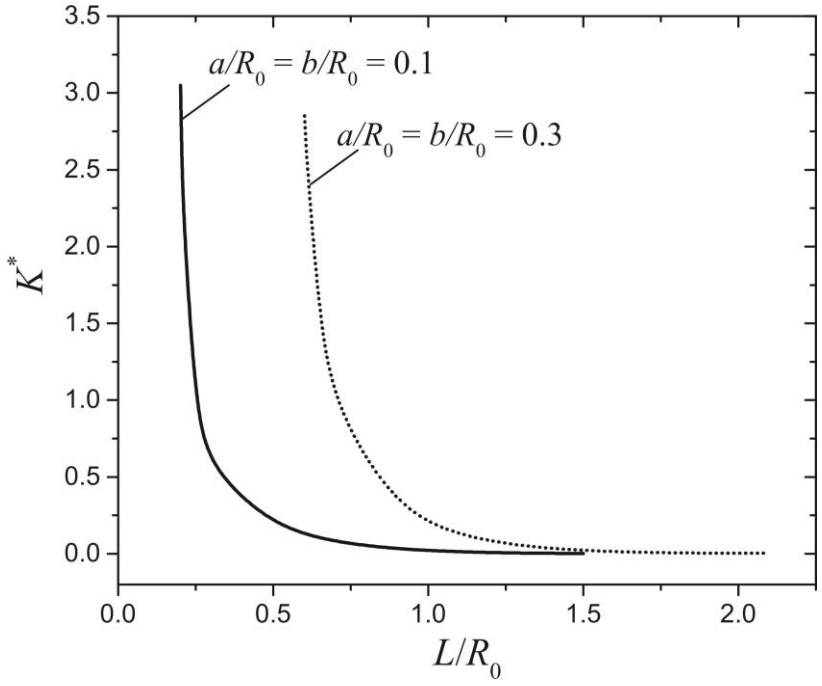

Figure 4.6: Normalized drag force coefficient K^* ($K^* = K_{ab} = K_{ba}$) with different particle sizes.

It is noteworthy that with given configuration, the coefficient K^* represents the contribution from the movement of the neighboring particle which indicates the hydrodynamic interactions between them. In such case, the drag force has the same direction as the neighboring particle which makes the coefficient K^* positive (Figure 4.6). In both cases, when the two particles are very close, the coefficient K^* has the maximum value which arises from the larger velocity gradient due to the neighboring particle. As the particle spacing increases, the coefficient decays to zero with similar tendency which indicates the hydrodynamic interaction can be neglected. The characteristic distance related to particle-particle interaction for the coefficient K is the same as the coefficient D.

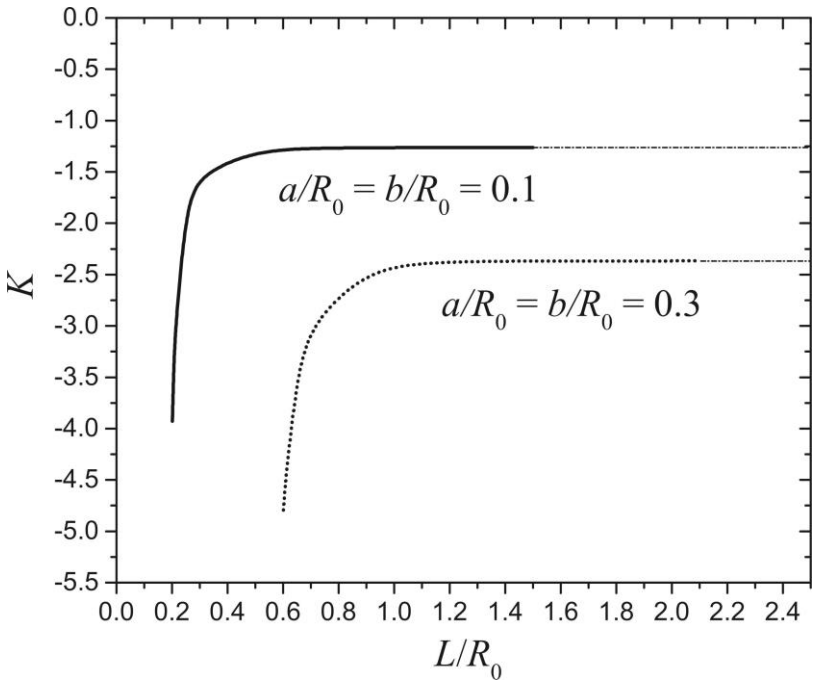

Figure 4.7: Normalized drag force coefficient K ($K = K_a = K_b$) with different particle sizes.

Unlike the previous coefficients, K demonstrates the drag force subjected to the movement of the particles themselves (Figure 4.7). The coefficient is negative since the drag force is against the direction of the particle motion. The increment of the magnitude of coefficient K at smaller particle spacing is attributed to the neighboring particle which enhances the velocity gradient. Furthermore, the bigger particle has stronger velocity gradient together with the larger magnitude of drag force coefficient for certain particle spacing.

The mechanism of low Reynolds number requires that the total drag force should be zero, implying the velocities of particles can be calculated (Figure 4.8). The velocities are normalized by the maximum value of the background flow U_0 and plotted as a function of particle spacing. From the kinematic reversibility, the velocity of particle A is the same as the one of particle B since the two particles are identical and the new variable U_z ($U_z = U_{az}\ U_{bz}$) is used to represent the velocity.

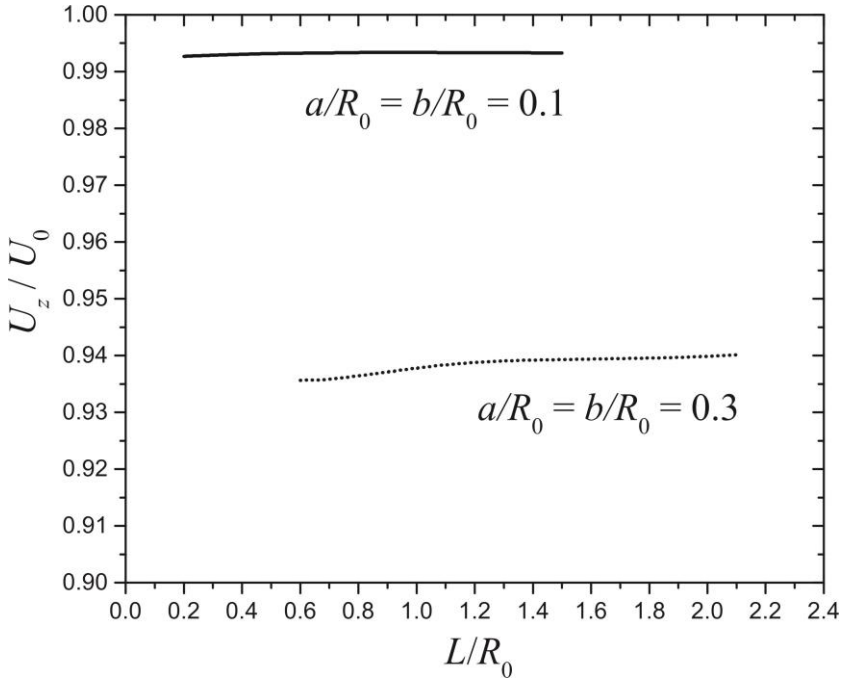

Figure 4.8: Normalized velocity of the two particles U_z ($U_z = U_{az} = U_{bz}$) with different particle sizes.

In Figure 4.8, the variation of translational velocity of both particles is very small. When the two particles are almost in contact, the velocity has a minimum value and increases to a constant as the particle spacing increasing. Furthermore, if the particle spacing is three times larger than the sum of particles radii, the particle-particle interaction can be neglected, which agrees well with the previous discussion.

4.1.2 Two particles with different sizes

A more informative analysis of the hydrodynamic interaction is provided by comparing the two particles with different sizes. We set the size of particle *A* as a/R_0=0.1 and vary the radius of particle *B* with b/a=2, 3, 4, 5. Figure 4.9 shows the normalized drag force coefficient D_a as a function of the normalized distance L/R_0. The horizontal line refers to the coefficient of a single particle case with a/R_0=0.1.

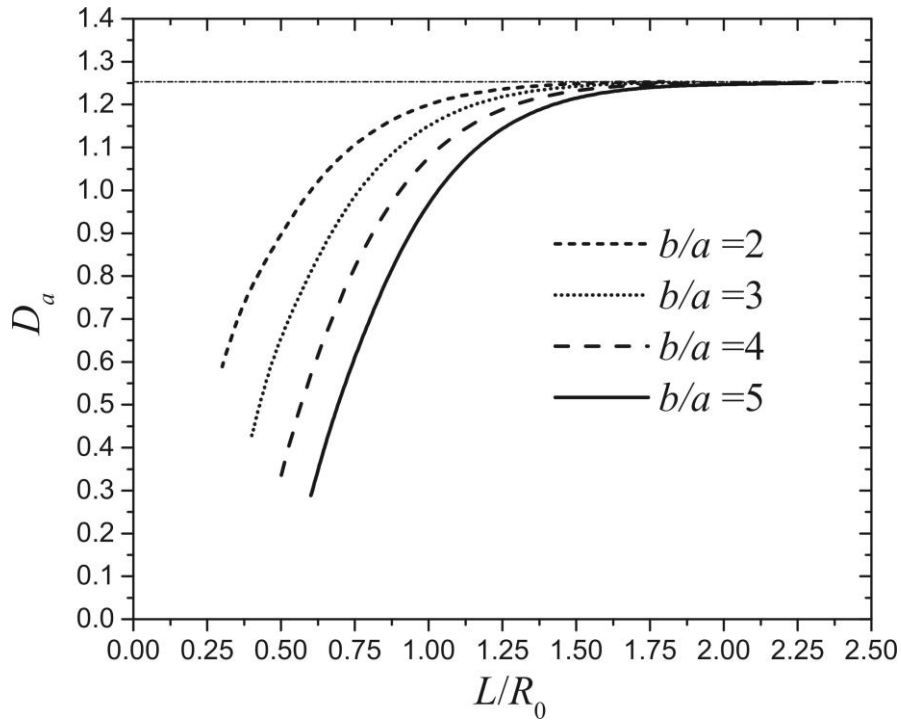

Figure 4.9: Normalized drag force coefficient D_a for two particles with different sizes. The horizontal line refers to the coefficient of a single particle case with a/R_0=0.1.

As we discussed above, when the two particles become sufficiently close together, a larger region where the velocity gradient of the fluid is negligible is developed in between them that causes the smaller D_a. Hence the bigger particle

B is moving ahead, smaller is the necessary value for coefficient D_a which stems from the stronger hydrodynamic interaction.

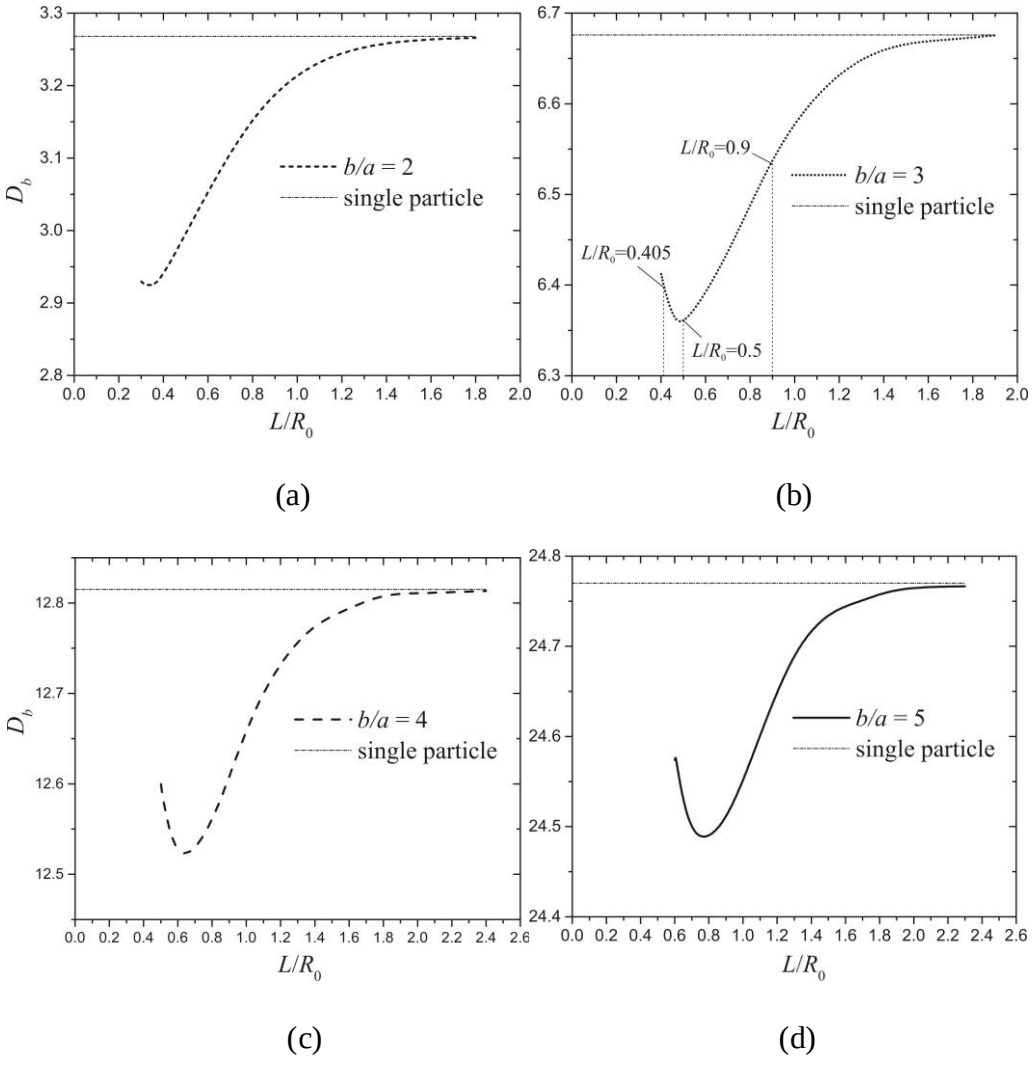

Figure 4.10: Normalized drag force coefficient D_b. It is plotted as L/R_0. We choose a/R_0=0.1 and (a) b/a=2, (b) b/a=3, (c) b/a=4, (d) b/a=5, respectively. The horizontal line refers to the coefficient of single particle case accordingly.

Interestingly, the variation of the drag force coefficient D_b is not monotonous when particle *B* is bigger than particle *A* (Figure 4.10). As the particle spacing increasing, the coefficient D_b decreases first to a minimum value and then

increases to a constant referring to the single particle case. We choose three characteristic particle spacing with b/a=3 (Figure 4.10(b)) and plot the streamlines.

The streamlines in Figure 4.11 show the flow field between the two particles. When the two particles are sufficiently close together, the remarkable distortion of the flow field is generated between them influencing the drag force. The characteristic feature is the asymmetric circulation area which is related to the coefficient D_b. When the two particles are very close (Figure 4.11(a)), there exists the strong viscous interaction. However, the circulation area is limited due to the small particle spacing. With L/R_0 increasing, the circulation area increases to a maximum value causing the minimum coefficient D_b (Figure 4.11(b)). If the two particles are far away, the circulation area vanishes with the larger coefficient D_b (Figure 4.11(c)). It is instructive to analyze the impact of the circulation area on the drag force. In the circulation area, both of the velocity magnitude and velocity gradient are significantly smaller than those outside. As mentioned earlier, the velocity gradient is responsible for the drag force acting on the surface of the particle. Hence the larger circulation area exists, smaller is the necessary value for coefficient D_b.

Figure 4.12 shows the velocity profile along the radial direction of the two particles with different configurations. It can be concluded that due to the presence of the particle, the previous parabolic flow has been pressed into an annular flow between the particle and the wall. Meanwhile, the velocity along

the radial direction on the surface of particle *A* is larger than the one of particle *B* since particle *A* is smaller.

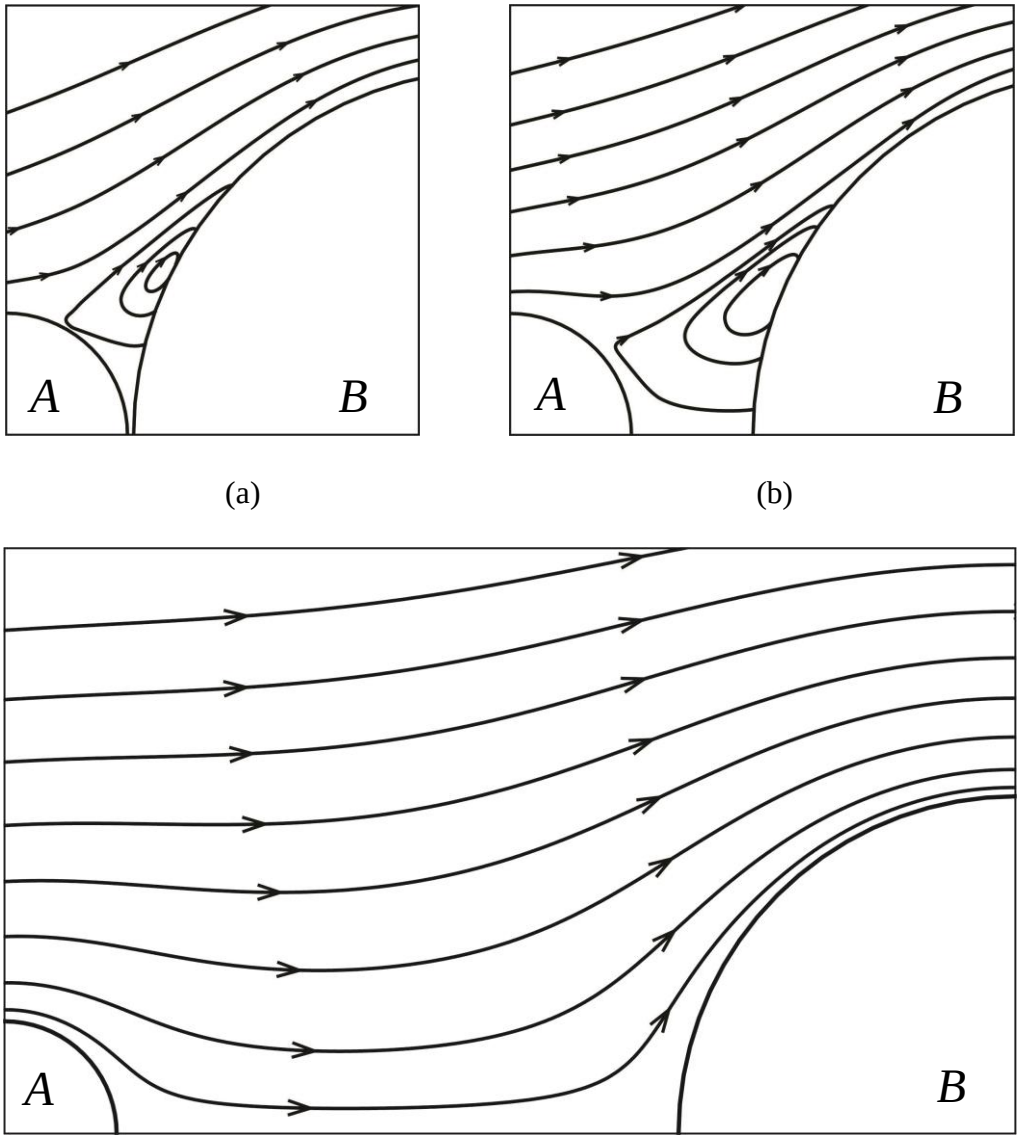

Figure 4.11: Streamlines with a/R_0=0.1 and b/a=3. We choose (a) L/R_0=0.405, (b) L/R_0=0.5, (c) L/R_0= 0.9, respectively. Since the geometry is under axisymmetric condition, we plot half of the streamlines with U_a=U_b=0 to represent the flow field.

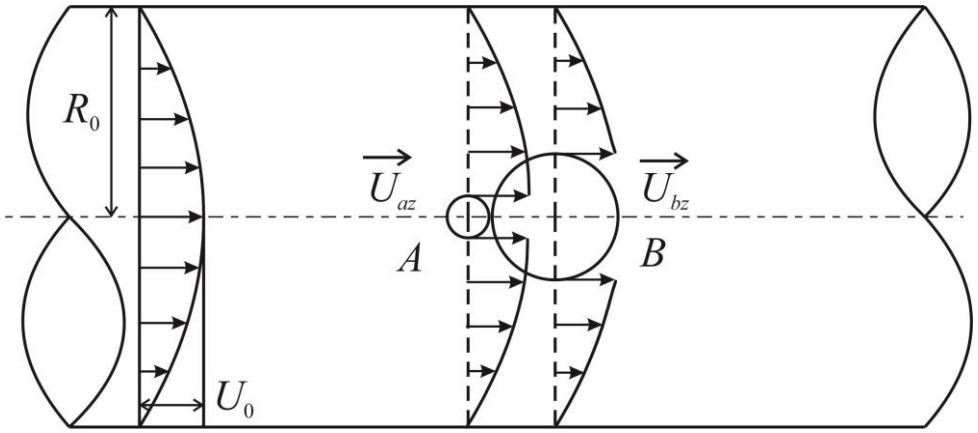

(a)

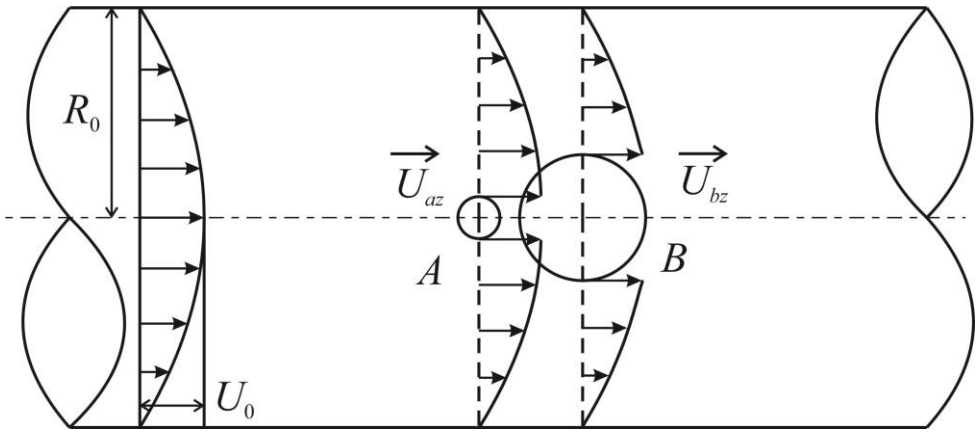

(b)

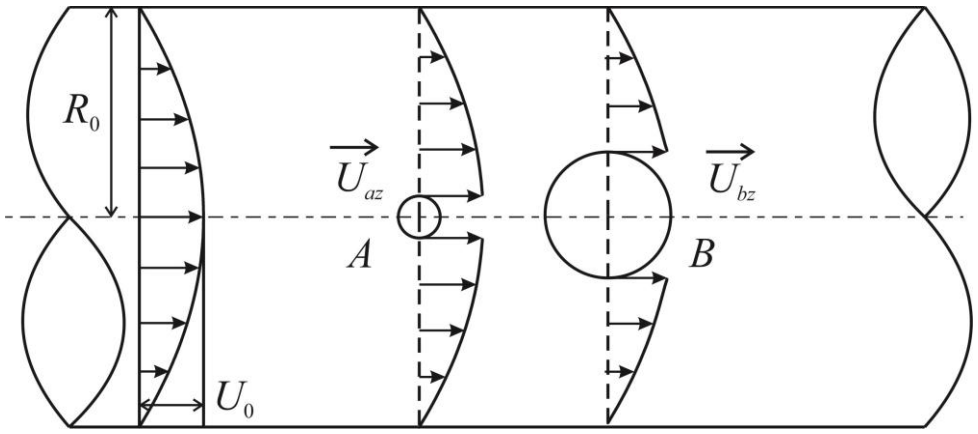

(c)

Figure 4.12: Velocity profile along the radial direction of the two particles with a/R_0=0.1 and b/a=3. We choose (a) L/R_0=0.405, (b) L/R_0=0.5, (c) L/R_0= 0.9, respectively.

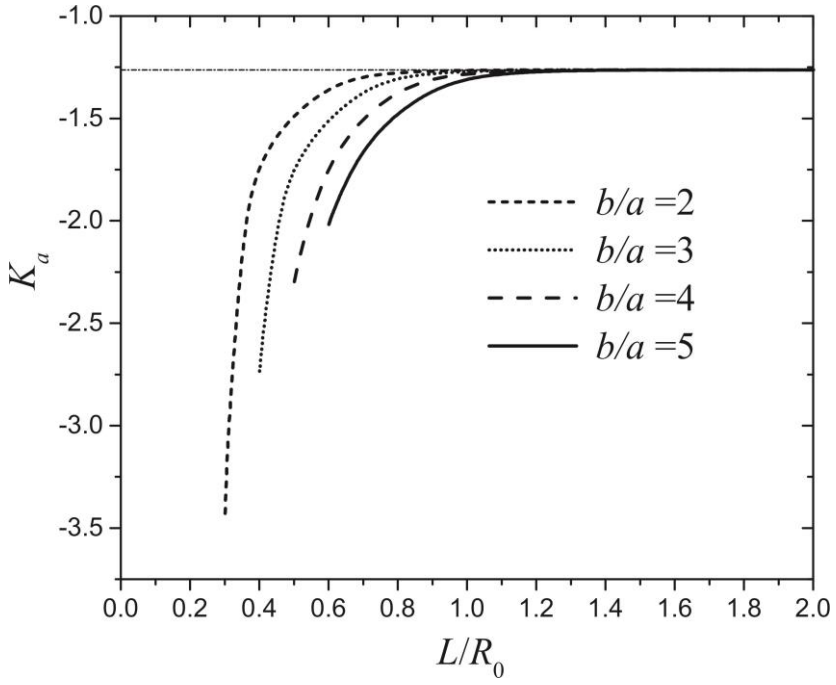

Figure 4.13: Normalized drag force coefficients K_a with different radii ratios.

Similar to the behavior described in Figure 4.7, K_a or K_b shows the drag force due to the movement of the particles themselves. Figure 4.13 represents the coefficient K_a related to the translational velocity of particle *A*. For a certain radii ratio, the magnitude of K_a decreases monotonously to a horizontal line which refers to the value of the single particle case. Furthermore, the bigger particle *B* moving ahead induces smaller velocity gradient between the two particles causing the coefficient *K* with smaller magnitude.

Similar tendency is also obtained for the coefficient K_b (Figure 4.14). The magnitude of the coefficient increases with the radius increasing which is similar with the phenomenon in figure 4.7.

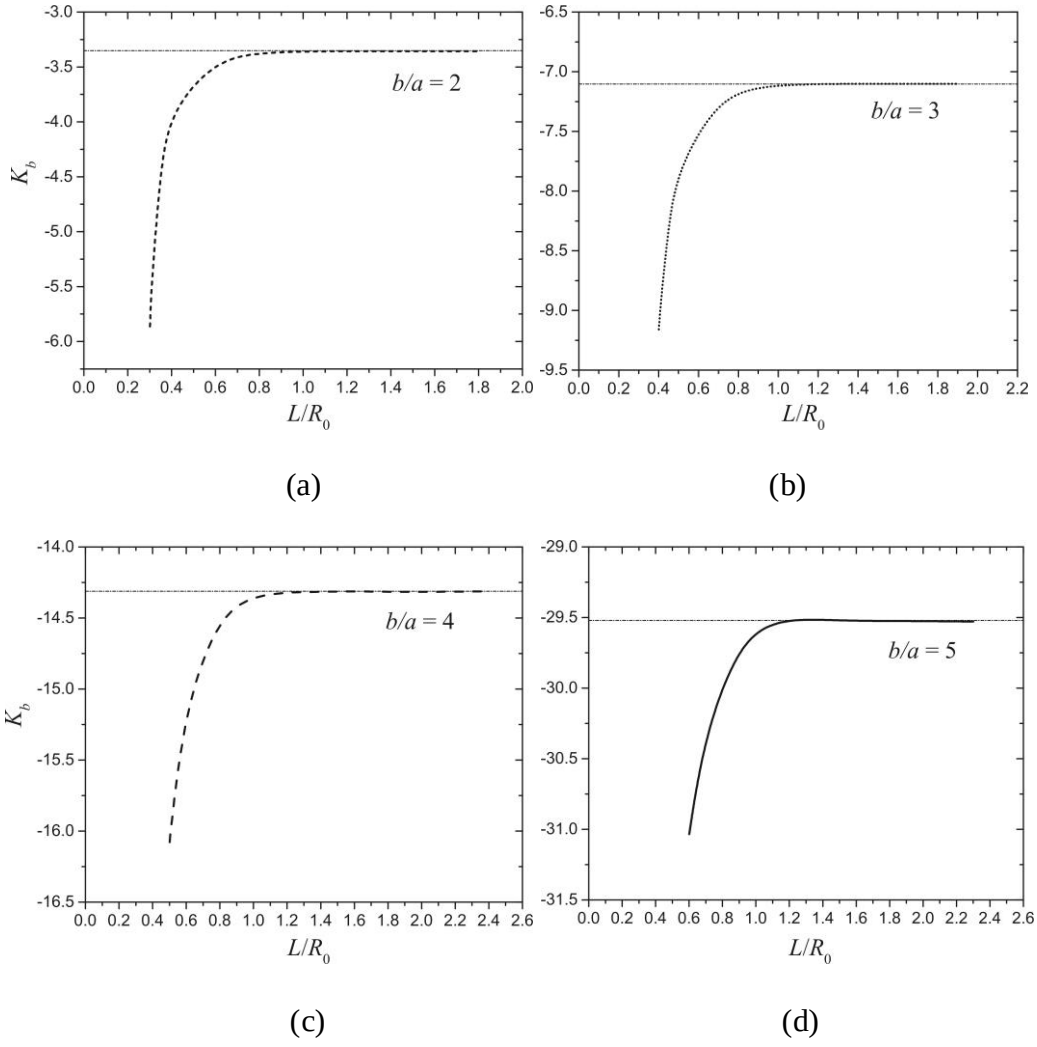

Figure 4.14: Normalized drag force coefficient D_b with different radii ratios.

The drag force coefficients corresponding to the hydrodynamic interactions (Figure 4.15) show a similar pattern to that of Figure 4.6. Our analytical results have validated that the two coefficients are identical which are represented by the new variable K^* ($K^* = K_{ab} = K_{ba}$). It is noted that these coefficients decrease monotonically to zero as L/R_0 increases which indicates that the particle-particle interaction is negligible. The kinematic reversibility does not rule out the possibility of K_{ab} being unequal to K_{ba}. Happel and Brenner have demonstrated

the identity of the coefficients based on the resistance matrix [90]. They showed that when the two particles travel in a low Reynolds number world, the resistance matrix is symmetric. That is why the two coefficients are still identical when the particle *B* is bigger.

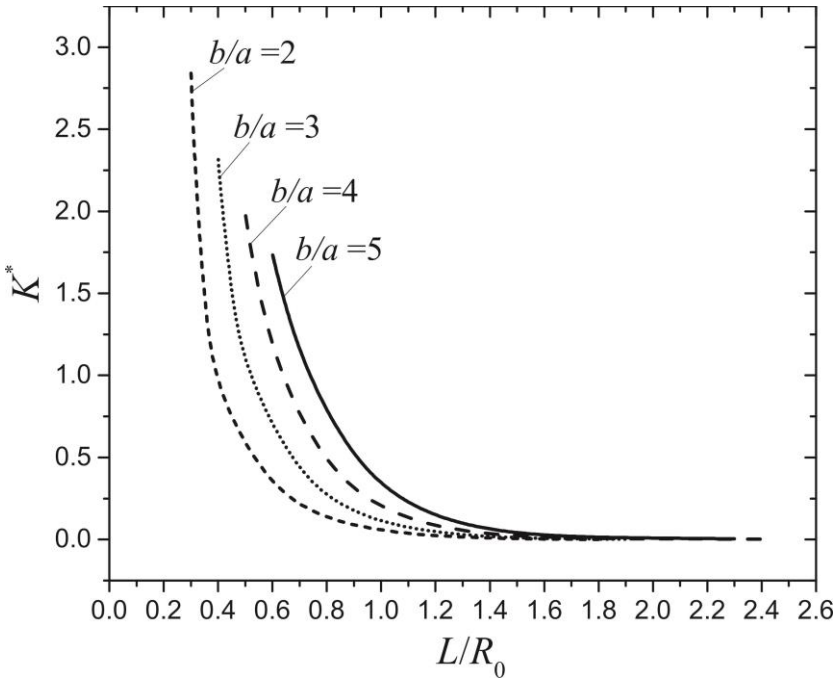

Figure 4.15: Normalized drag force coefficients K^* ($K^* = K_{ab} = K_{ba}$) with different radii ratios.

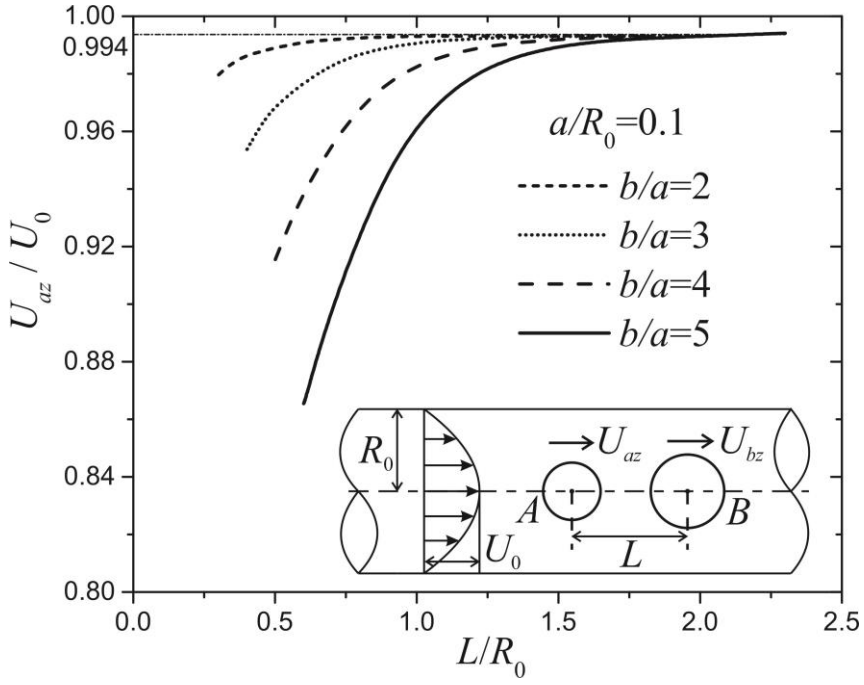

(a)

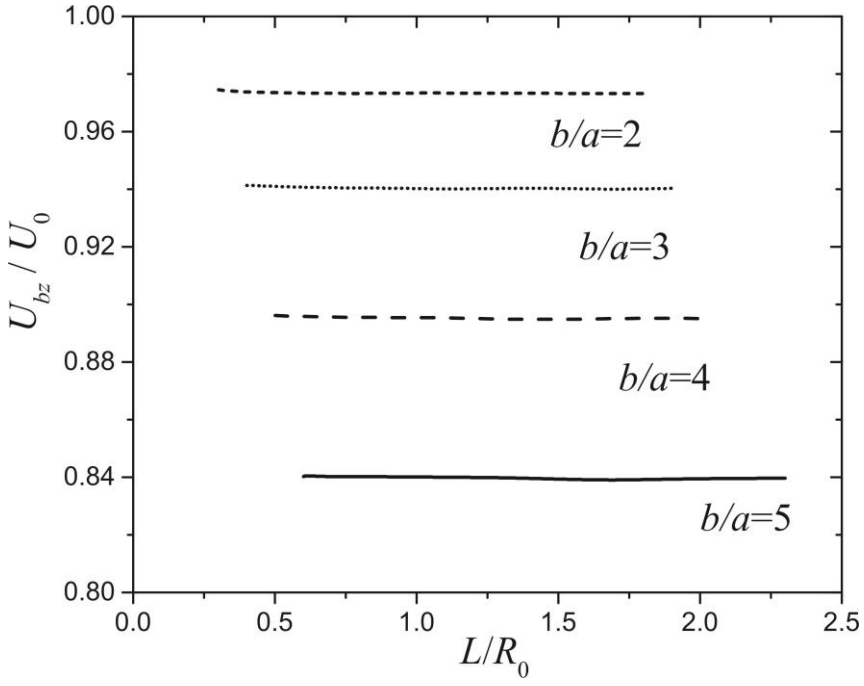

(b)

Figure 4.16: (a) Normalized velocity of particle *A*; (b) Normalized velocity of particle *B*.

The mechanism of low Reynolds number requires that the total drag force should be zero, implying the velocities of particles can be calculated. We investigate the effect of the particle spacing and radii ratios on the velocities of particle *A* and *B* (Figure 4.16). The velocities are normalized by the maximum value of the background flow U_0 and plotted as a function of particle spacing. In general, the nonlinear evolution of the particle velocities is related to the flow field around it. The horizontal line in Figure 4.16(a) refers to the velocity of a single particle travelling along the axis within a tube. As L/R_0 increasing, the velocity of particle *A* increases monotonously to a constant referring that the particle-particle interaction can be neglected. It is interesting, however, the effect of the interaction on particle *B* is weak.

As mentioned earlier, the total drag force is zero in a low Reynolds number world. The variation of the velocities of particles should be considered to represent the particle-particle interaction which is more informative. In such case, the characteristic distance related to this interaction can be obtained from Figure 4.16. When b/a= 4 and L/R_0 >1.5, for example, the particle-particle interaction is negligible since the difference between the velocity of particle *A* and the single particle case is less than 1 (Figure 4.16 (a)). Based on these results, we find that the particle-particle interaction can be neglected when the separation distance is three times larger than the sum of particles radii. Furthermore, as shown in this figure, the velocity of particle *A* is always larger than that of particle *B* when b/a>1. This implies the two particles are

approaching. Meanwhile, if we reverse the direction of the Poiseuille Flow, the two particles will repel subjected to the kinematic reversibility.

In this section, we investigate the flow behavior of the two particles travelling along the axis of the tube. The drag force coefficients are presented and the characteristic distance of the particle-particle interaction can be obtained corresponding to different cases. We find that the particle-particle interaction can affect the velocity gradient significantly which is responsible for the drag force coefficients. When the two particles are very close, the particle-particle interaction can enhance the drag force magnitude arising from the particle motion and reduce the one related to the background flow. Meanwhile, there exists a circulation area when the two particles have the different sizes. The presence of the circulation area can reduce the drag force since the velocity gradient inside the area is smaller than the one outside. Furthermore, it is noted that the movement of the particle can be influenced by the one moving ahead. The effect on the smaller particle is significantly stronger than the bigger one. The mechanism of such case is not only of fundamental interest for the hydrodynamic interactions of multi-particles flow field in the tube, but also contribute significantly to the insight of the aggregation and separation phenomena of particles.

4.2 Two spheres with one off the axis

In this section, we explore more general cases. The two particles have symmetrical positions with respect to *X*-axis (Figure 4.17). A lateral distance is given to particle *B*, named as L_b in the coordinate system. The kinematic reversibility indicates that a single particle cannot move laterally in a cylindrical tube. However, in the two particles case, with such lateral distance, particle *A* and particle *B* have translational velocities in *Z* and *X*-direction and rotational velocity in *Y*-direction.

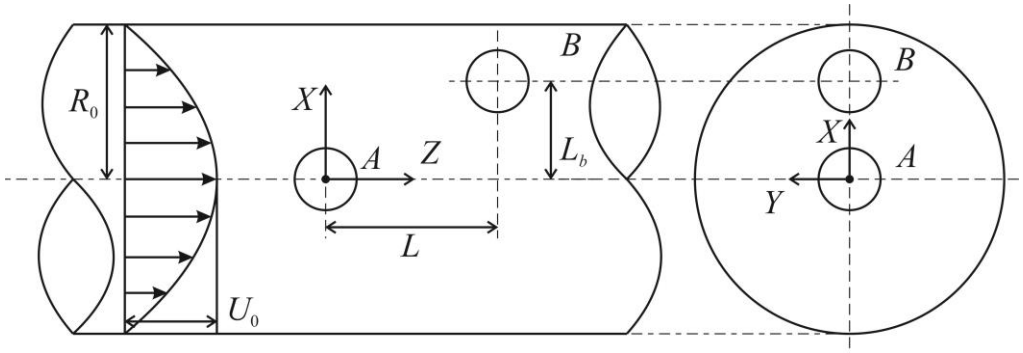

Figure 4.17: Schematics of two rigid particles with the symmetric positions in a cylindrical tube. Particle *A* is located on the axis and Particle *B* has a lateral distance perpendicular to the axis named as L_b.

To better analyze the flow behavior, it is necessary to set up different cases. Meanwhile, since the coefficients have been discussed in the previous section, we focus on the velocities of particles in the following sections.

4.2.1 Two particles with same size

We first consider these two particles with the same normalized radius $a/R_0=b/R_0=0.02$. Two different particle spacings are applied ($L/R_0=0.02$ and 0.05) and the normalized lateral distance L_b/R_0 is changed as a variable to analyze the velocities of the particles.

Figure 4.18 and 4.19 show the normalized velocities of the particles in the *X*-direction with two different particle spacings: $L/R_0=0.05$ and $L/R_0=0.02$. In these two cases, the fluid pushes the two particles into the opposite directions. Particle *A* moves downward with the negative translational velocity and particle *B* has the opposite movement.

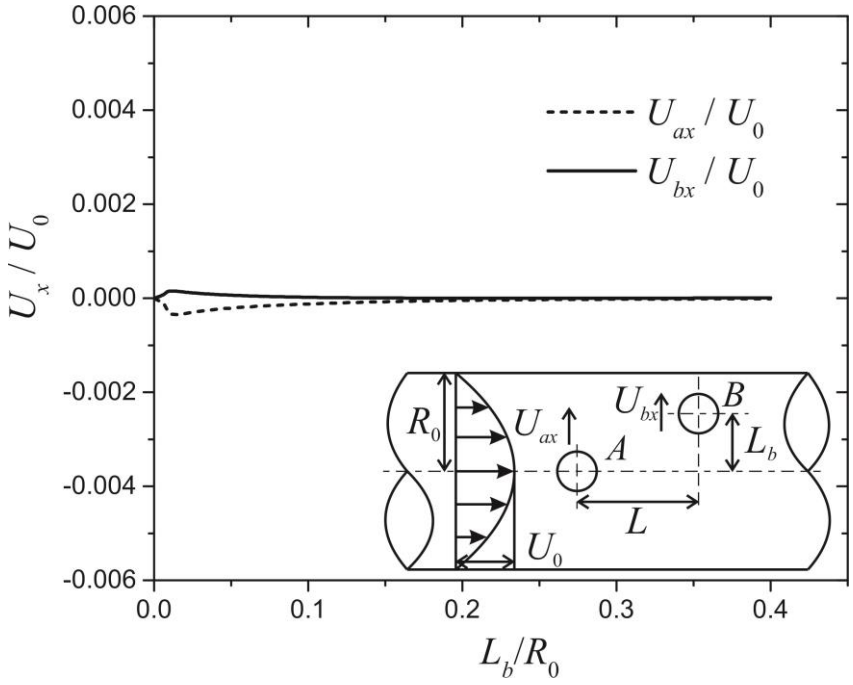

Figure 4.18: Normalized velocities the two particles in *X*-direction with $a/R_0=b/R_0=0.02$ and $L/R_0=0.05$.

In Figure 4.18, since the particle spacing is larger than the sum of the radii of particle *A* and particle *B*, the lateral distance L_b/R_0 can be varied from zero. When particle *B* is situated on the axis of the tube (L_b/R_0=0), the two particles have the axisymmetric geometry which makes the translational velocity in *X*-direction zero. As L_b/R_0 increasing, the lateral distance breaks the axisymmetric configuration and the two particles have velocities towards to the wall. The velocity increases to a maximum value and then decreases to zero which indicates the particle-particle interactions can be neglected. When the particle spacing is smaller (Figure 4.19), we vary L_b/R_0 from a minimum value to ensure the two particles will not collide. With L_b/R_0 increasing, the magnitude of the velocities decreases dramatically to zero form the maximum value which is significantly larger than previous case (Figure 4.18). This indicates the particle-particle interaction is stronger comparing with the larger particle spacing case.

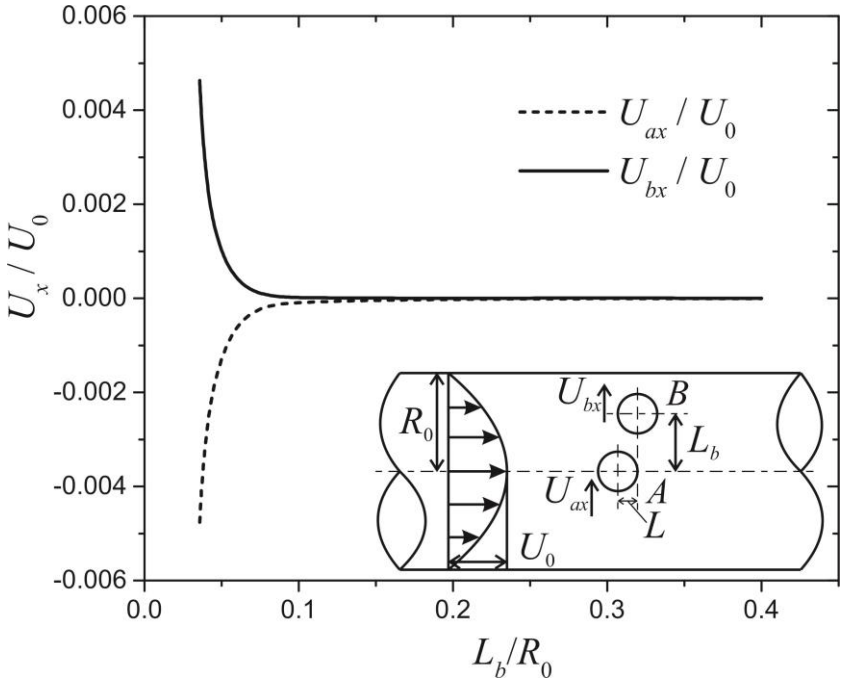

Figure 4.19: Normalized velocities the two particles in *X*-direction with $a/R_0=b/R_0=0.02$ and $L/R_0=0.02$.

Figure 4.20 and 4.21 shows the normalized velocities of the particles in *Z*-direction with the two different particle spacings. The *Z*-velocities of the two particles are dominated by the advection due to the Poiseuille Flow, so the two cases have similar pattern. The variation of U_{az}/U_0 is negligible and U_{bz}/U_0 decreases monotonously.

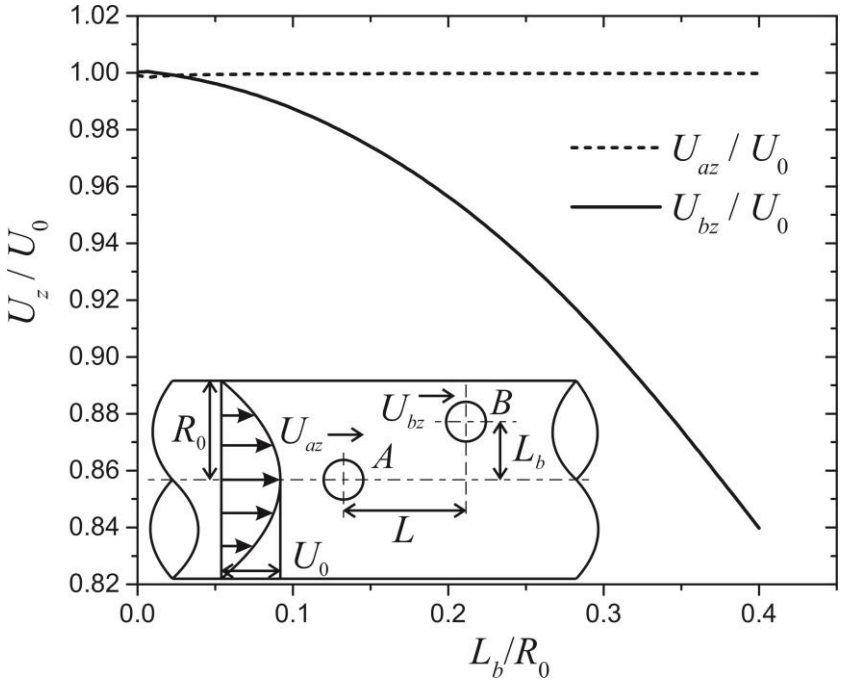

Figure 4.20: Normalized velocities the two particles in *Z*-direction with $a/R_0=b/R_0=0.02$ and $L/R_0=0.05$.

In the Poiseuille Flow, the fluid pushes the two particles moving forward. Particle *A* is set along the axis of the tube so the translational velocity is close to the maximum value of the Poiseuille Flow. Particle *B* is located with the lateral distance as a variable causing the velocity decreases nonlinearly corresponding to the Poiseuille Flow.

It should be noted that when the two particles are very close to each other, the particle-particle interactions can still impact the movements of the particles. In Figure 4.20, the velocity of particle *B* is larger than the one of particle *A* when L_b/R_0 is sufficiently small. As expected, the movement of particle *B* is enhanced by particle *A* moving behind. In the smaller particle spacing case (Figure 4.21), the impact is stronger due to the particle-particle interaction.

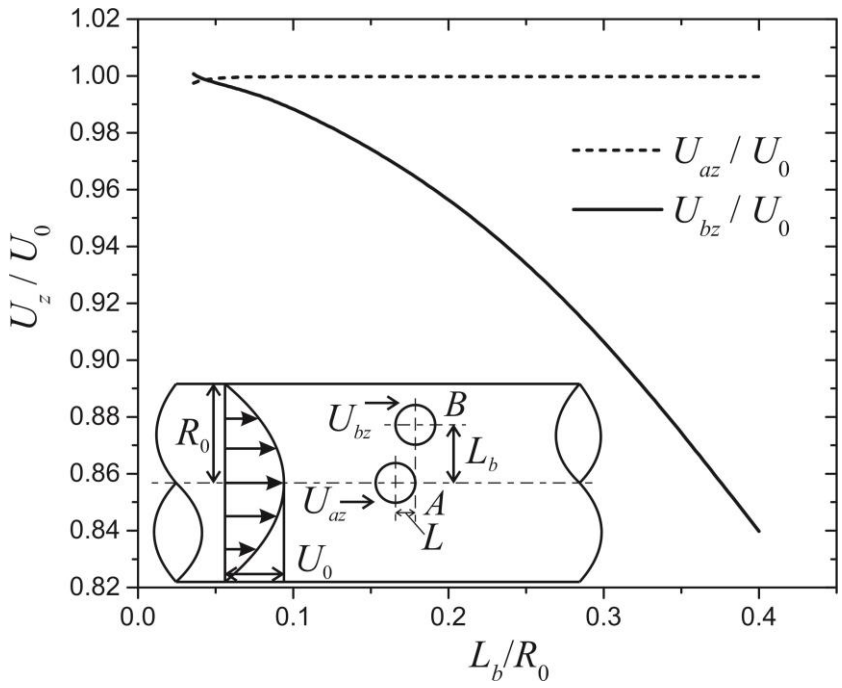

Figure 4.21: Normalized velocities the two particles in *Z*-direction with $a/R_0=b/R_0=0.02$ and $L/R_0=0.02$.

Unlike the translational velocity, the rotational velocity can be in the opposite direction when the two particles are very close to each other. When $L/R_0=0.05$ (Figure 4.22), the rotational velocity of particle *A* has little variation and particle *B* has a linear relationship with L_b/R_0 increasing due to the linear gradient of the Poiseuille Flow in the radial direction.

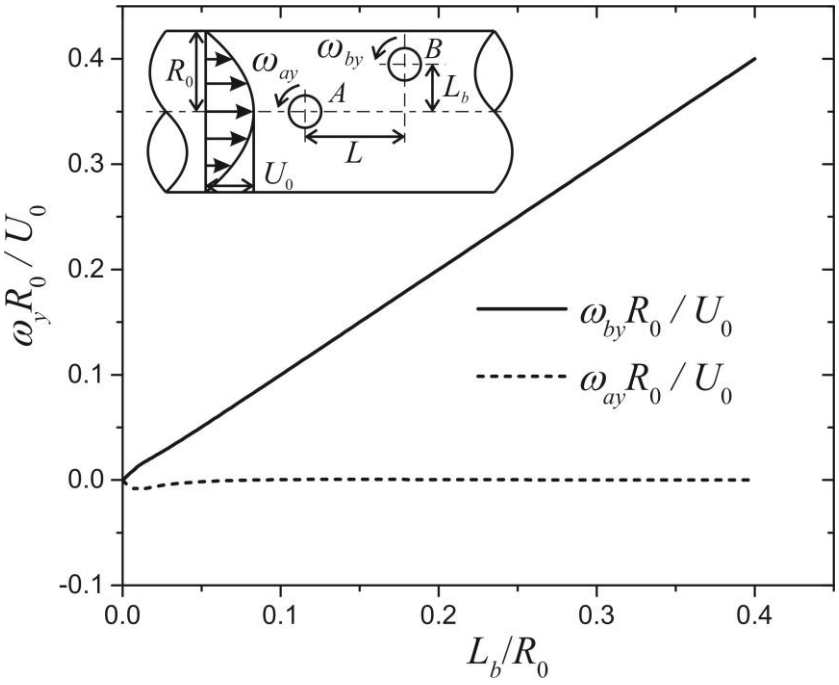

Figure 4.22: Normalized rotational velocities the two particles in *Y*-direction with $a/R_0=b/R_0=0.02$ and $L/R_0=0.05$.

It is interesting, however, particle *B* has a negative rotational velocity first and then turns to positive with L_b/R_0 increasing when $L/R_0 = 0.02$ (Figure 4.23). The reason behind such mechanism is the balance of the parabolic background flow and the particle-particle interactions. When a single particle travels towards to the wall in the positive *X*-direction from the axis position, it has the positive rotational velocity (anticlockwise in Figure 4.23) due to the parabolic profile. The magnitude is related to the velocity gradient. Hence the further the particle is from the axis, larger is the necessary value for rotational velocity. However, when the two particles are very close, the flow sustains a lower velocity between the particles due to the particle-particle interaction than for the flow nearer to the cylindrical tube. This makes the rotational velocity of particle *B*

negative (clockwise in Figure 4.23). As L_b/R_0 increasing, the Poiseuille Flow will dominate the particle motion with the linear and positive rotational velocity.

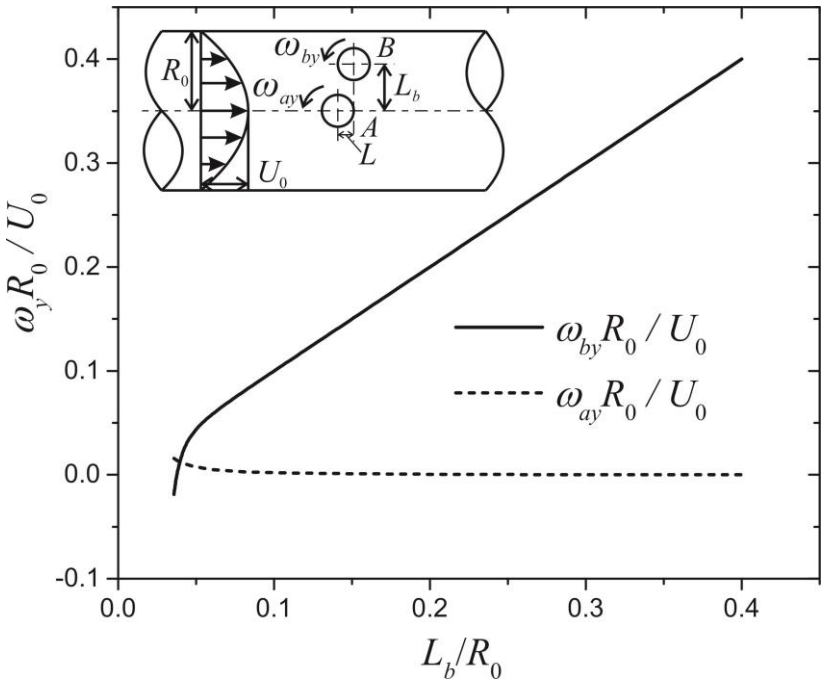

Figure 4.23: Normalized rotational velocities the two particles in *Y*-direction with $a/R_0=b/R_0=0.02$ and $L/R_0=0.02$.

As discussed earlier, the particle-particle interaction can be neglected when the separation distance is three times larger than the sum of particles radii, which is concluded from the case when the two particles are along the axis. However, when particle *B* has a lateral distance, the lateral and rotational velocities should be considered as well. When the two particle are identical and the separation distance is three times larger than the sum of particles radii, the particle-particle interaction can be neglected, which agrees with our previous discussion. With such configuration, the Poiseuille Flow dominates the translational velocity in

the *Z*-direction and rotational velocity in the *Y*-direction and the lateral velocity is negligible.

4.2.2 Two particles with different sizes

In this section, we set the two particles with different sizes: a/R_0=0.05 and b/R_0=0.1. Two particle spacings are also adopted to analyze the velocities of the particles with L/R_0=0.1 and 0.2. As described earlier, the normalized lateral distance L_b/R_0 is changed as a variable.

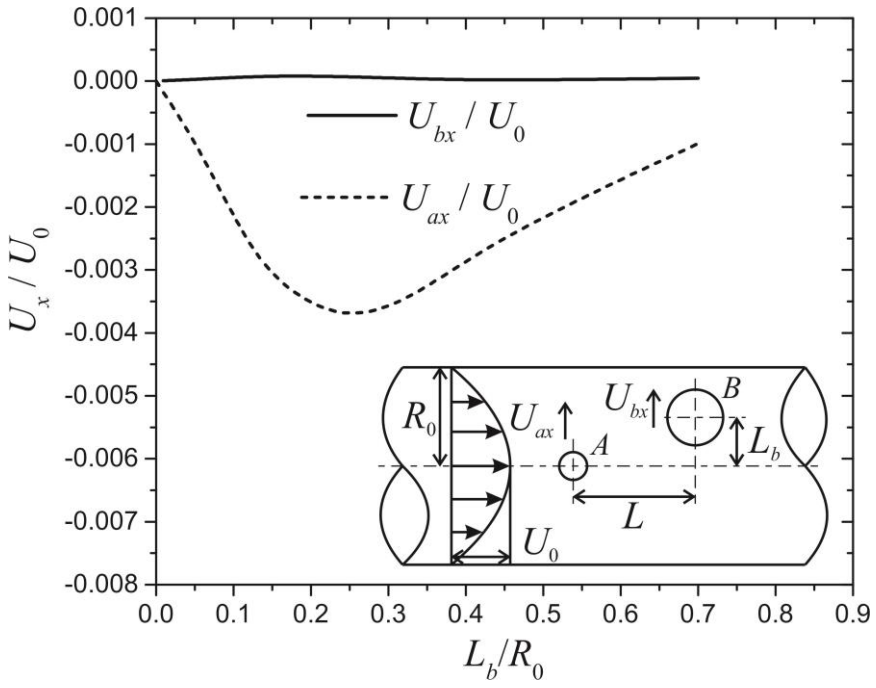

Figure 4.24: Normalized translational velocities of the two particles in *X*-direction with a/R_0=0.05, b/R_0=0.1 and L/R_0=0.2.

Figure 4.24 shows the translational velocities of the two particles in *X*-direction with the larger particle spacing L/R_0=0.2. Similar to the configuration described

earlier, the lateral distance L_b/R_0 can be changed from zero. As discussed in the previous section, particle *A* moves downward with the negative translational velocity. With L_b/R_0 increasing, the magnitude of the velocity increases to a maximum value and then decreases. Interestingly, the change rate of the velocity before and after the maximum magnitude is different. When $L_b/R_0=0$, it is an axisymmetric model. However, the presence of the lateral distance will break the axisymmetric conditions immediately. So when the flow passes around particle *A* and recovers back, the fluids above and below the axis are different due to the distortion of particle *B*. This variation causes the significant net movement of the fluid in the *X*-direction between the two particles which induces the lateral movements of them. With L_b/R_0 increasing, the fluid is easier to flow between the two particles causing the lateral velocity rapidly increases to the maximum value. As the two particles are far away from each other, the velocity decreases with smaller change rate indicating the particle-particle interaction weakens. However, the variation of the velocity of particle *B* is negligible indicating the particle-particle interaction on particle B is weak. This phenomenon is similar with the one discussed in Figure 4.16.

The case with the smaller particle spacing is also considered (Figure 4.25). We vary L_b/R_0 from a minimum value to ensure the two particles will not collide. When the two particles are very close to each other, the magnitude of the velocity of particle *A* does not reach the maximum value even the particle-particle interaction is the strongest. The reason is that the space between the two particles is narrow and the volume of the fluid going through is limited. As

L_b/R_0 increasing, the magnitude increases to the maximum value and then decreases indicating the particle-particle interaction dwindles. However, the change of the velocity of particle *B* is monotonous with L_b/R_0 increasing which is similar as the one described in Figure 4.19.

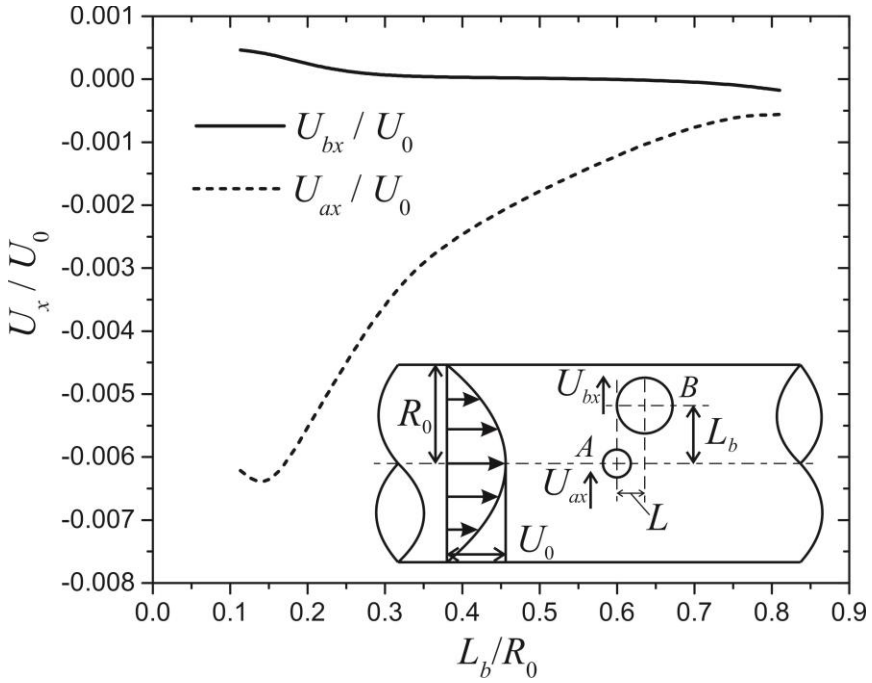

Figure 4. 25: Normalized translational velocities of the two particles in *X*-direction with a/R_0=0.05, b/R_0=0.1 and L/R_0=0.1.

Figure 4.26 and 4.27 represent the translational velocities in *Z*-direction of the two particles. The advection due to the Poiseuille Flow dominates the flow behavior even when the two particles are very close. The velocity of particle *A* is nearly a constant and always larger than the one of particle *B*.

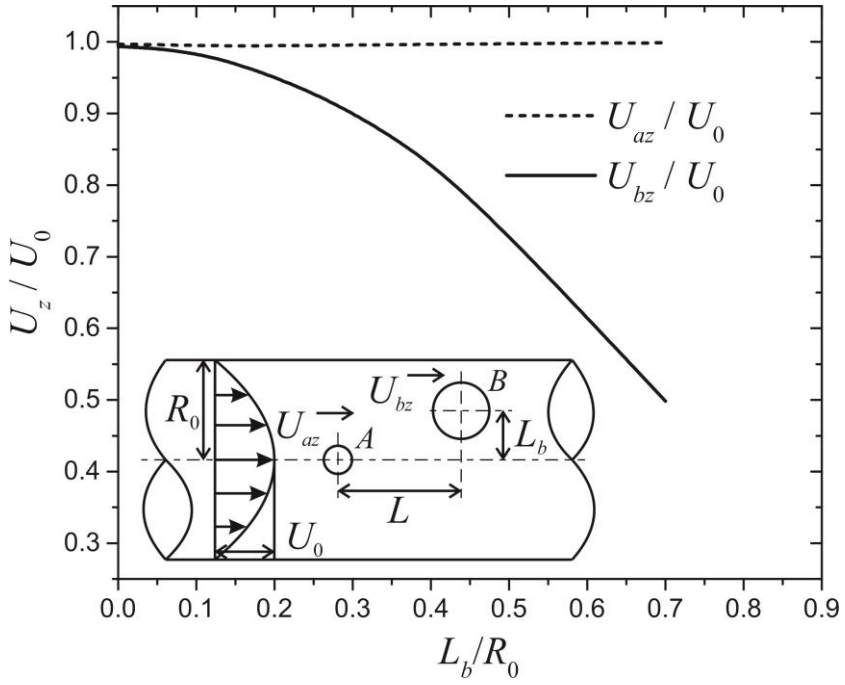

Figure 4.26: Normalized translational velocities of the two particles in *Z*-direction with a/R_0=0.05, b/R_0=0.1 and L/R_0=0.2.

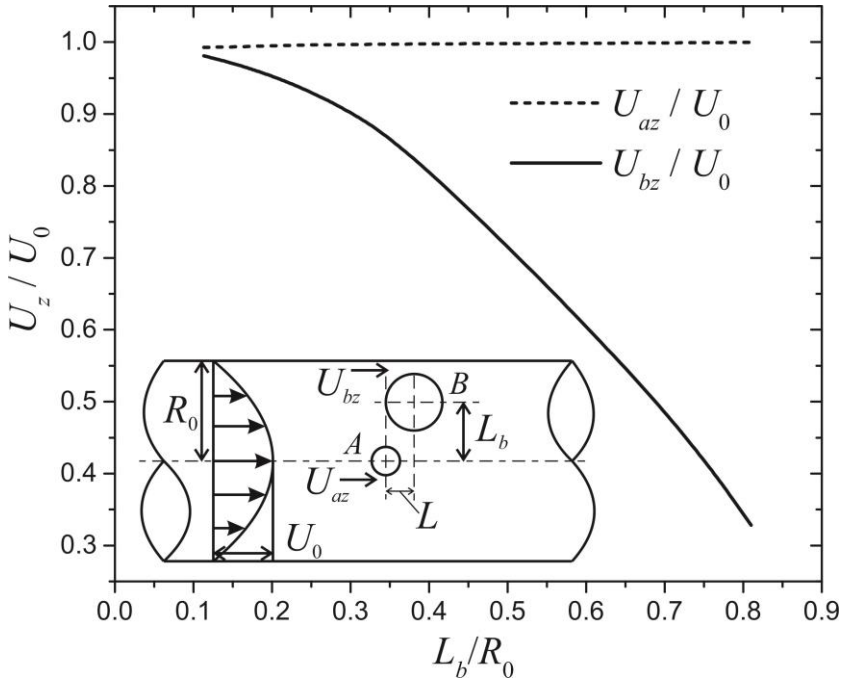

Figure 4.27: Normalized translational velocities the two particles in *Z*-direction with a/R_0=0.05, b/R_0=0.1 and L/R_0=0.1.

Unlike previous discussion, the particle-particle interaction on the rotational velocities of the two particles is weak (Figure 4.28 and 4.29). In these two figures, the rotational velocity of particle *B* follows a straight line due to the linear gradient of the Poiseuille Flow in the radial direction even when the two particles are very close. This indicates the particle-particle interaction on the rotational velocity of particle *B* is negligible.

The variation of the translational velocity of particle *A* is small. When the two particles are very close, the magnitude has a maximum value and then decreases to zero with the particle spacing increasing.

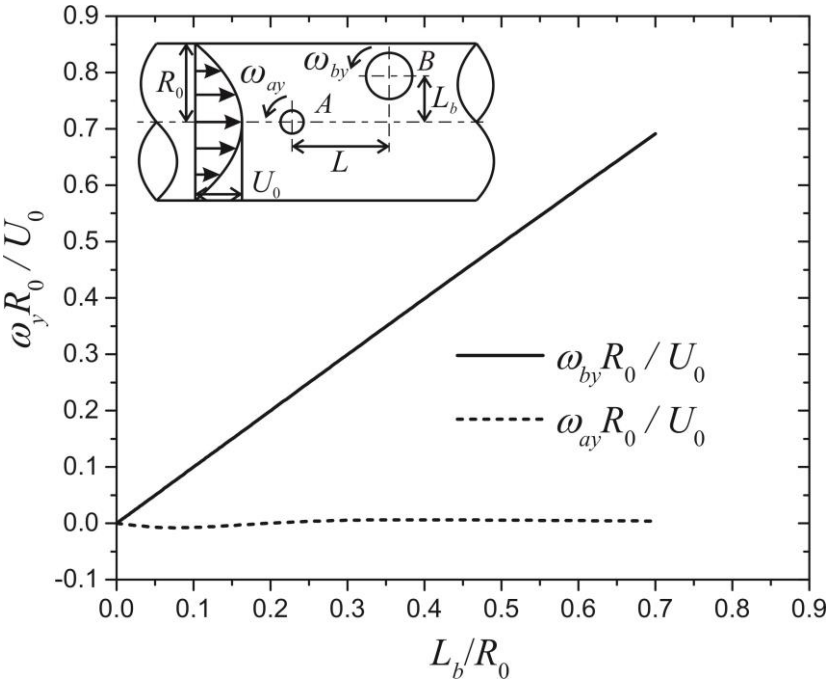

Figure 4.28: Normalized rotational velocities of the two particles in *Y*-direction with a/R_0=0.05, b/R_0=0.1 and L/R_0=0.2.

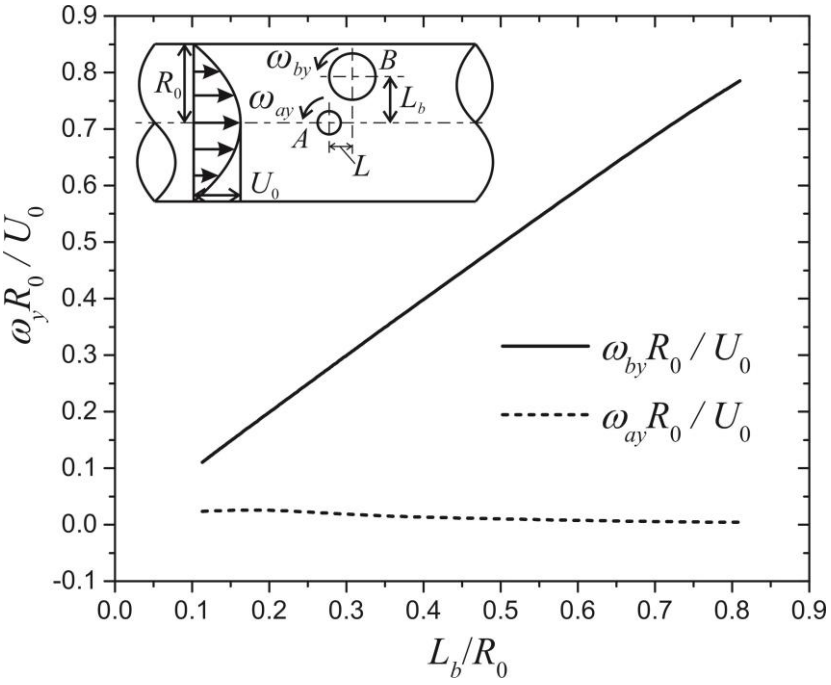

Figure 4.29: Normalized rotational velocities of the two particles in *Y*-direction with a/R_0=0.05, b/R_0=0.1 and L/R_0=0.1.

As discussed earlier, the particle-particle interaction can be neglected when the separation distance is three times larger than the sum of particles radii. It is interesting, when particle *B* is bigger, the particle-particle interaction cannot be neglected even if the separation distance is large. When the separation distance is three times larger than the sum of particles radii (Figure 4.24), the magnitude of the velocity of particle *A* is about eighty percent of the maximum value indicating the particle-particle interaction has certain influences on the particle behavior. Although the particle-particle interaction has negligible influences on the translational velocity in the *Z*-direction and rotational velocity in the *Y*-direction, it cannot be neglected. Nevertheless, by comparing Figure 4.24 with 4.26, we find that the translational velocities of the two particles in the *Z*-

direction are two orders of magnitudes higher than that in the lateral direction. This indicates the lateral shift is small. Therefore, the separation distance to neglect the particle-particle interaction should be considered depending on the specific application.

In this section, we focus on the velocities of the two particles with one off the axis. We find that when the two particles travel within the tube, the fluid can pushes them into opposite lateral directions which are different from the single particle case. The Poiseuille Flow dominates the translational velocities of the two particles along the axis. Meanwhile, the hydrodynamic interaction can make the particle rotate in an opposite direction of the single particle case. Such analysis can provide unprecedented flow prediction for the motion of multi particles case.

4.3 Two particles in the same cross sectional area

We also consider the two particles moving in the same cross sectional area (L=0). The two particles are identical with normalized radius a/R_0=b/R_0=0.02. We set particle A along the X-direction with lateral distance L_a/R_0=0.02 and particle B with L_b/R_0= 0.07 (Figure 4.30). The azimuthal angle φ_{ab} is changed as a variable to analyze the velocities of the two particles. To better highlight the velocities of particle B, we further construct a body-fixed frame xyz such that the origin is set at the center of particle B and its z-axis is always parallel to the axis of the tube. Due to this configuration, particle A has the translational velocity in Z direction (U_{aZ}) and rotational velocities in X (ω_{aX}) and Y-direction (ω_{aY}). Similarly, particle B has the translational velocity in z-direction (U_{bz}) and rotational velocities in x (ω_{bx}) and y-direction (ω_{by}) of the body-fixed frame.

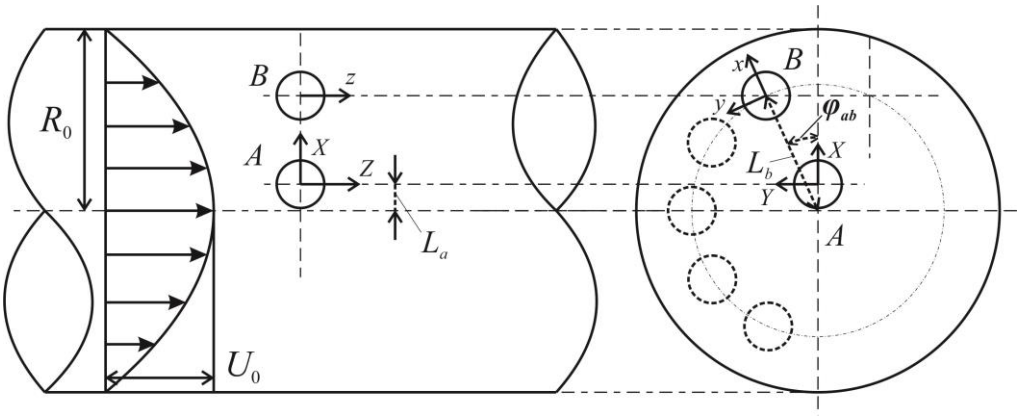

Figure 4.30: Schematics of two rigid particles in the same cross sectional area in a cylindrical tube.

Figure 4.31 shows the normalized translational velocities of the two particles in the same cross sectional area. As discussed earlier, the velocities of the two

particles are dominated by the advection due to the Poiseuille Flow. The velocities are nearly a constant and the magnitude for particle *A* is larger than the one for particle *B* since particle *A* is closer to the axis of the tube.

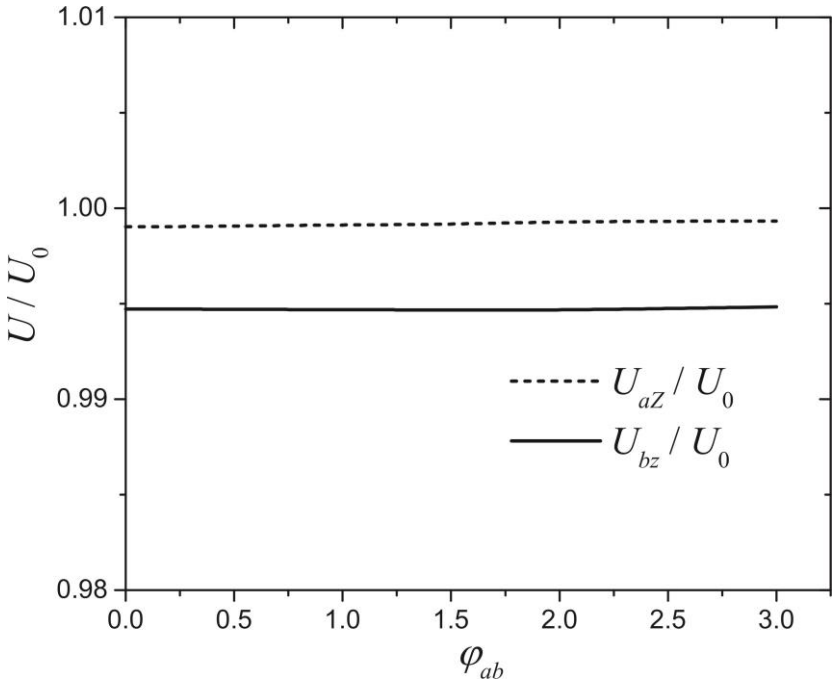

Figure 4.31: Normalized translational velocities of the two particles in the same cross sectional area.

Since the difference of the lateral distance of particle *A* and particle *B* is larger than the sum of the radii of the two particles, the azimuthal angle φ_{ab} can be varied from zero. When φ_{ab}=0, particle *B* is situated above particle *A* and the *x*-axis is parallel to the *X*-axis. The two particles have symmetrical positions with respect to the *X*-axis, so the rotational velocities ω_{aX} and ω_{bx} are zero (Figure 4.32). With φ_{ab} increasing, the fluid is allowed to flow between the two particles which pushes them rotate in the opposite directions. The magnitude of

the two velocities increases to a maximum value and then decreases to zero which indicate the particle-particle interaction can be neglected.

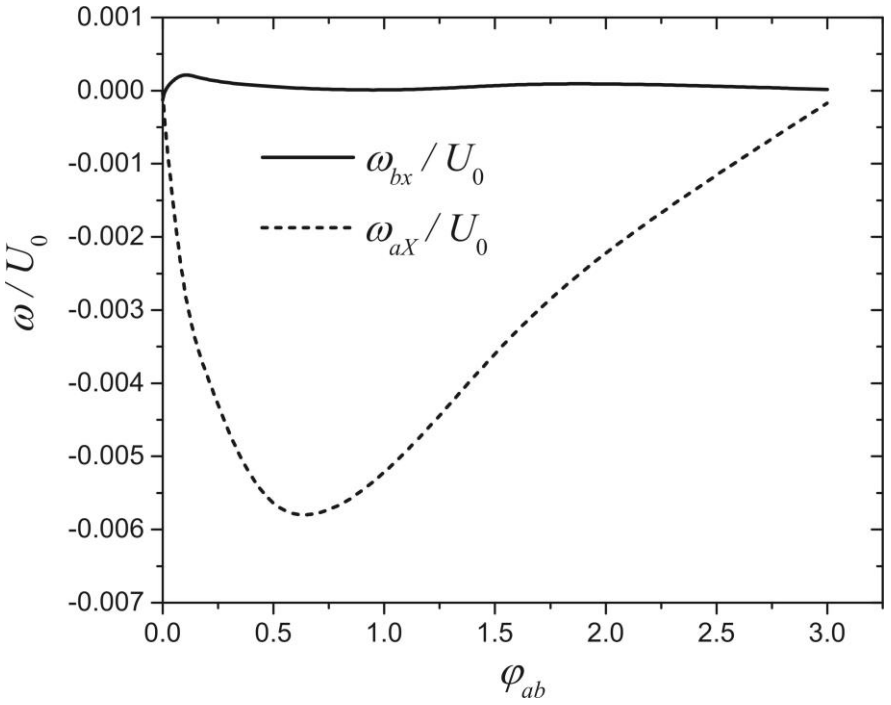

Figure 4.32: Normalized rotational velocities of the two particles in the same cross sectional area: ω_{aX}/U_0 and ω_{bx}/U_0.

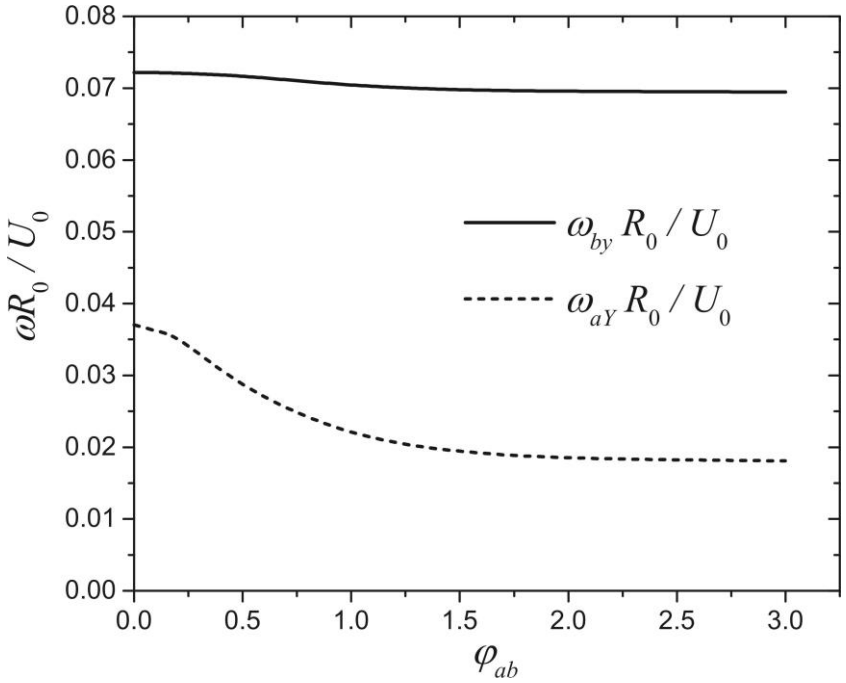

Figure 4.33: Normalized rotational velocities of the two particles in the same cross sectional area: ω_{aY}/U_0 and ω_{by}/U_0.

Figure 4.33 shows the rotational velocities of the two particles due to the Poiseuille Flow. When the two particles are very close, the magnitude of the velocities has a maximum value and then decreases to a constant with φ_{ab} increasing. Similar with the discussion of Figure 4.22, the velocity of particle *B* is larger than the one of particle *A*.

In this section, the motion of the two particles travelling in the same cross sectional area has been analyzed. The Poiseuille Flow dominates the translational velocity and the magnitude is nearly a constant. Unlike the single particle case, the particle-particle interaction can induce extra rotational velocities of the two particles. Such analysis can give us insights to predict the motion of multi particles case.

Chapter 5

Conclusions and Future Work

5.1 Conclusions

In this thesis, a systematic procedure to calculate the slow viscous flow of two particles with arbitrary positions travelling in a cylindrical tube is presented. This procedure is established with the method of reflections which can treat the boundary conditions of particles and the tube separately. Lamb's general solution is employed to calculate the flow field in spherical coordinates according to the spherical harmonics. In the cylindrical coordinates, a systematic procedure is proposed by using the orthogonally relationships and Fourier integral with reference to cylindrical harmonics which is more general than the previous method.

By utilizing this procedure, we investigate three specific cases of the two particles travelling in the cylindrical tube. The three characteristic cases can cover all the possible configurations, since the motion of two particles with arbitrary positions can be considered as a combination of the three cases. The main conclusions of this thesis consist of the following parts:

(1) The particle-particle interaction can affect the velocity gradient significantly which is responsible for the drag force coefficients. When the two particles travel along the axis of the tube, the particle-particle interaction can enhance the drag force magnitude arising from the particle motion and reduce the one related to the background flow.

(2) There exists an asymmetric circulation area when the two particles have the different sizes. The presence of the circulation area can reduce the drag force since the velocity gradient inside the area is smaller than the one outside. This indicates the circulation area can enhance the movement of the particle.

(3) The fluid can pushes the two particles into opposite lateral directions which are different from the single particle case. The magnitude of the lateral velocities of the two particles is two orders smaller than that in the axis direction. The effect of particle-particle interaction on the smaller particle is significantly stronger than the bigger one. The Poiseuille Flow dominates the flow behavior along the axis and the variation of the velocity in this direction is small. In addition, unlike the single particle case, the particle-particle interaction can induce extra rotational velocities of the two particles.

(4) The direction of Poiseuille Flow, particle position relative to the axis and particle size can make the two particles attract and repel. The particle-particle interaction can be neglected when the separation distance is three times larger than the sum of particles radii when the two particles are identical. If the two particles have different sizes, the separation distance to neglect the particle-particle interaction should be considered depending on the specific application. Such analysis can give us insights to understand the mechanisms of collision and aggregation of particles.

The main objective of this work has been achieved. A developed mathematical procedure which is capable of solving the motion of two particles with arbitrary positions in the tube has been successfully carried out. Furthermore, the two-particle approach can then be extended to multiple particles problem by extending the boundary conditions based on the method of reflections. The investigation on such case has provided significant flow prediction for the motion of particles travelling in a tube.

5.2 Future work

With the systematic procedure proposed in this thesis, the motion of two particles travelling in a cylindrical tube at low Reynolds number has been analyzed. The investigation has provided the insight to carry on the further research for particles travelling in a channel.

(1) In general, microfluidics channels have rectangular cross sections in the experiment due to the fabrication process of objects with small scale. As the extension of current study, the theory of slow viscous flow past two spheres in a rectangular channel will be investigated. For rectangular channel which is described in Cartesian coordinates, the general solution will be derived. We intend to employ conformal mapping method to transform the rectangular boundary into cylinder. The procedure we proposed in chapter 3 can be then used. Developing such model concerns the detailed flow field of particles in microchannel for microfluidic system, with the prospect of exploring the adaptability of such an instrument to industrial applications

(2) Furthermore, we intend to conduct experiments using a microfluidic system to validate the theoretical model. The rectangular channel can be fabricated using soft lithography technique or 3D printer. Using image processing technique, we can capture the velocity of two particles.

Reference

1. Schneider, T., *The general circulation of the atmosphere.* Annual Review of Earth and Planetary Sciences, 2006. **34**: p. 655-688.
2. Prather, K.A., C.D. Hatch, and V.H. Grassian, *Analysis of Atmospheric Aerosols.* Annual Review of Analytical Chemistry, 2008. **1**: p. 485-514.
3. McCave, I.N., *Size spectra and aggregation of suspended particles in the deep ocean.* Deep Sea Research Part A. Oceanographic Research Papers, 1984. **31**(4): p. 329-352.
4. Burd, A.B. and G.A. Jackson, *Particle aggregation.* Annual Review of Marine Science, 2009. **1**: p. 65-90.
5. Schoch, R.B., J.Y. Han, and P. Renaud, *Transport phenomena in nanofluidics.* Reviews of Modern Physics, 2008. **80**(3): p. 839-883.
6. Brenner, H., *The Stokes resistance of an arbitrary particle.* Chemical Engineering Science, 1963. **18**(1): p. 1-25.
7. Brenner, H., *The Stokes resistance of an arbitrary particle—II: An extension.* Chemical Engineering Science, 1964. **19**(9): p. 599-629.
8. Stimson, M. and G.B. Jeffery, *The motion of two spheres in a viscous fluid.* Proceedings of the Royal Society of London Series a-Containing Papers of a Mathematical and Physical Character, 1926. **111**(757): p. 110-116.
9. Goldman, A.J., R.G. Cox, and H. Brenner, *The slow motion of two identical arbitrarily oriented spheres through a viscous fluid.* Chemical Engineering Science, 1966. **21**(12): p. 1151-1170.
10. Jeffrey, D.J. and Y. Onishi, *Calculation of the resistance and mobility functions for two unequal rigid spheres in low-Reynolds-number flow.* Journal of Fluid Mechanics, 1984. **139**: p. 261-290.
11. Kim, S. and R.T. Mifflin, *The resistance and mobility functions of two equal spheres in low-Reynolds-number flow.* Physics of Fluids, 1985. **28**(7): p. 2033-2045.
12. Ardekani, A.M. and R.H. Rangel, *Unsteady motion of two solid spheres in Stokes flow.* Physics of Fluids, 2006. **18**(10).
13. Kim, S., *Stokes flow past three spheres: An analytic solution.* Physics of Fluids, 1987. **30**(8 , Aug. 1987): p. 2309-2314.
14. Wilson, H.J., *Stokes flow past three spheres.* Journal of Computational Physics, 2013. **245**: p. 302-316.
15. Ho, C.-M. and Y.-C. Tai, *Micro-electro-mechanical-systems (mems) and fluid flows.* Annual Review of Fluid Mechanics, 1998. **30**(1): p. 579.
16. Martinez, M.J. and K.S. Udell, *Axisymmetric creeping motion of drops through circular tubes.* Journal of Fluid Mechanics, 1990. **210**: p. 565-591.
17. Bhattacharya, S. and C. Mishra, *Analysis of general creeping motion of a sphere inside a cylinder.* Journal of Fluid Mechanics, 2010. **642**: p. 295-328.
18. Pozrikidis, C., *The buoyancy-driven motion of a train of viscous drops within a cylindrical tube.* Journal of Fluid Mechanics, 1992. **237**: p. 627-648.

19. Coulliette, C. and C. Pozrikidis, *Motion of an array of drops through a cylindrical tube.* Journal of Fluid Mechanics, 1998. **358**: p. 1-28.
20. Brenner, H. and J. Happel, *Slow viscous flow past a sphere in a cylindrical tube.* Journal of Fluid Mechanics, 1958. **4**(2): p. 195-213.
21. Greenstein, T. and J. Happel, *Theoretical study of the slow motion of a sphere and a fluid in a cylindrical tube.* Journal of Fluid Mechanics, 1968. **34**(04): p. 705-710.
22. Keh, H.J. and Y.C. Chang, *Creeping motion of a slip spherical particle in a circular cylindrical pore.* International Journal of Multiphase Flow, 2007. **33**(7): p. 726-741.
23. Sonshine, R.M. and H. Brenner, *The stokes translation of two or more particles along the axis of an infinitely long circular cylinder.* Applied Scientific Research, 1966. **16**(1): p. 425-454.
24. Greenste.T and J. Happel, *The slow motion of two particles symmetrically placed about the axis of a circular cylinder in a direction perpendicular to their line of centers.* Applied Scientific Research, 1970. **22**(5): p. 345-&.
25. Navardi, S. and S. Bhattacharya, *General methodology to evaluate two-particle hydrodynamic friction inside cylinder-bound viscous fluid.* Computers and Fluids, 2013. **76**: p. 149-169.
26. Brenner, H., *The Stokes resistance of an arbitrary particle—III: Shear fields.* Chemical Engineering Science, 1964. **19**(9): p. 631-651.
27. Brenner, H., *The Stokes resistance of an arbitrary particle—IV Arbitrary fields of flow.* Chemical Engineering Science, 1964. **19**(10): p. 703-727.
28. Yick, K.Y., et al., *Enhanced drag of a sphere settling in a stratified fluid at small Reynolds numbers.* Journal of Fluid Mechanics, 2009. **632**: p. 49-68.
29. Ardekani, A.M. and R. Stocker, *Stratlets: Low Reynolds Number Point-Force Solutions in a Stratified Fluid.* Physical Review Letters, 2010. **105**(8): p. 084502.
30. Prakash, J. and G.P.R. Sekhar, *Arbitrary oscillatory Stokes flow past a porous sphere using Brinkman model.* Meccanica, 2012. **47**(5): p. 1079-1095.
31. Yadav, P.K., *Slow Motion of a Porous Cylindrical Shell in a concentric cylindrical cavity.* Meccanica, 2013. **48**(7): p. 1607-1622.
32. Saad, E.I., *Stokes flow past an assemblage of axisymmetric porous spherical shell-in-cell models: effect of stress jump condition.* Meccanica, 2013. **48**(7): p. 1747-1759.
33. Brenner, H., *The slow motion of a sphere through a viscous fluid towards a plane surface.* Chemical Engineering Science, 1961. **16**(3-4): p. 242-251.
34. Goldman, A.J., R.G. Cox, and H. Brenner, *Slow viscous motion of a sphere parallel to a plane wall—I Motion through a quiescent fluid.* Chemical Engineering Science, 1967. **22**(4): p. 637-&.
35. Goldman, A.J., R.G. Cox, and H. Brenner, *Slow viscous motion of a sphere parallel to a plane wall—II Couette flow.* Chemical Engineering Science, 1967. **22**(4): p. 653-&.
36. Dagan, Z., R. Pfeffer, and S. Weinbaum, *Axisymmetric stagnation flow of a spherical particle near a finite planar surface at zero Reynolds number.* Journal of Fluid Mechanics, 1982. **122**(SEP): p. 273-294.
37. Oneill, M.E., *A sphere in contact with a plane wall in a slow linear shear flow.* Chemical Engineering Science, 1968. **23**(11): p. 1293-&.

38. Goren, S.L., *The normal force exerted by creeping flow on a small sphere touching a plane.* Journal of Fluid Mechanics, 1970. **41**: p. 619-&.
39. Sano, O. and H. Hasimoto, *The effect of two plane walls on the motion of a small sphere in a viscous fluid.* Journal of Fluid Mechanics, 1978. **87**(AUG): p. 673-694.
40. Ganatos, P., S. Weinbaum, and R. Pfeffer, *A strong interaction theory for the creeping motion of a sphere between plane parallel boundaries. Part 1. Perpendicular motion.* Journal of Fluid Mechanics, 1980. **99**(4 , Aug. 29, 1980): p. 739-753.
41. Ganatos, P., R. Pfeffer, and S. Weinbaum, *A strong interaction theory for the creeping motion of a sphere between plane parallel boundaries. Part 2. Parallel motion.* Journal of Fluid Mechanics, 1980. **99**(AUG): p. 755-783.
42. Dvinsky, A.S. and A.S. Popel, *Motion of a rigid cylinder between parallel plates in stokes flow: Part 1: Motion in a quiescent fluid and sedimentation.* Computers & Fluids, 1987. **15**(4): p. 391-404.
43. Dvinsky, A.S. and A.S. Popel, *Motion of a rigid cylinder between parallel plates in stokes flow: Part 2: Poiseuille and couette flow.* Computers & Fluids, 1987. **15**(4): p. 405-419.
44. Staben, M.E., A.Z. Zinchenko, and R.H. Davis, *Motion of a particle between two parallel plane walls in low-Reynolds-number Poiseuille flow.* Physics of Fluids, 2003. **15**(6): p. 1711-1733.
45. Staben, M.E., K.P. Galvin, and R.H. Davis, *Low-Reynolds-number motion of a heavy sphere between two parallel plane walls.* Chemical Engineering Science, 2006. **61**(6): p. 1932-1945.
46. Chang, Y.C. and H.J. Keh, *Slow motion of a slip spherical particle perpendicular to two plane walls.* Journal of Fluids and Structures, 2006. **22**(5): p. 647-661.
47. Lee, S.H., R.S. Chadwick, and L.G. Leal, *Motion of a sphere in the presence of a plane interface. Part 1. An approximate solution by generalization of the method of Lorentz.* Journal of Fluid Mechanics, 1979. **93**(pt 4): p. 705-726.
48. Lee, S.H. and L.G. Leal, *Motion of a sphere in the presence of a plane interface. Part 2. An exact solution in bipolar co-ordinates (Fluid Mechanics).* Journal of Fluid Mechanics, 1980. **98**(1): p. 193-224.
49. Berdan Ii, C. and L.G. Leal, *Motion of a sphere in the presence of a deformable interface: I. Perturbation of the interface from flat: the effects on drag and torque.* Journal of Colloid And Interface Science, 1982. **87**(1): p. 62-80.
50. Lee, S.H. and L.G. Leal, *The motion of a sphere in the presence of a deformable interface: II. A numerical study of the translation of a sphere normal to an interface.* Journal of Colloid And Interface Science, 1982. **87**(1): p. 81-106.
51. Yang, S.M. and L.G. Leal, *Particle motion in Stokes flow near a plane fluid-fluid interface. Part 1. Slender body in a quiescent fluid.* Journal of Fluid Mechanics, 1983. **136**(NOV): p. 393-421.
52. Yang, S.M. and L.G. Leal, *Particle motion in Stokes flow near a plane fluid–fluid interface. Part 2. Linear shear and axisymmetric straining flows.* Journal of Fluid Mechanics, 1984. **149**(DEC): p. 275-304.
53. Yang, S.M. and L.G. Leal, *Motions of a fluid drop near a deformable interface.* International Journal of Multiphase Flow, 1990. **16**(4): p. 597-616.

54. Chi, B.K. and L.G. Leal, *A theoretical study of the motion of a viscous drop toward a fluid interface at low Reynolds number.* Journal of Fluid Mechanics, 1989. **201**: p. 123-146.
55. Danov, K.D., et al., *Stokes flow caused by the motion of a rigid sphere close to a viscous interface.* Chemical Engineering Science, 1998. **53**(19): p. 3413-3434.
56. Pozrikidis, C., *Particle motion near and inside an interface.* Journal of Fluid Mechanics, 2007. **575**: p. 333-357.
57. Geller, A.S., S.H. Lee, and L.G. Leal, *The creeping motion of a spherical particle normal to a deformable interface.* Journal of Fluid Mechanics, 1986. **169**: p. 27-69.
58. Oneill, M.E. and S.R. Majumdar, *Asymmetrical slow viscous fluid motions caused by the translation or rotation of two spheres. Part I: The determination of exact solutions for any values of the ratio of radii and separation parameters.* Zeitschrift Fur Angewandte Mathematik Und Physik, 1970. **21**(2): p. 164-&.
59. Oneill, M.E. and S.R. Majumdar, *Asymmetrical slow viscous fluid motions caused by the translation or rotation of two spheres. Part II: Asymptotic forms of the solutions when the minimum clearance between the spheres approaches zero.* Zeitschrift Fur Angewandte Mathematik Und Physik, 1970. **21**(2): p. 180-&.
60. Keh, H.J. and S.H. Chen, *Low-Reynolds-number hydrodynamic interactions in a suspension of spherical particles with slip surfaces.* Chemical Engineering Science, 1997. **52**(11): p. 1789-1805.
61. Saad, E.I., *Motion of two spheres translating and rotating through a viscous fluid with slip surfaces.* Fluid Dynamics Research, 2012. **44**(5): p. 18.
62. Yoon, B.J. and S. Kim, *Note on the direct calculation of mobility functions for two equal-sized spheres in Stokes flow.* Journal of Fluid Mechanics, 1987. **185**: p. 437-446.
63. Ying, R.X. and M.H. Peters, *Hydrodynamic interaction of two unequal-sized spheres in a slightly rarefied gas: resistance and mobility functions.* Journal of Fluid Mechanics, 1989. **207**: p. 353-378.
64. Jeffrey, D.J., *The calculation of the low Reynolds number resistance functions for two unequal spheres.* Physics of Fluids a-Fluid Dynamics, 1992. **4**(1): p. 16-29.
65. Cooley, M.D.A. and M.E. Oneill, *On the slow motion of two spheres in contact along their line of centres through a viscous fluid.* Proceedings of the Cambridge Philosophical Society-Mathematical and Physical Sciences, 1969. **66**: p. 407-&.
66. Oneill, M.E., *On asymmetrical slow viscous flows caused by the motion of two equal spheres almost in contact.* Proceedings of the Cambridge Philosophical Society-Mathematical and Physical Sciences, 1969. **65**: p. 543-&.
67. Nir, A. and A. Acrivos, *On the creeping motion of two arbitrary-sized touching spheres in a linear shear field.* Journal of Fluid Mechanics, 1973. **59**(JUN19): p. 209-223.
68. Sun, R. and A.T. Chwang, *Interactions between two touching spherical particles in sedimentation.* Physical Review E, 2007. **76**(4).

69. Ekiel-Jezewska, M.L., et al., *Hydrodynamic interactions between two spheres at contact.* Physical Review E, 1999. **59**(3): p. 3182-3191.
70. Ekiel-Jezewska, M.L., et al., *Rotation due to hydrodynamic interactions between two spheres in contact.* Physical Review E, 2002. **66**(5).
71. Zhao, Y. and R.H. Davis, *Interaction of two touching spheres in a viscous fluid.* Chemical Engineering Science, 2002. **57**(11): p. 1997-2006.
72. Brenner, H. and M.E. Oneill, *On the Stokes resistance of multiparticle systems in a linear shear field.* Chemical Engineering Science, 1972. **27**(7): p. 1421-&.
73. Clercx, H.J.H. and P. Schram, *Three particle hydrodynamic interactions in suspensions.* Journal of Chemical Physics, 1992. **96**(4): p. 3137-3151.
74. Cichocki, B., et al., *Friction and mobility of many spheres in Stokes flow.* Journal of Chemical Physics, 1994. **100**(5): p. 3780-3790.
75. Haber, S. and H. Brenner, *Hydrodynamic interactions of spherical particles in quadratic Stokes flows.* International Journal of Multiphase Flow, 1999. **25**(6-7): p. 1009-1032.
76. Filippov, A.V., *Drag and torque on clusters of N-arbitrary spheres at low Reynolds number.* Journal of Colloid and Interface Science, 2000. **229**(1): p. 184-195.
77. Ekiel-Jezewska, M.L. and E. Wajnryb, *Equilibria for the relative motion of three heavy spheres in Stokes fluid flow.* Physical Review E, 2006. **73**(4).
78. Ekiel-Jezewska, M.L. and B.U. Felderhof, *Hydrodynamic interactions between a sphere and a number of small particles.* Journal of Chemical Physics, 2015. **142**(1): p. 5.
79. Hollander, W. and S.K. Zaripov, *Hydrodynamically interacting droplets at small Reynolds numbers.* International Journal of Multiphase Flow, 2005. **31**(1): p. 53-68.
80. Faltas, M.S., H.H. Sherief, and E.A. Ashmawy, *Interaction of two spherical particles rotating in a micropolar fluid.* Mathematical and Computer Modelling, 2012. **56**(9-10): p. 229-239.
81. Fuentes, Y.O., S. Kim, and D.J. Jeffrey, *Mobility functions for two unequal viscous drops in Stokes flow. I. Axisymmetric motions.* Physics of Fluids, 1988. **31**(9): p. 2445-2455.
82. Fuentes, Y.O., S. Kim, and D.J. Jeffrey, *Mobility functions for two unequal viscous drops in Stokes flow. II. Asymmetric motions.* Physics of Fluids A, 1989. **1**(1): p. 61-76.
83. Stoos, J.A., S.M. Yang, and L.G. Leal, *Hydrodynamic interaction of a small fluid particle and a spherical drop in low-reynolds number flow.* International Journal of Multiphase Flow, 1992. **18**(6): p. 1019-1044.
84. Keh, H.J. and Y.K. Tseng, *Slow motion of multiple droplets in arbitrary three-dimensional configurations.* Aiche Journal, 1992. **38**(12): p. 1881-1904.
85. Baldessari, F. and L.G. Leal, *Two touching spherical drops in uniaxial extensional flow: Analytic solution to the creeping flow problem.* Journal of Colloid And Interface Science, 2005. **289**(1): p. 262-270.
86. Pozrikidis, C., *Interception of two spherical drops in linear Stokes flow.* Journal of Engineering Mathematics, 2010. **66**(4): p. 353-379.
87. Wang, H. and R. Skalak, *Viscous flow in a cylindrical tube containing a line of spherical particles.* Journal of Fluid Mechanics, 1969. **38**: p. 75-&.

88. Chen, T.C. and R. Skalak, *Stokes flow in a cylindrical tube containing a line of spheroidal particles.* Applied Scientific Research, 1970. **22**(6): p. 403-&.
89. Leichtberg, S., R. Pfeffer, and S. Weinbaum, *Stokes flow past finite coaxial clusters of spheres in a circular cylinder.* International Journal of Multiphase Flow, 1976. **3**(2): p. 147-169.
90. Happel, J.R. and H. Brenner, *Low Reynolds Number Hydrodynamics: With Special Applications to Particulate Media*. 1965: Prentice-Hall.
91. Kim, S. and S.J. Karrila, *Microhydrodynamics: Principles And Selected Applications*. 1991: Dover.
92. Lamb, H., *Hydrodynamics*. 1895: At the University Press.
93. Hobson, E.W., *The theory of spherical and ellipsoidal harmonics / E.W. Hobson*. 2012: Cambridge : Cambridge University Press, 2012.
94. MacRobert, T.M. and I.N. Sneddon, *Spherical harmonics : an elementary treatise on harmonic functions with applications / by T. M. Macrobert*. International series of monographs in pure and applied mathematics: v. 98. 1967: Oxford ; New York : Pergamon Press, 1967.3d ed. rev. / with the assistance of I.N. Sneddon.
95. Kreyszig, E., *Advanced engineering mathematics / Erwin Kreyszig*. 1993: New York : Wiley, c1993.7th ed.
96. Lamb, H.S., *Hydrodynamics / by Sir Horace Lamb*. 1993: Cambridge : Cambridge University Press, 1993.6th ed.

Appendix

Mathematica code: Solution of slow viscous flow of two particles travelling along the axis of a cylindrical tube. The two particles have different sizes with a/R_0=0.1 and b/R_0=0.3. a and b are the radius of particle A and particle B respectively. The particle spacing is L/R_0=0.5. The two particles only have the translational velocity in the axial direction.

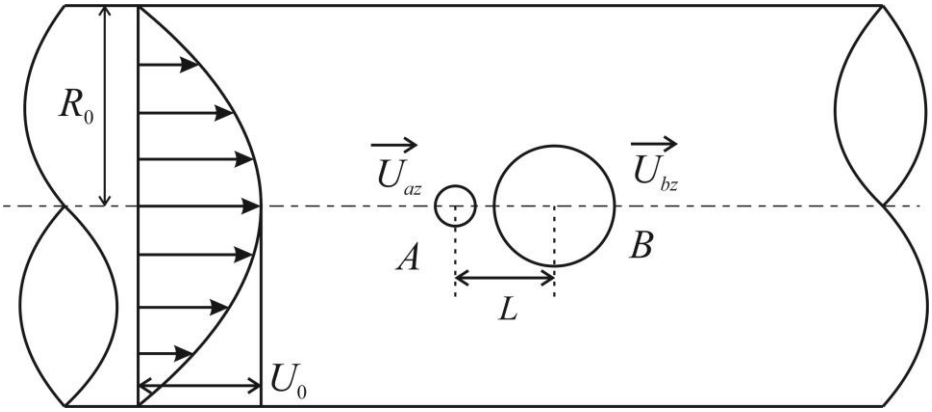

```
(*Initial conditions*)
mat = {{Sin[θa] * Cos[ϕa], Cos[θa] * Cos[ϕa], -Sin[ϕa]},
    {Sin[θa] * Sin[ϕa], Cos[θa] * Sin[ϕa], Cos[ϕa]},
    {Cos[θa], -Sin[θa], 0}};
mata = {{Cos[ϕa] Sin[θa], Sin[θa] Sin[ϕa], Cos[θa]},
    {Cos[θa] Cos[ϕa], Cos[θa] Sin[ϕa], -Sin[θa]},
    {-Sin[ϕa], Cos[ϕa], 0}};
mbt = {{Sin[θb] * Cos[ϕb], Cos[θb] * Cos[ϕb], -Sin[ϕb]},
    {Sin[θb] * Sin[ϕb], Cos[θb] * Sin[ϕb], Cos[ϕb]},
    {Cos[θb], -Sin[θb], 0}};
mbtb = {{Cos[ϕb] Sin[θb], Sin[θb] Sin[ϕb], Cos[θb]},
    {Cos[θb] Cos[ϕb], Cos[θb] Sin[ϕb], -Sin[θb]},
    {-Sin[ϕb], Cos[ϕb], 0}};
mct = {{Cos[Φ], -Sin[Φ], 0}, {Sin[Φ], Cos[Φ], 0}, {0, 0, 1}};
mctc = {{Cos[Φ], Sin[Φ], 0}, {-Sin[Φ], Cos[Φ], 0}, {0, 0, 1}};
rc0 = 1.;
a = 0.1;
b = 0.3;
La = 0.;
Lb = 0.;
L = 0.5;
ϕab = 0.;
kh = 1;
sphenumber = 4;
slimitupp = 0.00005;
slimitup = 0.00005;
h = 1000;
λh = 40;
ωax = 0;
ωay = 0;
ωaz = 0;
ωbx = 0;
ωby = 0;
ωbz = 0;
v[0] = {0, 0, U0 * (1 - rc * rc * rc0^-1 * rc0^-1) - Ua}
ωa = {ωax, ωay, ωaz};
ωb = {ωbx, ωby, ωbz};
rav = {ram * Sin[θa] * Cos[ϕa],
    ram * Sin[θa] * Sin[ϕa], ram * Cos[θa]};
rbv = {rbm * Sin[θb] * Cos[ϕb], rbm * Sin[θb] * Sin[ϕb],
    rbm * Cos[θb]};
```

```
vam = Cross[ωa, rav] - v[0] /.
  {rc → √(a^2 * Sin[θa] * Sin[θa] + La * La +
       2 * La * a * Sin[θa] * Cos[ϕa]), ram → a}

(*Spherical harmonics with reference to particle A*)

fgetXa[vam_] :=
  (Vaxm = ({Sin[θa] * Cos[ϕa], Sin[θa] * Sin[ϕa], Cos[θa]}).
      (vam) /. ϕa → 0.2;
   For[i = 1, i < sphenumber + 1, i++,
    Xa[i] = Chop[(2 * i + 1) * 4^-1 * π^-1 *
       (Ua * NIntegrate[2 * π * Sin[θa] * (Coefficient[Vaxm, Ua,
             1]) * LegendreP[i, Cos[θa]], {θa, 0, π},
          AccuracyGoal → 5] + U0 * NIntegrate[2 * π *
           Sin[θa] * (Coefficient[Vaxm, U0, 1]) * LegendreP[
            i, Cos[θa]], {θa, 0, π}, AccuracyGoal → 5] +
        Ub * NIntegrate[2 * π * Sin[θa] * (Coefficient[
             Vaxm, Ub, 1]) * LegendreP[i, Cos[θa]], {θa, 0, π},
          AccuracyGoal → 5]) * LegendreP[i, Cos[θa]]]]);
fgetYa[vam_] :=
  (Vaym = (-D[({0, 1, 0}.(Sin[θa] * (mata.vam))), θa] / Sin[θa] -
      ({1, 0, 0}.(mata.vam)) * 2) /. ϕa → 0.2;
   For[i = 1, i < sphenumber + 1, i++,
    Ya[i] = Chop[(2 * i + 1) * 4^-1 * π^-1 *
       (Ua * NIntegrate[2 * π * Sin[θa] * (Coefficient[Vaym, Ua,
             1]) * LegendreP[i, Cos[θa]], {θa, 0, π},
          AccuracyGoal → 5] + U0 * NIntegrate[2 * π *
           Sin[θa] * (Coefficient[Vaym, U0, 1]) * LegendreP[
            i, Cos[θa]], {θa, 0, π}, AccuracyGoal → 5] +
        Ub * NIntegrate[2 * π * Sin[θa] * (Coefficient[
             Vaym, Ub, 1]) * LegendreP[i, Cos[θa]], {θa, 0, π},
          AccuracyGoal → 5]) * LegendreP[i, Cos[θa]]]]);
```

```
fgetXa[vam];
fgetYa[vam];
For[i = 1, i < sphenumber + 1, i++, pa[-(i + 1)] = μ * (2 * i - 1) *
    a^-1 * (i + 1)^-1 * (a / ra)^(i+1) * ((i + 2) * Xa[i] + Ya[i])];
For[i = 1, i < sphenumber + 1, i++, Φa[-(i + 1)] =
   2^-1 * a * (i + 1)^-1 * (a / ra)^(i+1) * (i * Xa[i] + Ya[i])];
v[1] = Chop[mat.Sum[ Grad[Φa[-(i + 1)], {ra, θa, φa},
       "Spherical"] - (i - 2) * ra * ra * μ^-1 * 2^-1 * i^-1 * (2 * i - 1)^-1 *
       Grad[pa[-(i + 1)], {ra, θa, φa}, "Spherical"] +
      (i + 1) * μ^-1 * i^-1 * (2 * i - 1)^-1 * {ra, 0, 0} * pa[-(i + 1)],
     {i, sphenumber}]]
F[1] = FullSimplify[mat.
    (-4 * π * Grad[ra^3 * pa[-2], {ra, θa, φa}, "Spherical"])]

(*Coordinate transformation*)

vbm =
  Chop[Cross[ωb, rbv] + {0, 0, Ub - Ua} - v[0] - TrigExpand[v[1]] /.
    {rc → b * Sin[θb], rbm → b,
     Cos[θa] → (L + b * Cos[θb]) / √(b^2 + 2 * b * (L * Cos[θb]) + L * L),
     Sin[θa] → √(1 - (L + b * Cos[θb])^2 / (b^2 + L^2 + 2 * b * L * Cos[θb])),
     Cos[φa] → (Lb * Cos[φab] + b * Sin[θb] * Cos[φb] - La) /
       ((√(b^2 + 2 * b * Lb * Sin[θb] * Cos[(φab - φb)] +
             2 * b * (L * Cos[θb] - La * Sin[θb] * Cos[φb]) +
             La * La + Lb * Lb + L * L - 2 * La * Lb * Cos[φab])) *
         √(1 - (L + b * Cos[θb])^2 / (b^2 + L^2 + La^2 + Lb^2 + 2 *
                b * L * Cos[θb] - 2 * La * Lb * Cos[φab] + 2 * b *
                (Lb * Cos[φab - φb] - La * Cos[φb]) Sin[θb]))),
     Sin[φa] → (Lb * Sin[φab] + b * Sin[θb] * Sin[φb]) /
       ((√(b^2 + 2 * b * Lb * Sin[θb] * Cos[(φab - φb)] +
             2 * b * (L * Cos[θb] - La * Sin[θb] * Cos[φb]) +
             La * La + Lb * Lb + L * L - 2 * La * Lb * Cos[φab])) *
         √(1 - (L + b * Cos[θb])^2 / (b^2 + L^2 + La^2 + Lb^2 + 2 * b *
                L * Cos[θb] - 2 * La * Lb * Cos[φab] + 2 * b *
                (Lb * Cos[φab - φb] - La * Cos[φb]) Sin[θb]))),
     ra → √(b^2 + 2 * b * Lb * Sin[θb] * Cos[(φab - φb)] +
          2 * b * (L * Cos[θb] - La * Sin[θb] * Cos[φb]) +
          La * La + Lb * Lb + L * L - 2 * La * Lb * Cos[φab]),
     Tan[θa] → √(1 - (L + b * Cos[θb])^2 / (b^2 + L^2 + La^2 + Lb^2 +
                2 * b * L * Cos[θb] - 2 * La * Lb * Cos[φab] + 2 * b *
                (Lb * Cos[φab - φb] - La * Cos[φb]) Sin[θb])) /
```

```
((L + b * Cos[θb]) / √(b^2 + 2 * b * Lb * Sin[θb] *
        Cos[(ϕab - ϕb)] +
       2 * b * (L * Cos[θb] - La * Sin[θb] * Cos[ϕb]) +
       La * La + Lb * Lb + L * L - 2 * La * Lb * Cos[ϕab])),
Cot[θa] → (L + b * Cos[θb]) / √(b^2 + 2 * b * Lb *
       Sin[θb] * Cos[(ϕab - ϕb)] +
      2 * b * (L * Cos[θb] - La * Sin[θb] * Cos[ϕb]) +
      La * La + Lb * Lb + L * L - 2 * La * Lb * Cos[ϕab]) /
  (√(1 - (L + b * Cos[θb])^2 / (b^2 + L^2 + La^2 + Lb^2 +
         2 * b * L * Cos[θb] - 2 * La * Lb * Cos[ϕab] + 2 * b *
          (Lb * Cos[ϕab - ϕb] - La * Cos[ϕb]) Sin[θb]))),
Sec[θa] → √(b^2 + 2 * b * Lb * Sin[θb] * Cos[(ϕab - ϕb)] +
     2 * b * (L * Cos[θb] - La * Sin[θb] * Cos[ϕb]) +
     La * La + Lb * Lb + L * L - 2 * La * Lb * Cos[ϕab]) /
  ((L + b * Cos[θb])), Csc[θa] →
 1 / √(1 - (L + b * Cos[θb])^2 / (b^2 + L^2 + La^2 + Lb^2 +
        2 * b * L * Cos[θb] - 2 * La * Lb * Cos[ϕab] + 2 * b *
         (Lb * Cos[ϕab - ϕb] - La * Cos[ϕb]) Sin[θb]))}];

(*Spherical harmonics with reference to particle B*)
```

```
fgetXb[vbm_] :=
  (Vbxm = ({Sin[θb] * Cos[ϕb], Sin[θb] * Sin[ϕb], Cos[θb]}) .
      (vbm) /. ϕb → 0.2;
   For[i = 1, i < sphenumber + 1, i++,
    Xb[i] = Chop[(2 * i + 1) * 4^-1 * π^-1 *
       (Ua * NIntegrate[2 * π * Sin[θb] * (Coefficient[Vbxm, Ua,
             1]) * LegendreP[i, Cos[θb]], {θb, 0, π},
          AccuracyGoal → 5] + U0 * NIntegrate[2 * π *
           Sin[θb] * (Coefficient[Vbxm, U0, 1]) * LegendreP[
            i, Cos[θb]], {θb, 0, π}, AccuracyGoal → 5] +
        Ub * NIntegrate[2 * π * Sin[θb] * (Coefficient[
             Vbxm, Ub, 1]) * LegendreP[i, Cos[θb]], {θb, 0, π},
          AccuracyGoal → 5]) * LegendreP[i, Cos[θb]]]]);
fgetYb[vbm_] :=
  (Vbym = (-D[({0, 1, 0}.(Sin[θb] * (mbtb.vbm))), θb] / Sin[θb] -
      ({1, 0, 0}.(mbtb.vbm)) * 2) /. ϕb → 0.2;
   For[i = 1, i < sphenumber + 1, i++,
    Yb[i] = Chop[(2 * i + 1) * 4^-1 * π^-1 *
       (Ua * NIntegrate[2 * π * Sin[θb] * (Coefficient[Vbym, Ua,
             1]) * LegendreP[i, Cos[θb]], {θb, 0, π},
          AccuracyGoal → 5] + U0 * NIntegrate[2 * π *
           Sin[θb] * (Coefficient[Vbym, U0, 1]) * LegendreP[
            i, Cos[θb]], {θb, 0, π}, AccuracyGoal → 5] +
        Ub * NIntegrate[2 * π * Sin[θb] * (Coefficient[
             Vbym, Ub, 1]) * LegendreP[i, Cos[θb]], {θb, 0, π},
          AccuracyGoal → 5]) * LegendreP[i, Cos[θb]]]]);

fgetXb[vbm];
fgetYb[vbm];
For[i = 1, i < sphenumber + 1, i++, pb[-(i + 1)] = μ * (2 * i - 1) *
    b^-1 * (i + 1)^-1 * (b / rb)^(i+1) * ((i + 2) * Xb[i] + Yb[i])];
For[i = 1, i < sphenumber + 1, i++, Φb[-(i + 1)] =
   2^-1 * b * (i + 1)^-1 * (b / rb)^(i+1) * (i * Xb[i] + Yb[i])];
v[2] = Chop[mbt.Sum[Grad[Φb[-(i + 1)], {rb, θb, ϕb},
      "Spherical"] - (i - 2) * rb * rb * μ^-1 * 2^-1 * i^-1 * (2 * i - 1)^-1 *
      Grad[pb[-(i + 1)], {rb, θb, ϕb}, "Spherical"] +
     (i + 1) * μ^-1 * i^-1 * (2 * i - 1)^-1 * {rb, 0, 0} * pb[-(i + 1)],
    {i, sphenumber}]]
F[2] = Chop[FullSimplify[mbt.
     (-4 * π * Grad[rb^3 * pb[-2], {rb, θb, ϕb}, "Spherical"])]];

(*Coordinate transformation*)
```

```
vm[2] = Chop[(-TrigExpand[-v[1] - v[2]] /.
      {(1 - Cos[θa]^2) → Sin[θa]^2, (1 - Cos[θb]^2) → Sin[θb]^2}) /.
    {ra → Sqrt[rc0^2 + Z * Z], Cos[θa] → Z / Sqrt[rc0^2 + Z * Z],
     Sin[θa] → rc0 / Sqrt[rc0^2 + Z * Z], Cos[ϕa] → Cos[Φ],
     Sin[ϕa] → Sin[Φ], rb → Sqrt[rc0^2 + (Z - L) * (Z - L)],
     Tan[θa] → rc0 / Z, Cot[θa] → Z / rc0,
     Sec[θa] → Sqrt[rc0^2 + Z * Z] / Z, Csc[θa] → Sqrt[rc0^2 + Z * Z] / rc0,
     Cos[θb] → (Z - L) / Sqrt[rc0^2 + (Z - L) * (Z - L)],
     Sin[θb] → rc0 / Sqrt[rc0^2 + (Z - L) * (Z - L)],
     Tan[θb] → rc0 / (Z - L), Cot[θb] → (Z - L) / rc0, Cos[ϕb] →
      Cos[Φ], Sec[θb] → Sqrt[rc0^2 + (Z - L) * (Z - L)] / (Z - L),
     Csc[θb] → Sqrt[rc0^2 + (Z - L) * (Z - L)] / rc0, Sin[ϕb] → Sin[Φ]}];

(*Cylindrical harmonics*)

fgetcharmonics[vm_] := (
  UaR = (Coefficient[(vm.{Cos[Φ], Sin[Φ], 0}), Ua, 1]);
  U0R = (Coefficient[(vm.{Cos[Φ], Sin[Φ], 0}), U0, 1]);
  UbR = (Coefficient[(vm.{Cos[Φ], Sin[Φ], 0}), Ub, 1]);
  UaZ = (Coefficient[(vm.{0, 0, 1}), Ua, 1]);
  U0Z = (Coefficient[(vm.{0, 0, 1}), U0, 1]);
  UbZ = (Coefficient[(vm.{0, 0, 1}), Ub, 1]);
  (cosAR[0] =
    1 * π^-1 * (Ua * (Integrate[Fit[Table[{Z, 2 * π * UaR /. Φ → 0.2},
                {Z, -h - slimitupp, -40 - slimitupp, 100}],
              {Z^-1, Z^-2, Z^-3, Z^-4}, Z] * Cos[λ * Z],
            {Z, -h, -40. - slimitupp}] + Integrate[
            Fit[Table[{Z, 2 * π * UaR /. Φ → 0.2},
                {Z, 42. + slimitupp, h + slimitupp, 100}],
              {Z^-1, Z^-2, Z^-3, Z^-4}, Z] * Cos[λ * Z],
            {Z, 42. + slimitupp, +h + slimitupp}] + Sum[
            Integrate[Fit[Table[{Z, (2 * π * UaR /. Φ → 0.2)}, {Z,
                  i * 10 - slimitupp, i * 10 + 10 - slimitupp, 1}],
                {1, Z, Z^2}, Z] * Cos[λ * Z], {Z, i * 10 - slimitupp,
              i * 10 + 10 - slimitupp}], {i, -4, -2, 1}] +
          Integrate[Fit[Table[{Z, (2 * π * UaR /. Φ → 0.2)},
                {Z, -10. - slimitupp, -6. - slimitupp, 0.5}],
              {1, Z, Z^2}, Z] * Cos[λ * Z],
```

```
 {Z, -10. - slimitupp, -6. - slimitupp}] +
Sum[Integrate[Fit[Table[{Z, (2 * π * UaR /. Φ → 0.2)},
      {Z, i - slimitupp, i + 1 - slimitupp, 0.1}],
     {1, Z, Z^2}, Z] * Cos[λ * Z], {Z, i - slimitupp,
    i + 1 - slimitupp}], {i, -6, -3, 1}] +
Sum[Integrate[Fit[Table[{Z, (2 * π * UaR /. Φ → 0.2)},
      {Z, i * 0.5 - slimitupp, i * 0.5 + 0.5 - slimitupp,
       0.1}], {1, Z, Z^2}, Z] * Cos[λ * Z],
   {Z, i * 0.5 - slimitupp, i * 0.5 + 0.5 - slimitupp}],
  {i, -4, -1, 1}] + Sum[Integrate[
   Fit[Table[{Z, (2 * π * UaR /. Φ → 0.2)}, {Z,
      i * 0.25 + slimitupp, i * 0.25 + 0.25 + slimitupp,
      0.05}], {1, Z, Z^2}, Z] * Cos[λ * Z],
   {Z, i * 0.25 + slimitupp, i * 0.25 + 0.25 +
     slimitupp}], {i, 0, 15, 1}] +
Sum[Integrate[Fit[Table[{Z, (2 * π * UaR /. Φ → 0.2)},
      {Z, i * 0.5 + slimitupp, i * 0.5 + 0.5 + slimitupp,
       0.1}], {1, Z, Z^2}, Z] * Cos[λ * Z],
   {Z, i * 0.5 + slimitupp, i * 0.5 + 0.5 + slimitupp}],
  {i, 8, 13, 1}] + Sum[Integrate[
   Fit[Table[{Z, (2 * π * UaR /. Φ → 0.2)}, {Z,
      i + slimitupp, i + 1 + slimitupp, 0.1}],
     {1, Z, Z^2}, Z] * Cos[λ * Z], {Z, i + slimitupp,
    i + 1 + slimitupp}], {i, 7, 11, 1}] +
Sum[Integrate[Fit[Table[{Z, (2 * π * UaR /. Φ → 0.2)},
      {Z, i * 10 + 2 + slimitupp, i * 10 + 10 + 2 +
        slimitupp, 0.1}], {1, Z, Z^2}, Z] *
    Cos[λ * Z], {Z, i * 10 + 2 + slimitupp,
    i * 10 + 10 + 2 + slimitupp}], {i, 1, 3, 1}]) +
U0 * (Integrate[Fit[Table[{Z, 2 * π * U0R /. Φ → 0.2},
      {Z, -h - slimitupp, -40 - slimitupp, 50}],
     {Z^-1, Z^-2, Z^-3, Z^-4}, Z] * Cos[λ * Z],
  {Z, -h, -40. - slimitupp}] + Integrate[
  Fit[Table[{Z, 2 * π * U0R /. Φ → 0.2},
      {Z, 40. + slimitupp, h + slimitupp, 50}],
     {Z^-1, Z^-2, Z^-3, Z^-4}, Z] * Cos[λ * Z],
  {Z, 40. + slimitupp, +h}] + Sum[Integrate[
   Fit[Table[{Z, (2 * π * U0R /. Φ → 0.2)}, {Z,
      i * 10 - slimitupp, i * 10 + 10 - slimitupp, 0.1}],
     {1, Z, Z^2}, Z] * Cos[λ * Z], {Z, i * 10 - slimitupp,
    i * 10 + 10 - slimitupp}], {i, -4, -2, 1}] +
 Integrate[Fit[Table[{Z, (2 * π * U0R /. Φ → 0.2)},
```

```
    {Z, -10. - slimitupp, -6. - slimitupp, 0.1}],
   {1, Z, Z^2}, Z] * Cos[λ * Z],
 {Z, -10. - slimitupp, -6. - slimitupp}] +
Sum[Integrate[Fit[Table[{Z, (2 * π * U0R /. Φ → 0.2)},
     {Z, i - slimitupp, i + 1 - slimitupp, 0.1}],
    {1, Z, Z^2}, Z] * Cos[λ * Z], {Z, i - slimitupp,
   i + 1 - slimitupp}], {i, -6, -3, 1}] +
Sum[Integrate[Fit[Table[{Z, (2 * π * U0R /. Φ → 0.2)},
     {Z, i * 0.5 - slimitupp, i * 0.5 + 0.5 - slimitupp,
      0.1}], {1, Z, Z^2}, Z] * Cos[λ * Z],
  {Z, i * 0.5 - slimitupp, i * 0.5 + 0.5 - slimitupp}],
 {i, -4, -1, 1}] + Sum[Integrate[
  Fit[Table[{Z, (2 * π * U0R /. Φ → 0.2)}, {Z,
     i * 0.25 + slimitupp, i * 0.25 + 0.25 + slimitupp,
     0.05}], {1, Z, Z^2}, Z] * Cos[λ * Z],
  {Z, i * 0.25 + slimitupp, i * 0.25 + 0.25 +
    slimitupp}], {i, 0, 1, 1}] +
Sum[Integrate[Fit[Table[{Z, (2 * π * U0R /. Φ → 0.2)},
     {Z, i * 0.1 + slimitupp, i * 0.1 + 0.1 + slimitupp,
      0.02}], {1, Z, Z^2}, Z] * Cos[λ * Z],
  {Z, i * 0.1 + slimitupp, i * 0.1 + 0.1 + slimitupp}],
 {i, 5, 9, 1}] + Sum[Integrate[
  Fit[Table[{Z, (2 * π * U0R /. Φ → 0.2)}, {Z,
     i * 0.25 + slimitupp, i * 0.25 + 0.25 + slimitupp,
     0.05}], {1, Z, Z^2}, Z] * Cos[λ * Z],
  {Z, i * 0.25 + slimitupp, i * 0.25 + 0.25 +
    slimitupp}], {i, 4, 11, 1}] +
Sum[Integrate[Fit[Table[{Z, (2 * π * U0R /. Φ → 0.2)},
     {Z, i * 0.5 + slimitupp, i * 0.5 + 0.5 + slimitupp,
      0.1}], {1, Z, Z^2}, Z] * Cos[λ * Z],
  {Z, i * 0.5 + slimitupp, i * 0.5 + 0.5 + slimitupp}],
 {i, 6, 11, 1}] + Sum[Integrate[
  Fit[Table[{Z, (2 * π * U0R /. Φ → 0.2)}, {Z,
     i + slimitupp, i + 1 + slimitupp, 0.1}],
    {1, Z, Z^2}, Z] * Cos[λ * Z], {Z, i + slimitupp,
   i + 1 + slimitupp}], {i, 6, 9, 1}] +
Sum[Integrate[Fit[Table[{Z, (2 * π * U0R /. Φ → 0.2)},
     {Z, i * 5 + slimitupp, i * 5 + 5 + slimitupp, 1}],
    {1, Z, Z^2}, Z] * Cos[λ * Z],
  {Z, i * 5 + slimitupp, i * 5 + 5 + slimitupp}],
 {i, 2, 3, 1}] + Sum[Integrate[
  Fit[Table[{Z, (2 * π * U0R /. Φ → 0.2)}, {Z,
```

```
          i * 10 + slimitupp, i * 10 + 10 + slimitupp, 0.1}],
        {1, Z, Z^2}, Z] * Cos[λ * Z], {Z, i * 10 + slimitupp,
       i * 10 + 10 + slimitupp}], {i, 2, 3, 1}]) +
Ub * (Integrate[Fit[Table[{Z, 2 * π * UbR /. Φ → 0.2},
        {Z, -h - slimitupp, -40 - slimitupp, 50}],
       {Z^-1, Z^-2, Z^-3, Z^-4}, Z] * Cos[λ * Z],
     {Z, -h, -40. - slimitupp}] + Integrate[
     Fit[Table[{Z, 2 * π * UbR /. Φ → 0.2},
        {Z, 40. + slimitupp, h + slimitupp, 50}],
       {Z^-1, Z^-2, Z^-3, Z^-4}, Z] * Cos[λ * Z],
     {Z, 40. + slimitupp, +h}] + Sum[Integrate[
      Fit[Table[{Z, (2 * π * UbR /. Φ → 0.2)}, {Z,
          i * 10 - slimitupp, i * 10 + 10 - slimitupp, 0.1}],
        {1, Z, Z^2}, Z] * Cos[λ * Z], {Z, i * 10 - slimitupp,
       i * 10 + 10 - slimitupp}], {i, -4, -2, 1}] +
    Integrate[Fit[Table[{Z, (2 * π * UbR /. Φ → 0.2)},
        {Z, -10. - slimitupp, -6. - slimitupp, 0.1}],
       {1, Z, Z^2}, Z] * Cos[λ * Z],
     {Z, -10. - slimitupp, -6. - slimitupp}] +
    Sum[Integrate[Fit[Table[{Z, (2 * π * UbR /. Φ → 0.2)},
          {Z, i - slimitupp, i + 1 - slimitupp, 0.1}],
        {1, Z, Z^2}, Z] * Cos[λ * Z], {Z, i - slimitupp,
       i + 1 - slimitupp}], {i, -6, -3, 1}] +
    Sum[Integrate[Fit[Table[{Z, (2 * π * UbR /. Φ → 0.2)},
          {Z, i * 0.5 - slimitupp, i * 0.5 + 0.5 - slimitupp,
           0.1}], {1, Z, Z^2}, Z] * Cos[λ * Z],
      {Z, i * 0.5 - slimitupp, i * 0.5 + 0.5 - slimitupp}],
     {i, -4, -1, 1}] + Sum[Integrate[
      Fit[Table[{Z, (2 * π * UbR /. Φ → 0.2)}, {Z,
          i * 0.25 + slimitupp, i * 0.25 + 0.25 + slimitupp,
           0.05}], {1, Z, Z^2}, Z] * Cos[λ * Z],
      {Z, i * 0.25 + slimitupp, i * 0.25 + 0.25 +
        slimitupp}], {i, 0, 13, 1}] +
    Sum[Integrate[Fit[Table[{Z, (2 * π * UbR /. Φ → 0.2)},
          {Z, i * 0.5 + slimitupp, i * 0.5 + 0.5 + slimitupp,
           0.1}], {1, Z, Z^2}, Z] * Cos[λ * Z],
      {Z, i * 0.5 + slimitupp, i * 0.5 + 0.5 + slimitupp}],
     {i, 7, 11, 1}] + Sum[Integrate[
      Fit[Table[{Z, (2 * π * UbR /. Φ → 0.2)}, {Z,
          i + slimitupp, i + 1 + slimitupp, 0.1}],
        {1, Z, Z^2}, Z] * Cos[λ * Z], {Z, i + slimitupp,
       i + 1 + slimitupp}], {i, 6, 9, 1}] +
```

```
        Sum[Integrate[Fit[Table[{Z, (2 * π * UbR /. Φ → 0.2)},
              {Z, i * 5 + slimitupp, i * 5 + 5 + slimitupp, 1}],
            {1, Z, Z^2}, Z] * Cos[λ * Z],
          {Z, i * 5 + slimitupp, i * 5 + 5 + slimitupp}],
         {i, 2, 3, 1}] + Sum[Integrate[
          Fit[Table[{Z, (2 * π * UbR /. Φ → 0.2)}, {Z,
              i * 10 + slimitupp, i * 10 + 10 + slimitupp, 1}],
            {1, Z, Z^2}, Z] * Cos[λ * Z], {Z, i * 10 + slimitupp,
           i * 10 + 10 + slimitupp}], {i, 2, 3, 1}]));
cosBR[0] = 1 * π^-1 * (Ua * (Integrate[Fit[Table[{Z, 2 * π * UaR /.
              Φ → 0.2}, {Z, -h - slimitupp, -40 - slimitupp,
             100}], {Z^-1, Z^-2, Z^-3, Z^-4}, Z] *
          Sin[λ * Z], {Z, -h, -40. - slimitupp}] +
        Integrate[Fit[Table[{Z, 2 * π * UaR /. Φ → 0.2},
            {Z, 42. + slimitupp, h + slimitupp, 100}],
          {Z^-1, Z^-2, Z^-3, Z^-4}, Z] * Sin[λ * Z],
         {Z, 42. + slimitupp, +h + slimitupp}] + Sum[
         Integrate[Fit[Table[{Z, (2 * π * UaR /. Φ → 0.2)}, {Z,
              i * 10 - slimitupp, i * 10 + 10 - slimitupp, 1}],
            {1, Z, Z^2}, Z] * Sin[λ * Z], {Z, i * 10 - slimitupp,
           i * 10 + 10 - slimitupp}], {i, -4, -2, 1}] +
        Integrate[Fit[Table[{Z, (2 * π * UaR /. Φ → 0.2)},
            {Z, -10. - slimitupp, -6. - slimitupp, 0.5}],
          {1, Z, Z^2}, Z] * Sin[λ * Z],
         {Z, -10. - slimitupp, -6. - slimitupp}] +
        Sum[Integrate[Fit[Table[{Z, (2 * π * UaR /. Φ → 0.2)},
              {Z, i - slimitupp, i + 1 - slimitupp, 0.1}],
            {1, Z, Z^2}, Z] * Sin[λ * Z], {Z, i - slimitupp,
           i + 1 - slimitupp}], {i, -6, -3, 1}] +
        Sum[Integrate[Fit[Table[{Z, (2 * π * UaR /. Φ → 0.2)},
              {Z, i * 0.5 - slimitupp, i * 0.5 + 0.5 - slimitupp,
               0.1}], {1, Z, Z^2}, Z] * Sin[λ * Z],
          {Z, i * 0.5 - slimitupp, i * 0.5 + 0.5 - slimitupp}],
         {i, -4, -1, 1}] + Sum[Integrate[
          Fit[Table[{Z, (2 * π * UaR /. Φ → 0.2)}, {Z,
              i * 0.25 + slimitupp, i * 0.25 + 0.25 + slimitupp,
              0.05}], {1, Z, Z^2}, Z] * Sin[λ * Z],
          {Z, i * 0.25 + slimitupp, i * 0.25 + 0.25 +
            slimitupp}], {i, 0, 15, 1}] +
        Sum[Integrate[Fit[Table[{Z, (2 * π * UaR /. Φ → 0.2)},
              {Z, i * 0.5 + slimitupp, i * 0.5 + 0.5 + slimitupp,
               0.1}], {1, Z, Z^2}, Z] * Sin[λ * Z],
```

```
    {Z, i * 0.5 + slimitupp, i * 0.5 + 0.5 + slimitupp}],
   {i, 8, 13, 1}] + Sum[Integrate[
    Fit[Table[{Z, (2 * π * UaR /. Φ → 0.2)}, {Z,
        i + slimitupp, i + 1 + slimitupp, 0.1}],
      {1, Z, Z^2}, Z] * Sin[λ * Z], {Z, i + slimitupp,
     i + 1 + slimitupp}], {i, 7, 11, 1}] +
  Sum[Integrate[Fit[Table[{Z, (2 * π * UaR /. Φ → 0.2)},
      {Z, i * 10 + 2 + slimitupp, i * 10 + 10 + 2 +
        slimitupp, 0.1}], {1, Z, Z^2}, Z] *
    Sin[λ * Z], {Z, i * 10 + 2 + slimitupp,
    i * 10 + 10 + 2 + slimitupp}], {i, 1, 3, 1}]) +
U0 * (Integrate[Fit[Table[{Z, 2 * π * U0R /. Φ → 0.2},
      {Z, -h - slimitupp, -40 - slimitupp, 50}],
    {Z^-1, Z^-2, Z^-3, Z^-4}, Z] * Sin[λ * Z],
   {Z, -h, -40. - slimitupp}] + Integrate[
   Fit[Table[{Z, 2 * π * U0R /. Φ → 0.2},
      {Z, 40. + slimitupp, h + slimitupp, 50}],
    {Z^-1, Z^-2, Z^-3, Z^-4}, Z] * Sin[λ * Z],
   {Z, 40. + slimitupp, +h}] + Sum[Integrate[
    Fit[Table[{Z, (2 * π * U0R /. Φ → 0.2)}, {Z,
        i * 10 - slimitupp, i * 10 + 10 - slimitupp, 0.1}],
      {1, Z, Z^2}, Z] * Sin[λ * Z], {Z, i * 10 - slimitupp,
     i * 10 + 10 - slimitupp}], {i, -4, -2, 1}] +
  Integrate[Fit[Table[{Z, (2 * π * U0R /. Φ → 0.2)},
      {Z, -10. - slimitupp, -6. - slimitupp, 0.1}],
    {1, Z, Z^2}, Z] * Sin[λ * Z],
   {Z, -10. - slimitupp, -6. - slimitupp}] +
  Sum[Integrate[Fit[Table[{Z, (2 * π * U0R /. Φ → 0.2)},
      {Z, i - slimitupp, i + 1 - slimitupp, 0.1}],
    {1, Z, Z^2}, Z] * Sin[λ * Z], {Z, i - slimitupp,
    i + 1 - slimitupp}], {i, -6, -3, 1}] +
  Sum[Integrate[Fit[Table[{Z, (2 * π * U0R /. Φ → 0.2)},
      {Z, i * 0.5 - slimitupp, i * 0.5 + 0.5 - slimitupp,
       0.1}], {1, Z, Z^2}, Z] * Sin[λ * Z],
    {Z, i * 0.5 - slimitupp, i * 0.5 + 0.5 - slimitupp}],
   {i, -4, -1, 1}] + Sum[Integrate[
    Fit[Table[{Z, (2 * π * U0R /. Φ → 0.2)}, {Z,
        i * 0.25 + slimitupp, i * 0.25 + 0.25 + slimitupp,
        0.05}], {1, Z, Z^2}, Z] * Sin[λ * Z],
    {Z, i * 0.25 + slimitupp, i * 0.25 + 0.25 +
      slimitupp}], {i, 0, 1, 1}] +
  Sum[Integrate[Fit[Table[{Z, (2 * π * U0R /. Φ → 0.2)},
```

```
        {Z, i * 0.1 + slimitupp, i * 0.1 + 0.1 + slimitupp,
         0.02}], {1, Z, Z^2}, Z] * Sin[λ * Z],
       {Z, i * 0.1 + slimitupp, i * 0.1 + 0.1 + slimitupp}],
     {i, 5, 9, 1}] + Sum[Integrate[
      Fit[Table[{Z, (2 * π * U0R /. Φ → 0.2)}, {Z,
          i * 0.25 + slimitupp, i * 0.25 + 0.25 + slimitupp,
          0.05}], {1, Z, Z^2}, Z] * Sin[λ * Z],
       {Z, i * 0.25 + slimitupp, i * 0.25 + 0.25 +
         slimitupp}], {i, 4, 11, 1}] +
    Sum[Integrate[Fit[Table[{Z, (2 * π * U0R /. Φ → 0.2)},
        {Z, i * 0.5 + slimitupp, i * 0.5 + 0.5 + slimitupp,
         0.1}], {1, Z, Z^2}, Z] * Sin[λ * Z],
       {Z, i * 0.5 + slimitupp, i * 0.5 + 0.5 + slimitupp}],
     {i, 6, 11, 1}] + Sum[Integrate[
      Fit[Table[{Z, (2 * π * U0R /. Φ → 0.2)}, {Z,
          i + slimitupp, i + 1 + slimitupp, 0.1}],
        {1, Z, Z^2}, Z] * Sin[λ * Z], {Z, i + slimitupp,
       i + 1 + slimitupp}], {i, 6, 9, 1}] +
    Sum[Integrate[Fit[Table[{Z, (2 * π * U0R /. Φ → 0.2)},
        {Z, i * 5 + slimitupp, i * 5 + 5 + slimitupp, 1}],
       {1, Z, Z^2}, Z] * Sin[λ * Z],
       {Z, i * 5 + slimitupp, i * 5 + 5 + slimitupp}],
     {i, 2, 3, 1}] + Sum[Integrate[
      Fit[Table[{Z, (2 * π * U0R /. Φ → 0.2)}, {Z,
          i * 10 + slimitupp, i * 10 + 10 + slimitupp, 0.1}],
        {1, Z, Z^2}, Z] * Sin[λ * Z], {Z, i * 10 + slimitupp,
       i * 10 + 10 + slimitupp}], {i, 2, 3, 1}]) +
 Ub * (Integrate[Fit[Table[{Z, 2 * π * UbR /. Φ → 0.2},
        {Z, -h - slimitupp, -40 - slimitupp, 50}],
       {Z^-1, Z^-2, Z^-3, Z^-4}, Z] * Sin[λ * Z],
     {Z, -h, -40. - slimitupp}] + Integrate[
     Fit[Table[{Z, 2 * π * UbR /. Φ → 0.2},
        {Z, 40. + slimitupp, h + slimitupp, 50}],
       {Z^-1, Z^-2, Z^-3, Z^-4}, Z] * Sin[λ * Z],
     {Z, 40. + slimitupp, +h}] + Sum[Integrate[
      Fit[Table[{Z, (2 * π * UbR /. Φ → 0.2)}, {Z,
          i * 10 - slimitupp, i * 10 + 10 - slimitupp, 0.1}],
        {1, Z, Z^2}, Z] * Sin[λ * Z], {Z, i * 10 - slimitupp,
       i * 10 + 10 - slimitupp}], {i, -4, -2, 1}] +
    Integrate[Fit[Table[{Z, (2 * π * UbR /. Φ → 0.2)},
        {Z, -10. - slimitupp, -6. - slimitupp, 0.1}],
       {1, Z, Z^2}, Z] * Sin[λ * Z],
```

```
    {Z, -10. - slimitupp, -6. - slimitupp}] +
   Sum[Integrate[Fit[Table[{Z, (2 * π * UbR /. Φ → 0.2)},
        {Z, i - slimitupp, i + 1 - slimitupp, 0.1}],
      {1, Z, Z^2}, Z] * Sin[λ * Z], {Z, i - slimitupp,
     i + 1 - slimitupp}], {i, -6, -3, 1}] +
   Sum[Integrate[Fit[Table[{Z, (2 * π * UbR /. Φ → 0.2)},
        {Z, i * 0.5 - slimitupp, i * 0.5 + 0.5 - slimitupp,
         0.1}], {1, Z, Z^2}, Z] * Sin[λ * Z],
    {Z, i * 0.5 - slimitupp, i * 0.5 + 0.5 - slimitupp}],
   {i, -4, -1, 1}] + Sum[Integrate[
    Fit[Table[{Z, (2 * π * UbR /. Φ → 0.2)}, {Z,
        i * 0.25 + slimitupp, i * 0.25 + 0.25 + slimitupp,
        0.05}], {1, Z, Z^2}, Z] * Sin[λ * Z],
    {Z, i * 0.25 + slimitupp, i * 0.25 + 0.25 +
      slimitupp}], {i, 0, 13, 1}] +
   Sum[Integrate[Fit[Table[{Z, (2 * π * UbR /. Φ → 0.2)},
        {Z, i * 0.5 + slimitupp, i * 0.5 + 0.5 + slimitupp,
         0.1}], {1, Z, Z^2}, Z] * Sin[λ * Z],
    {Z, i * 0.5 + slimitupp, i * 0.5 + 0.5 + slimitupp}],
   {i, 7, 11, 1}] + Sum[Integrate[
    Fit[Table[{Z, (2 * π * UbR /. Φ → 0.2)}, {Z,
        i + slimitupp, i + 1 + slimitupp, 0.1}],
      {1, Z, Z^2}, Z] * Sin[λ * Z], {Z, i + slimitupp,
     i + 1 + slimitupp}], {i, 6, 9, 1}] +
   Sum[Integrate[Fit[Table[{Z, (2 * π * UbR /. Φ → 0.2)},
        {Z, i * 5 + slimitupp, i * 5 + 5 + slimitupp, 1}],
      {1, Z, Z^2}, Z] * Sin[λ * Z],
    {Z, i * 5 + slimitupp, i * 5 + 5 + slimitupp}],
   {i, 2, 3, 1}] + Sum[Integrate[
    Fit[Table[{Z, (2 * π * UbR /. Φ → 0.2)}, {Z,
        i * 10 + slimitupp, i * 10 + 10 + slimitupp, 1}],
      {1, Z, Z^2}, Z] * Sin[λ * Z], {Z, i * 10 + slimitupp,
     i * 10 + 10 + slimitupp}], {i, 2, 3, 1}]));
sinAR[0] = 0;
sinBR[0] = 0;
cosAΦ[0] = 0;
cosBΦ[0] = 0;
sinAΦ[0] = 0;
sinBΦ[0] = 0;
cosAZ[0] =
 1 * π^-1 * (Ua * (Integrate[Fit[Table[{Z, 2 * π * UaZ /. Φ → 0.2},
       {Z, -h - slimitupp, -40 - slimitupp, 50}],
```

```
   {Z^-1, Z^-2, Z^-3, Z^-4}, Z] * Cos[λ * Z],
 {Z, -h, -40. - slimitupp}] + Integrate[
 Fit[Table[{Z, 2 * π * UaZ /. Φ → 0.2},
    {Z, 40. + slimitupp, h + slimitupp, 50}],
   {Z^-1, Z^-2, Z^-3, Z^-4}, Z] * Cos[λ * Z],
 {Z, 40. + slimitupp, +h}] + Sum[Integrate[
  Fit[Table[{Z, (2 * π * UaZ /. Φ → 0.2)}, {Z,
      i * 10 - slimitupp, i * 10 + 10 - slimitupp, 0.1}],
    {1, Z, Z^2}, Z] * Cos[λ * Z], {Z, i * 10 - slimitupp,
   i * 10 + 10 - slimitupp}], {i, -4, -2, 1}] +
Integrate[Fit[Table[{Z, (2 * π * UaZ /. Φ → 0.2)},
    {Z, -10. - slimitupp, -6. - slimitupp, 0.1}],
   {1, Z, Z^2}, Z] * Cos[λ * Z],
 {Z, -10. - slimitupp, -6. - slimitupp}] +
Sum[Integrate[Fit[Table[{Z, (2 * π * UaZ /. Φ → 0.2)},
     {Z, i - slimitupp, i + 1 - slimitupp, 0.1}],
    {1, Z, Z^2}, Z] * Cos[λ * Z], {Z, i - slimitupp,
   i + 1 - slimitupp}], {i, -6, -3, 1}] +
Sum[Integrate[Fit[Table[{Z, (2 * π * UaZ /. Φ → 0.2)},
     {Z, i * 0.5 - slimitupp, i * 0.5 + 0.5 - slimitupp,
      0.1}], {1, Z, Z^2}, Z] * Cos[λ * Z],
  {Z, i * 0.5 - slimitupp, i * 0.5 + 0.5 - slimitupp}],
 {i, -4, -1, 1}] + Sum[Integrate[
  Fit[Table[{Z, (2 * π * UaZ /. Φ → 0.2)}, {Z,
      i * 0.2 + slimitupp, i * 0.2 + 0.2 + slimitupp,
      0.05}], {1, Z, Z^2}, Z] * Cos[λ * Z],
  {Z, i * 0.2 + slimitupp, i * 0.2 + 0.2 + slimitupp}],
 {i, 0, 4, 1}] + Sum[Integrate[
  Fit[Table[{Z, (2 * π * UaZ /. Φ → 0.2)}, {Z,
      i * 0.5 + slimitupp, i * 0.5 + 0.5 + slimitupp,
      0.1}], {1, Z, Z^2}, Z] * Cos[λ * Z],
  {Z, i * 0.5 + slimitupp, i * 0.5 + 0.5 + slimitupp}],
 {i, 2, 9, 1}] + Sum[Integrate[
  Fit[Table[{Z, (2 * π * UaZ /. Φ → 0.2)}, {Z,
      i + slimitupp, i + 1 + slimitupp, 0.1}],
    {1, Z, Z^2}, Z] * Cos[λ * Z], {Z, i + slimitupp,
   i + 1 + slimitupp}], {i, 5, 9, 1}] +
Sum[Integrate[Fit[Table[{Z, (2 * π * UaZ /. Φ → 0.2)},
     {Z, i * 5 + slimitupp, i * 5 + 5 + slimitupp, 1}],
    {1, Z, Z^2}, Z] * Cos[λ * Z], {Z, i * 5 + slimitupp,
   i * 5 + 5 + slimitupp}], {i, 2, 3, 1}] + Sum[
 Integrate[Fit[Table[{Z, (2 * π * UaZ /. Φ → 0.2)}, {Z,
```

```
          i * 10 + slimitupp, i * 10 + 10 + slimitupp, 1}],
        {1, Z, Z^2}, Z] * Cos[λ * Z], {Z, i * 10 + slimitupp,
       i * 10 + 10 + slimitupp}], {i, 2, 3, 1}]) +
U0 * (Integrate[Fit[Table[{Z, 2 * π * U0Z /. Φ → 0.2},
        {Z, -h - slimitupp, -40 - slimitupp, 50}],
       {Z^-1, Z^-2, Z^-3, Z^-4}, Z] * Cos[λ * Z],
     {Z, -h, -40. - slimitupp}] + Integrate[
     Fit[Table[{Z, 2 * π * U0Z /. Φ → 0.2},
        {Z, 40. + slimitupp, h + slimitupp, 50}],
       {Z^-1, Z^-2, Z^-3, Z^-4}, Z] * Cos[λ * Z],
     {Z, 40. + slimitupp, +h}] + Sum[Integrate[
      Fit[Table[{Z, (2 * π * U0Z /. Φ → 0.2)}, {Z,
          i * 10 - slimitupp, i * 10 + 10 - slimitupp, 0.1}],
        {1, Z, Z^2}, Z] * Cos[λ * Z], {Z, i * 10 - slimitupp,
       i * 10 + 10 - slimitupp}], {i, -4, -2, 1}] +
    Integrate[Fit[Table[{Z, (2 * π * U0Z /. Φ → 0.2)},
        {Z, -10. - slimitupp, -6. - slimitupp, 0.1}],
       {1, Z, Z^2}, Z] * Cos[λ * Z],
     {Z, -10. - slimitupp, -6. - slimitupp}] +
    Sum[Integrate[Fit[Table[{Z, (2 * π * U0Z /. Φ → 0.2)},
         {Z, i - slimitupp, i + 1 - slimitupp, 0.1}],
        {1, Z, Z^2}, Z] * Cos[λ * Z], {Z, i - slimitupp,
       i + 1 - slimitupp}], {i, -6, -3, 1}] +
    Sum[Integrate[Fit[Table[{Z, (2 * π * U0Z /. Φ → 0.2)},
         {Z, i * 0.5 - slimitupp, i * 0.5 + 0.5 - slimitupp,
          0.1}], {1, Z, Z^2}, Z] * Cos[λ * Z],
      {Z, i * 0.5 - slimitupp, i * 0.5 + 0.5 - slimitupp}],
     {i, -4, -1, 1}] + Sum[Integrate[
      Fit[Table[{Z, (2 * π * U0Z /. Φ → 0.2)}, {Z,
          i * 0.25 + slimitupp, i * 0.25 + 0.25 + slimitupp,
          0.05}], {1, Z, Z^2}, Z] * Cos[λ * Z],
      {Z, i * 0.25 + slimitupp, i * 0.25 + 0.25 +
        slimitupp}], {i, 0, 9, 1}] +
    Sum[Integrate[Fit[Table[{Z, (2 * π * U0Z /. Φ → 0.2)},
         {Z, i * 0.5 + slimitupp, i * 0.5 + 0.5 + slimitupp,
          0.1}], {1, Z, Z^2}, Z] * Cos[λ * Z],
      {Z, i * 0.5 + slimitupp, i * 0.5 + 0.5 + slimitupp}],
     {i, 5, 7, 1}] + Sum[Integrate[
      Fit[Table[{Z, (2 * π * U0Z /. Φ → 0.2)}, {Z,
          i + slimitupp, i + 1 + slimitupp, 0.1}],
        {1, Z, Z^2}, Z] * Cos[λ * Z], {Z, i + slimitupp,
       i + 1 + slimitupp}], {i, 4, 9, 1}] +
```

```
    Sum[Integrate[Fit[Table[{Z, (2 * π * U0Z /. Φ → 0.2)},
          {Z, i * 5 + slimitupp, i * 5 + 5 + slimitupp, 1}],
         {1, Z, Z^2}, Z] * Cos[λ * Z],
        {Z, i * 5 + slimitupp, i * 5 + 5 + slimitupp}],
       {i, 2, 3, 1}] + Sum[Integrate[
        Fit[Table[{Z, (2 * π * U0Z /. Φ → 0.2)}, {Z,
            i * 10 + slimitupp, i * 10 + 10 + slimitupp, 1}],
         {1, Z, Z^2}, Z] * Cos[λ * Z], {Z, i * 10 + slimitupp,
        i * 10 + 10 + slimitupp}], {i, 2, 3, 1}]) +
  Ub * (Integrate[Fit[Table[{Z, 2 * π * UbZ /. Φ → 0.2},
          {Z, -h - slimitupp, -40 - slimitupp, 50}],
         {Z^-1, Z^-2, Z^-3, Z^-4}, Z] * Cos[λ * Z],
       {Z, -h, -40. - slimitupp}] + Integrate[
       Fit[Table[{Z, 2 * π * UbZ /. Φ → 0.2},
          {Z, 40. + slimitupp, h + slimitupp, 50}],
         {Z^-1, Z^-2, Z^-3, Z^-4}, Z] * Cos[λ * Z],
       {Z, 40 + slimitupp, +h}] + Sum[Integrate[
        Fit[Table[{Z, (2 * π * UbZ /. Φ → 0.2)}, {Z,
            i * 10 - slimitupp, i * 10 + 10 - slimitupp, 0.1}],
         {1, Z, Z^2}, Z] * Cos[λ * Z], {Z, i * 10 - slimitupp,
        i * 10 + 10 - slimitupp}], {i, -4, -2, 1}] +
    Integrate[Fit[Table[{Z, (2 * π * UbZ /. Φ → 0.2)},
          {Z, -10. - slimitupp, -6. - slimitupp, 0.1}],
         {1, Z, Z^2}, Z] * Cos[λ * Z],
       {Z, -10. - slimitupp, -6. - slimitupp}] +
    Sum[Integrate[Fit[Table[{Z, (2 * π * UbZ /. Φ → 0.2)},
          {Z, i - slimitupp, i + 1 - slimitupp, 0.1}],
         {1, Z, Z^2}, Z] * Cos[λ * Z], {Z, i - slimitupp,
        i + 1 - slimitupp}], {i, -6, -3, 1}] +
    Sum[Integrate[Fit[Table[{Z, (2 * π * UbZ /. Φ → 0.2)},
          {Z, i * 0.5 - slimitupp, i * 0.5 + 0.5 - slimitupp,
           0.1}], {1, Z, Z^2}, Z] * Cos[λ * Z],
       {Z, i * 0.5 - slimitupp, i * 0.5 + 0.5 - slimitupp}],
      {i, -4, -1, 1}] + Sum[Integrate[
       Fit[Table[{Z, (2 * π * UbZ /. Φ → 0.2)}, {Z,
           i * 0.25 + slimitupp, i * 0.25 + 0.25 + slimitupp,
           0.05}], {1, Z, Z^2}, Z] * Cos[λ * Z],
       {Z, i * 0.25 + slimitupp, i * 0.25 + 0.25 +
         slimitupp}], {i, 0, 15, 1}] +
    Sum[Integrate[Fit[Table[{Z, (2 * π * UbZ /. Φ → 0.2)},
          {Z, i + slimitupp, i + 1 + slimitupp, 0.1}],
         {1, Z, Z^2}, Z] * Cos[λ * Z],
```

```
    {Z, i + slimitupp, i + 1 + slimitupp}], {i, 4, 9, 1}] +
  Sum[Integrate[Fit[Table[{Z, (2 * π * UbZ /. Φ → 0.2)},
       {Z, i * 5 + slimitupp, i * 5 + 5 + slimitupp, 1}],
      {1, Z, Z^2}, Z] * Cos[λ * Z],
    {Z, i * 5 + slimitupp, i * 5 + 5 + slimitupp}],
   {i, 2, 3, 1}] + Sum[Integrate[
    Fit[Table[{Z, (2 * π * UbZ /. Φ → 0.2)}, {Z,
       i * 10 + slimitupp, i * 10 + 10 + slimitupp, 1}],
      {1, Z, Z^2}, Z] * Cos[λ * Z], {Z, i * 10 + slimitupp,
     i * 10 + 10 + slimitupp}], {i, 2, 3, 1}]));
cosBZ[0] = 1 * π^-1 * (Ua * (Integrate[Fit[Table[{Z, 2 * π * UaZ /.
        Φ → 0.2}, {Z, -h - slimitupp, -40 - slimitupp,
       50}], {Z^-1, Z^-2, Z^-3, Z^-4}, Z] *
    Sin[λ * Z], {Z, -h, -40. - slimitupp}] +
  Integrate[Fit[Table[{Z, 2 * π * UaZ /. Φ → 0.2},
     {Z, 40. + slimitupp, h + slimitupp, 50}],
    {Z^-1, Z^-2, Z^-3, Z^-4}, Z] * Sin[λ * Z],
   {Z, 40. + slimitupp, +h}] + Sum[Integrate[
    Fit[Table[{Z, (2 * π * UaZ /. Φ → 0.2)}, {Z,
       i * 10 - slimitupp, i * 10 + 10 - slimitupp, 0.1}],
      {1, Z, Z^2}, Z] * Sin[λ * Z], {Z, i * 10 - slimitupp,
     i * 10 + 10 - slimitupp}], {i, -4, -2, 1}] +
  Integrate[Fit[Table[{Z, (2 * π * UaZ /. Φ → 0.2)},
     {Z, -10. - slimitupp, -6. - slimitupp, 0.1}],
    {1, Z, Z^2}, Z] * Sin[λ * Z],
   {Z, -10. - slimitupp, -6. - slimitupp}] +
  Sum[Integrate[Fit[Table[{Z, (2 * π * UaZ /. Φ → 0.2)},
       {Z, i - slimitupp, i + 1 - slimitupp, 0.1}],
      {1, Z, Z^2}, Z] * Sin[λ * Z], {Z, i - slimitupp,
     i + 1 - slimitupp}], {i, -6, -3, 1}] +
  Sum[Integrate[Fit[Table[{Z, (2 * π * UaZ /. Φ → 0.2)},
       {Z, i * 0.5 - slimitupp, i * 0.5 + 0.5 - slimitupp,
        0.1}], {1, Z, Z^2}, Z] * Sin[λ * Z],
    {Z, i * 0.5 - slimitupp, i * 0.5 + 0.5 - slimitupp}],
   {i, -4, -1, 1}] + Sum[Integrate[
    Fit[Table[{Z, (2 * π * UaZ /. Φ → 0.2)}, {Z,
       i * 0.2 + slimitupp, i * 0.2 + 0.2 + slimitupp,
       0.05}], {1, Z, Z^2}, Z] * Sin[λ * Z],
    {Z, i * 0.2 + slimitupp, i * 0.2 + 0.2 + slimitupp}],
   {i, 0, 4, 1}] + Sum[Integrate[
    Fit[Table[{Z, (2 * π * UaZ /. Φ → 0.2)}, {Z,
       i * 0.5 + slimitupp, i * 0.5 + 0.5 + slimitupp,
```

```
          0.1}], {1, Z, Z^2}, Z] * Sin[λ * Z],
       {Z, i * 0.5 + slimitupp, i * 0.5 + 0.5 + slimitupp}],
      {i, 2, 9, 1}] + Sum[Integrate[
       Fit[Table[{Z, (2 * π * UaZ /. Φ → 0.2)}, {Z,
            i + slimitupp, i + 1 + slimitupp, 0.1}],
         {1, Z, Z^2}, Z] * Sin[λ * Z], {Z, i + slimitupp,
        i + 1 + slimitupp}], {i, 5, 9, 1}] +
    Sum[Integrate[Fit[Table[{Z, (2 * π * UaZ /. Φ → 0.2)},
          {Z, i * 5 + slimitupp, i * 5 + 5 + slimitupp, 1}],
         {1, Z, Z^2}, Z] * Sin[λ * Z],
       {Z, i * 5 + slimitupp, i * 5 + 5 + slimitupp}],
      {i, 2, 3, 1}] + Sum[Integrate[
       Fit[Table[{Z, (2 * π * UaZ /. Φ → 0.2)}, {Z,
            i * 10 + slimitupp, i * 10 + 10 + slimitupp, 1}],
         {1, Z, Z^2}, Z] * Sin[λ * Z], {Z, i * 10 + slimitupp,
        i * 10 + 10 + slimitupp}], {i, 2, 3, 1}]) +
  U0 * (Integrate[Fit[Table[{Z, 2 * π * U0Z /. Φ → 0.2},
          {Z, -h - slimitupp, -40 - slimitupp, 50}],
         {Z^-1, Z^-2, Z^-3, Z^-4}, Z] * Sin[λ * Z],
       {Z, -h, -40. - slimitupp}] + Integrate[
       Fit[Table[{Z, 2 * π * U0Z /. Φ → 0.2},
          {Z, 40. + slimitupp, h + slimitupp, 50}],
         {Z^-1, Z^-2, Z^-3, Z^-4}, Z] * Sin[λ * Z],
       {Z, 40. + slimitupp, +h}] + Sum[Integrate[
       Fit[Table[{Z, (2 * π * U0Z /. Φ → 0.2)}, {Z,
            i * 10 - slimitupp, i * 10 + 10 - slimitupp, 0.1}],
         {1, Z, Z^2}, Z] * Sin[λ * Z], {Z, i * 10 - slimitupp,
        i * 10 + 10 - slimitupp}], {i, -4, -2, 1}] +
    Integrate[Fit[Table[{Z, (2 * π * U0Z /. Φ → 0.2)},
          {Z, -10. - slimitupp, -6. - slimitupp, 0.1}],
         {1, Z, Z^2}, Z] * Sin[λ * Z],
       {Z, -10. - slimitupp, -6. - slimitupp}] +
    Sum[Integrate[Fit[Table[{Z, (2 * π * U0Z /. Φ → 0.2)},
          {Z, i - slimitupp, i + 1 - slimitupp, 0.1}],
         {1, Z, Z^2}, Z] * Sin[λ * Z], {Z, i - slimitupp,
        i + 1 - slimitupp}], {i, -6, -3, 1}] +
    Sum[Integrate[Fit[Table[{Z, (2 * π * U0Z /. Φ → 0.2)},
          {Z, i * 0.5 - slimitupp, i * 0.5 + 0.5 - slimitupp,
           0.1}], {1, Z, Z^2}, Z] * Sin[λ * Z],
       {Z, i * 0.5 - slimitupp, i * 0.5 + 0.5 - slimitupp}],
      {i, -4, -1, 1}] + Sum[Integrate[
       Fit[Table[{Z, (2 * π * U0Z /. Φ → 0.2)}, {Z,
```

```
          i * 0.25 + slimitupp, i * 0.25 + 0.25 + slimitupp,
          0.05}], {1, Z, Z^2}, Z] * Sin[λ * Z],
       {Z, i * 0.25 + slimitupp, i * 0.25 + 0.25 +
         slimitupp}], {i, 0, 9, 1}] +
    Sum[Integrate[Fit[Table[{Z, (2 * π * U0Z /. Φ → 0.2)},
        {Z, i * 0.5 + slimitupp, i * 0.5 + 0.5 + slimitupp,
         0.1}], {1, Z, Z^2}, Z] * Sin[λ * Z],
       {Z, i * 0.5 + slimitupp, i * 0.5 + 0.5 + slimitupp}],
      {i, 5, 7, 1}] + Sum[Integrate[
      Fit[Table[{Z, (2 * π * U0Z /. Φ → 0.2)}, {Z,
          i + slimitupp, i + 1 + slimitupp, 0.1}],
        {1, Z, Z^2}, Z] * Sin[λ * Z], {Z, i + slimitupp,
       i + 1 + slimitupp}], {i, 4, 9, 1}] +
    Sum[Integrate[Fit[Table[{Z, (2 * π * U0Z /. Φ → 0.2)},
        {Z, i * 5 + slimitupp, i * 5 + 5 + slimitupp, 1}],
       {1, Z, Z^2}, Z] * Sin[λ * Z],
       {Z, i * 5 + slimitupp, i * 5 + 5 + slimitupp}],
      {i, 2, 3, 1}] + Sum[Integrate[
      Fit[Table[{Z, (2 * π * U0Z /. Φ → 0.2)}, {Z,
          i * 10 + slimitupp, i * 10 + 10 + slimitupp, 1}],
        {1, Z, Z^2}, Z] * Sin[λ * Z], {Z, i * 10 + slimitupp,
       i * 10 + 10 + slimitupp}], {i, 2, 3, 1}]) +
Ub * (Integrate[Fit[Table[{Z, 2 * π * UbZ /. Φ → 0.2},
        {Z, -h - slimitupp, -40 - slimitupp, 50}],
       {Z^-1, Z^-2, Z^-3, Z^-4}, Z] * Sin[λ * Z],
      {Z, -h, -40. - slimitupp}] + Integrate[
      Fit[Table[{Z, 2 * π * UbZ /. Φ → 0.2},
        {Z, 40. + slimitupp, h + slimitupp, 50}],
       {Z^-1, Z^-2, Z^-3, Z^-4}, Z] * Sin[λ * Z],
      {Z, 40. + slimitupp, +h}] + Sum[Integrate[
      Fit[Table[{Z, (2 * π * UbZ /. Φ → 0.2)}, {Z,
          i * 10 - slimitupp, i * 10 + 10 - slimitupp, 0.1}],
        {1, Z, Z^2}, Z] * Sin[λ * Z], {Z, i * 10 - slimitupp,
       i * 10 + 10 - slimitupp}], {i, -4, -2, 1}] +
    Integrate[Fit[Table[{Z, (2 * π * UbZ /. Φ → 0.2)},
        {Z, -10. - slimitupp, -6. - slimitupp, 0.1}],
       {1, Z, Z^2}, Z] * Sin[λ * Z],
      {Z, -10. - slimitupp, -6. - slimitupp}] +
    Sum[Integrate[Fit[Table[{Z, (2 * π * UbZ /. Φ → 0.2)},
        {Z, i - slimitupp, i + 1 - slimitupp, 0.1}],
       {1, Z, Z^2}, Z] * Sin[λ * Z], {Z, i - slimitupp,
       i + 1 - slimitupp}], {i, -6, -3, 1}] +
```

```
        Sum[Integrate[Fit[Table[{Z, (2 * π * UbZ /. Φ → 0.2)},
              {Z, i * 0.5 - slimitupp, i * 0.5 + 0.5 - slimitupp,
               0.1}], {1, Z, Z^2}, Z] * Sin[λ * Z],
            {Z, i * 0.5 - slimitupp, i * 0.5 + 0.5 - slimitupp}],
          {i, -4, -1, 1}] + Sum[Integrate[
           Fit[Table[{Z, (2 * π * UbZ /. Φ → 0.2)}, {Z,
               i * 0.25 + slimitupp, i * 0.25 + 0.25 + slimitupp,
               0.05}], {1, Z, Z^2}, Z] * Sin[λ * Z],
            {Z, i * 0.25 + slimitupp, i * 0.25 + 0.25 +
              slimitupp}], {i, 0, 15, 1}] +
        Sum[Integrate[Fit[Table[{Z, (2 * π * UbZ /. Φ → 0.2)},
              {Z, i + slimitupp, i + 1 + slimitupp, 0.1}],
            {1, Z, Z^2}, Z] * Sin[λ * Z],
            {Z, i + slimitupp, i + 1 + slimitupp}], {i, 4, 9, 1}] +
        Sum[Integrate[Fit[Table[{Z, (2 * π * UbZ /. Φ → 0.2)},
              {Z, i * 5 + slimitupp, i * 5 + 5 + slimitupp, 1}],
            {1, Z, Z^2}, Z] * Sin[λ * Z],
            {Z, i * 5 + slimitupp, i * 5 + 5 + slimitupp}],
          {i, 2, 3, 1}] + Sum[Integrate[
           Fit[Table[{Z, (2 * π * UbZ /. Φ → 0.2)}, {Z,
               i * 10 + slimitupp, i * 10 + 10 + slimitupp, 1}],
            {1, Z, Z^2}, Z] * Sin[λ * Z], {Z, i * 10 + slimitupp,
             i * 10 + 10 + slimitupp}], {i, 2, 3, 1}]));
sinAZ[0] = 0;
sinBZ[0] = 0;
ωca[0] = 0;
ωcb[0] = 0;
ωsa[0] = 0;
ωsb[0] = 0;
ψca[0] =
 (-1.` λ BesselI[1, λ] cosAR[0] - 0.5` λ BesselI[2, λ] cosBZ[
      0] + BesselI[0, λ] (-1.` cosAR[0] - 0.5` λ cosBZ[0])) /
  (1.` λ BesselI[0, λ]^2 - 2.` λ BesselI[1, λ]^2 + BesselI[0, λ]
     (-2.` BesselI[1, λ] + 1.` λ BesselI[2, λ]));
ψcb[0] = (0.5` λ BesselI[2, λ] cosAZ[0] +
    BesselI[0, λ] (0.5` λ cosAZ[0] - 1.` cosBR[0]) -
    1.` λ BesselI[1, λ] cosBR[0]) /
  (1.` λ BesselI[0, λ]^2 - 2.` λ BesselI[1, λ]^2 + BesselI[0, λ]
     (-2.` BesselI[1, λ] + 1.` λ BesselI[2, λ]));
ψsa[0] = 0;
ψsb[0] = 0;
γca[0] =
```

```
    (1.` BesselI[0, λ] cosAR[0] + 1.` BesselI[1, λ] cosBZ[0]) /
     (1.` λ BesselI[0, λ]^2 - 2.` λ BesselI[1, λ]^2 + BesselI[0, λ]
        (-2.` BesselI[1, λ] + 1.` λ BesselI[2, λ]));
   γcb[0] = (-1.` BesselI[1, λ] cosAZ[0] +
       1.` BesselI[0, λ] cosBR[0]) /
     (1.` λ BesselI[0, λ]^2 - 2.` λ BesselI[1, λ]^2 + BesselI[0, λ]
        (-2.` BesselI[1, λ] + 1.` λ BesselI[2, λ]));
   γsa[0] = 0;
   γsb[0] = 0;
  ))

fgetcharmonics[vm[2]]

v[3] =
  Chop[mct.{-π^-1 * (Cos[0] * (ψca[0] * (0.5 * (BesselI[1, λ * rc] +
                    BesselI[-1, λ * rc])) + γca[0] * λ * rc *
              (0.25 * (BesselI[-2, λ * rc] + 2 * BesselI[0, λ * rc] +
                    BesselI[+2, λ * rc]))) * Cos[λ * Z] +
         Cos[0] * (ψcb[0] * (0.5 * (BesselI[+1, λ * rc] +
                    BesselI[-1, λ * rc])) + γcb[0] * λ * rc *
              (0.25 * (BesselI[-2, λ * rc] + 2 * BesselI[0, λ * rc] +
                    BesselI[+2, λ * rc]))) * Sin[λ * Z]), 0,
     -π^-1 * (Cos[0] * (ψcb[0] * BesselI[0, λ * rc] + γcb[0] * λ * rc *
              (0.5 * (BesselI[+1, λ * rc] + BesselI[-1, λ * rc])) +
            γcb[0] * BesselI[0, λ * rc]) * Cos[λ * Z] +
         Cos[0] * (-ψca[0] * BesselI[0, λ * rc] - γca[0] * λ * rc *
              (0.5 * (BesselI[+1, λ * rc] + BesselI[-1, λ * rc])) -
            γca[0] * BesselI[0, λ * rc]) * Sin[λ * Z])}];
```

```
fgetcXa[vam_] :=
  (Vacxm = ({Sin[θa] * Cos[ϕa], Sin[θa] * Sin[ϕa], Cos[θa]}).
      (vam) /. ϕa → 0.2;
   For[i = 1, i < sphenumber + 1, i++,
    Xca[i] = Chop[(2 * i + 1) * 4^-1 * π^-1 *
       (Ua * NIntegrate[2 * π * Sin[θa] * (Coefficient[Vacxm,
             Ua, 1]) * LegendreP[i, Cos[θa]],
          {θa, 0, π}, {λ, slimitup, Infinity}, Method →
           {"GlobalAdaptive", Method → "CartesianRule"},
          AccuracyGoal → 3] + U0 * NIntegrate[
          2 * π * Sin[θa] * (Coefficient[Vacxm, U0, 1]) *
           LegendreP[i, Cos[θa]], {θa, 0, π}, {λ, slimitup,
           Infinity}, Method → {"GlobalAdaptive",
            Method → "CartesianRule"}, AccuracyGoal → 3] +
        Ub * NIntegrate[2 * π * Sin[θa] * (Coefficient[
             Vacxm, Ub, 1]) * LegendreP[i, Cos[θa]],
          {θa, 0, π}, {λ, slimitup, Infinity}, Method →
           {"GlobalAdaptive", Method → "CartesianRule"},
          AccuracyGoal → 3]) * LegendreP[i, Cos[θa]]]]);
fgetcYa[vam_] :=
  (Vacym =
    (-D[({0, 1, 0}.(Sin[θa] * (mata.vam))), θa] / Sin[θa] -
       ({1, 0, 0}.(mata.vam)) * 2) /. ϕa → 0.2;
   For[i = 1, i < sphenumber + 1, i++,
    Yca[i] = Chop[(2 * i + 1) * 4^-1 * π^-1 *
       (Ua * NIntegrate[2 * π * Sin[θa] * (Coefficient[Vacym,
             Ua, 1]) * LegendreP[i, Cos[θa]],
          {θa, 0, π}, {λ, slimitup, Infinity}, Method →
           {"GlobalAdaptive", Method → "CartesianRule"},
          AccuracyGoal → 3] + U0 * NIntegrate[
          2 * π * Sin[θa] * (Coefficient[Vacym, U0, 1]) *
           LegendreP[i, Cos[θa]], {θa, 0, π}, {λ, slimitup,
           Infinity}, Method → {"GlobalAdaptive",
            Method → "CartesianRule"}, AccuracyGoal → 3] +
        Ub * NIntegrate[2 * π * Sin[θa] * (Coefficient[
             Vacym, Ub, 1]) * LegendreP[i, Cos[θa]],
          {θa, 0, π}, {λ, slimitup, Infinity}, Method →
           {"GlobalAdaptive", Method → "CartesianRule"},
          AccuracyGoal → 3]) * LegendreP[i, Cos[θa]]]]);
```

```
fgetcXb[vbm_] :=
  (Vbcxm = ({Sin[θb] * Cos[ϕb], Sin[θb] * Sin[ϕb], Cos[θb]}).
      (vbm) /. ϕb → 0.2;
   For[i = 1, i < sphenumber + 1, i++,
    Xcb[i] = Chop[(2 * i + 1) * 4^-1 * π^-1 *
       (Ua * NIntegrate[2 * π * Sin[θb] * (Coefficient[Vbcxm,
             Ua, 1]) * LegendreP[i, Cos[θb]],
          {θb, 0, π}, {λ, slimitup, Infinity}, Method →
           {"GlobalAdaptive", Method → "CartesianRule"},
          AccuracyGoal → 3] + U0 * NIntegrate[
          2 * π * Sin[θb] * (Coefficient[Vbcxm, U0, 1]) *
           LegendreP[i, Cos[θb]], {θb, 0, π}, {λ, slimitup,
           Infinity}, Method → {"GlobalAdaptive",
            Method → "CartesianRule"}, AccuracyGoal → 3] +
        Ub * NIntegrate[2 * π * Sin[θb] * (Coefficient[
             Vbcxm, Ub, 1]) * LegendreP[i, Cos[θb]],
          {θb, 0, π}, {λ, slimitup, Infinity}, Method →
           {"GlobalAdaptive", Method → "CartesianRule"},
          AccuracyGoal → 3]) * LegendreP[i, Cos[θb]]]]);
fgetcYb[vbm_] :=
  (Vbcym =
    (-D[({0, 1, 0}.(Sin[θb] * (mbtb.vbm))), θb] / Sin[θb] -
       ({1, 0, 0}.(mbtb.vbm)) * 2) /. ϕb → 0.2;
   For[i = 1, i < sphenumber + 1, i++,
    Ycb[i] = Chop[(2 * i + 1) * 4^-1 * π^-1 *
       (Ua * NIntegrate[2 * π * Sin[θb] * (Coefficient[Vbcym,
             Ua, 1]) * LegendreP[i, Cos[θb]],
          {θb, 0, π}, {λ, slimitup, Infinity}, Method →
           {"GlobalAdaptive", Method → "CartesianRule"},
          AccuracyGoal → 3] + U0 * NIntegrate[
          2 * π * Sin[θb] * (Coefficient[Vbcym, U0, 1]) *
           LegendreP[i, Cos[θb]], {θb, 0, π}, {λ, slimitup,
           Infinity}, Method → {"GlobalAdaptive",
            Method → "CartesianRule"}, AccuracyGoal → 3] +
        Ub * NIntegrate[2 * π * Sin[θb] * (Coefficient[
             Vbcym, Ub, 1]) * LegendreP[i, Cos[θb]],
          {θb, 0, π}, {λ, slimitup, Infinity}, Method →
           {"GlobalAdaptive", Method → "CartesianRule"},
          AccuracyGoal → 3]) * LegendreP[i, Cos[θb]]]]);

(*calculation procedure with loop*)

For[n = 4,
 Abs[Re[Coefficient[Chop[F[n - 2].{0, 0, 1} / μ], Ub, 1]]] >
```

```
  0.001 || Abs[
    Re[Coefficient[Chop[F[n - 3].{0, 0, 1} / μ], Ub, 1]]] > 0.001,
n = n + 3, vm[n] = -TrigExpand[v[n - 2]] /. {rc → a * Sin[θa],
    Z → a * Cos[θa], Cos[Φ] → Cos[ϕa], Sin[Φ] → Sin[ϕa],
    Cos[θb] → (a * Cos[θa] - L) / Sqrt[(a^2 + L^2 - 2 * a * L * Cos[θa])],
    Sin[θb] → Sqrt[(1 - (a * Cos[θa] - L)^2 / (a^2 + L^2 - 2 * a * L * Cos[θa]))],
    Cos[ϕb] → Cos[ϕa], Sin[ϕb] → Sin[ϕa],
    rb → Sqrt[(a^2 + L^2 - 2 * a * L * Cos[θa])],
    Tan[θb] → Sqrt[(1 - (a * Cos[θa] - L)^2 / (a^2 + L^2 - 2 * a * L * Cos[θa]))] /
      ((a * Cos[θa] - L) / Sqrt[(a^2 + L^2 - 2 * a * L * Cos[θa])]),
    Cot[θb] → (a * Cos[θa] - L) / Sqrt[(a^2 + L^2 - 2 * a * L * Cos[θa])] /
      (Sqrt[(1 - (a * Cos[θa] - L)^2 / (a^2 + L^2 - 2 * a * L * Cos[θa]))]),
    Sec[θb] → Sqrt[(a^2 + L^2 - 2 * a * L * Cos[θa])] / ((a * Cos[θa] - L)),
    Csc[θb] → 1 / Sqrt[(1 - (a * Cos[θa] - L)^2 / (a^2 + L^2 - 2 * a * L * Cos[θa]))]};
fgetXa[vm[n]]; fgetYa[vm[n]];
vcm[n] = -v[n - 1] /. {rc → a * Sin[θa],
    Z → a * Cos[θa], Cos[Φ] → Cos[ϕa], Sin[Φ] → Sin[ϕa],
    Cos[θb] → (a * Cos[θa] - L) / Sqrt[(a^2 + L^2 - 2 * a * L * Cos[θa])],
    Sin[θb] → Sqrt[(1 - (a * Cos[θa] - L)^2 / (a^2 + L^2 - 2 * a * L * Cos[θa]))],
    Cos[ϕb] → Cos[ϕa], Sin[ϕb] → Sin[ϕa],
    rb → Sqrt[(a^2 + L^2 - 2 * a * L * Cos[θa])],
    Tan[θb] → Sqrt[(1 - (a * Cos[θa] - L)^2 / (a^2 + L^2 - 2 * a * L * Cos[θa]))] /
      ((a * Cos[θa] - L) / Sqrt[(a^2 + L^2 - 2 * a * L * Cos[θa])]),
    Cot[θb] → (a * Cos[θa] - L) / Sqrt[(a^2 + L^2 - 2 * a * L * Cos[θa])] /
      (Sqrt[(1 - (a * Cos[θa] - L)^2 / (a^2 + L^2 - 2 * a * L * Cos[θa]))]),
    Sec[θb] → Sqrt[(a^2 + L^2 - 2 * a * L * Cos[θa])] / ((a * Cos[θa] - L)),
```

$$\text{Csc}[\theta b] \to 1 \Big/ \sqrt{\left(1 - \frac{(a * \text{Cos}[\theta a] - L)^2}{\left(a^2 + L^2 - 2 * a * L * \text{Cos}[\theta a]\right)}\right)}\Big\};$$

```
fgetcXa[vcm[n]]; fgetcYa[vcm[n]];
For[i = 1, i < sphenumber + 1, i++, Xta[i] = Xa[i] + Xca[i]];
For[i = 1, i < sphenumber + 1, i++, Yta[i] = Ya[i] + Yca[i]];
For[i = 1, i < sphenumber + 1, i++,
 pa[-(i + 1)] = μ * (2 * i - 1) * a^-1 * (i + 1)^-1 *
   (a / ra)^(i+1) * ((i + 2) * Xta[i] + Yta[i])];
For[i = 1, i < sphenumber + 1, i++, Φa[-(i + 1)] =
  2^-1 * a * (i + 1)^-1 * (a / ra)^(i+1) * (i * Xta[i] + Yta[i])];
v[n] = Chop[mat.Sum[ Grad[Φa[-(i + 1)], {ra, θa, φa},
       "Spherical"] - (i - 2) * ra * ra * μ^-1 * 2^-1 * i^-1 * (2 * i - 1)^-1 *
       Grad[pa[-(i + 1)], {ra, θa, φa}, "Spherical"] +
      (i + 1) * μ^-1 * i^-1 * (2 * i - 1)^-1 * {ra, 0, 0} * pa[-(i + 1)],
    {i, sphenumber}]];
F[n] = Chop[FullSimplify[Chop[mat.(-4 * π *
        Grad[ra^3 * pa[-2], {ra, θa, φa}, "Spherical"])]]];
Print["F[n]", "=", F[n]];
vm[n + 1] =
 -TrigExpand[v[n]] /. {rc → b * Sin[θb], Z → b * Cos[θb] + L,
   Cos[Φ] → Cos[φb], Sin[Φ] → Sin[φb], rbm → b, Cos[θa] →
    (L + b * Cos[θb]) / Sqrt[b^2 + 2 * b * (L * Cos[θb]) + L * L], Sin[θa] →
    Sqrt[1 - (L + b * Cos[θb])^2 / (b^2 + L^2 + 2 * b * L * Cos[θb])], Cos[φa] → Cos[φb],
   Sin[φa] → Sin[φb], ra → Sqrt[b^2 + 2 * b * (L * Cos[θb]) + L * L],
   Tan[θa] → Sqrt[1 - (L + b * Cos[θb])^2 / (b^2 + L^2 + 2 * b * L * Cos[θb])] /
     ((L + b * Cos[θb]) / Sqrt[b^2 + 2 * b * (L * Cos[θb]) + L * L]),
   Cot[θa] → (L + b * Cos[θb]) / Sqrt[b^2 + 2 * b * (L * Cos[θb]) + L * L] /
     (Sqrt[1 - (L + b * Cos[θb])^2 / (b^2 + L^2 + 2 * b * L * Cos[θb])]), Sec[θa] →
    Sqrt[b^2 + 2 * b * (L * Cos[θb]) + L * L] / ((L + b * Cos[θb])),
   Csc[θa] → 1 / Sqrt[1 - (L + b * Cos[θb])^2 / (b^2 + L^2 + 2 * b * L * Cos[θb])]};
fgetXb[vm[n + 1]]; fgetYb[vm[n + 1]];
vcm[n + 1] = -v[n - 1] /. {rc → b * Sin[θb], Z → b * Cos[θb] + L,
   Cos[Φ] → Cos[φb], Sin[Φ] → Sin[φb], rbm → b,
```

```
    Cos[θa] → (L + b * Cos[θb]) / √(b^2 + 2 * b * (L * Cos[θb]) + L * L ,
    Sin[θa] → √(1 - (L + b * Cos[θb])^2 / (b^2 + L^2 + 2 * b * L * Cos[θb])),
    Cos[ϕa] → Cos[ϕb], Sin[ϕa] → Sin[ϕb],
    ra → √(b^2 + 2 * b * (L * Cos[θb]) + L * L ,
    Tan[θa] → √(1 - (L + b * Cos[θb])^2 / (b^2 + L^2 + 2 * b * L * Cos[θb])) /
      ((L + b * Cos[θb]) / √(b^2 + 2 * b * (L * Cos[θb]) + L * L)),
    Cot[θa] → (L + b * Cos[θb]) / √(b^2 + 2 * b * (L * Cos[θb]) + L * L) /
      (√(1 - (L + b * Cos[θb])^2 / (b^2 + L^2 + 2 * b * L * Cos[θb]))), Sec[θa] →
     √(b^2 + 2 * b * (L * Cos[θb]) + L * L) / ((L + b * Cos[θb])),
    Csc[θa] → 1 / √(1 - (L + b * Cos[θb])^2 / (b^2 + L^2 + 2 * b * L * Cos[θb]))};
fgetcXb[vcm[n + 1]]; fgetcYb[vcm[n + 1]];
For[i = 1, i < sphenumber + 1, i++, Xtb[i] = Xb[i] + Xcb[i]];
For[i = 1, i < sphenumber + 1, i++, Ytb[i] = Yb[i] + Ycb[i]];
For[i = 1, i < sphenumber + 1, i++,
 pb[-(i + 1)] = μ * (2 * i - 1) * b^-1 * (i + 1)^-1 *
   (b / rb)^(i+1) * ((i + 2) * Xtb[i] + Ytb[i])];
For[i = 1, i < sphenumber + 1, i++, Φb[-(i + 1)] =
  2^-1 * b * (i + 1)^-1 * (b / rb)^(i+1) * (i * Xtb[i] + Ytb[i])];
v[n + 1] = Chop[mbt.Sum[ Grad[Φb[-(i + 1)], {rb, θb, ϕb},
      "Spherical"] - (i - 2) * rb * rb * μ^-1 * 2^-1 * i^-1 * (2 * i - 1)^-1 *
      Grad[pb[-(i + 1)], {rb, θb, ϕb}, "Spherical"] +
     (i + 1) * μ^-1 * i^-1 * (2 * i - 1)^-1 * {rb, 0, 0} * pb[-(i + 1)],
    {i, sphenumber}]];
F[n + 1] = Chop[FullSimplify[mbt.
    (-4 * π * Grad[rb^3 * pb[-2], {rb, θb, ϕb}, "Spherical"])]];
Print["F[n+1]", "=", F[n + 1]];
vm[n + 2] =
 Chop[-((-v[n + 1] - v[n] /. {Cos[2 ϕa] → Cos[ϕa]^2 - Sin[ϕa]^2,
          Sin[2 ϕa] → 2 * Cos[ϕa] * Sin[ϕa],
          Cos[3 ϕa] → Cos[ϕa]^3 - 3 * Cos[ϕa] * Sin[ϕa]^2,
          Sin[3 ϕa] → 3 * Cos[ϕa]^2 * Sin[ϕa] - Sin[ϕa]^3,
          Cos[2 ϕb] → Cos[ϕb]^2 - Sin[ϕb]^2,
          Sin[2 ϕb] → 2 * Cos[ϕb] * Sin[ϕb],
          Cos[3 ϕb] → Cos[ϕb]^3 - 3 * Cos[ϕb] * Sin[ϕb]^2,
```

```
        Sin[3 ϕb] → 3 * Cos[ϕb]^2 * Sin[ϕb] - Sin[ϕb]^3}) /.
      {(1 - Cos[θa]^2) → Sin[θa]^2, (1 - Cos[θb]^2) → Sin[θb]^2}) /.
    {ra → Sqrt[rc0^2 + Z * Z] , Cos[θa] → Z / Sqrt[rc0^2 + Z * Z] ,
     Sin[θa] → rc0 / Sqrt[rc0^2 + Z * Z] ,
     Cos[ϕa] → Cos[Φ], Sin[ϕa] → Sin[Φ],
     rb → Sqrt[rc0^2 + (Z - L) * (Z - L)] ,
     Tan[θa] → rc0 / Z, Cot[θa] → Z / rc0,
     Sec[θa] → Sqrt[rc0^2 + Z * Z] / Z,
     Csc[θa] → Sqrt[rc0^2 + Z * Z] / rc0,
     Cos[θb] → (Z - L) / Sqrt[rc0^2 + (Z - L) * (Z - L)] ,
     Sin[θb] → rc0 / Sqrt[rc0^2 + (Z - L) * (Z - L)] ,
     Tan[θb] → rc0 / (Z - L),
     Cot[θb] → (Z - L) / rc0, Cos[ϕb] → Cos[Φ],
     Sec[θb] → Sqrt[rc0^2 + (Z - L) * (Z - L)] / (Z - L),
     Csc[θb] → Sqrt[rc0^2 + (Z - L) * (Z - L)] / rc0,
     Sin[ϕb] → Sin[Φ]}];
 fgetcharmonics[vm[n + 2]];
 Print["n+2", "=", n + 2];
 v[n + 2] = Chop[mct.{-π^-1 * (Cos[0] * (ψca[0] *
              (0.5 * (BesselI[1, λ * rc] + BesselI[-1, λ * rc])) +
             γca[0] * λ * rc * (0.25 * (BesselI[-2, λ * rc] +
                  2 * BesselI[0, λ * rc] + BesselI[+2, λ * rc]))) *
          Cos[λ * Z] + Cos[0] * (ψcb[0] * (0.5 * (BesselI[+1,
                λ * rc] + BesselI[-1, λ * rc])) + γcb[0] * λ * rc *
             (0.25 * (BesselI[-2, λ * rc] + 2 * BesselI[0, λ * rc] +
                  BesselI[+2, λ * rc]))) * Sin[λ * Z]), 0,
     -π^-1 * (Cos[0] * (ψcb[0] * BesselI[0, λ * rc] + γcb[0] * λ * rc *
              (0.5 * (BesselI[+1, λ * rc] + BesselI[-1, λ * rc])) +
             γcb[0] * BesselI[0, λ * rc]) * Cos[λ * Z] +
         Cos[0] * (-ψca[0] * BesselI[0, λ * rc] - γca[0] * λ * rc *
              (0.5 * (BesselI[+1, λ * rc] + BesselI[-1, λ * rc])) -
             γca[0] * BesselI[0, λ * rc]) * Sin[λ * Z])}];]

Fa = FullSimplify[Sum[F[i], {i, 1, n - 3, 3}]]

Fb = FullSimplify[Sum[F[i], {i, 2, n - 2, 3}]]

Solve[Fa.{0, 0, 1} == 0 && Fb.{0, 0, 1} == 0, {Ua, Ub}]
```